Fakultät für Mathematik, Informatik und Naturwissenschaften | RWTH AACHEN UNIVERSITY

„pH dependent migration and transcription in glioblastoma cancer stem cells“

Von der Fakultät für Mathematik, Informatik und Naturwissenschaften der RWTH Aachen University zur Erlangung des akademischen Grades eines Doktors der Naturwissenschaften genehmigte Dissertation

vorgelegt von

„Klaus-Daniel, Cortes Franco, Master of Science“

aus

„Hamburg, Deutschland“

Berichter*:* *Prof. Dr. rer. nat., Stefan Gründer*

Prof. Dr. rer. nat., Geraldine Zimmer-Bensch

Tag der mündlichen Prüfung*:* *06.12.2023*

Acknowledgements

Hereby I express my sincere gratitude to **Prof. Stefan Gründer**, for giving me this opportunity to be part of the research group in the physiology department, providing not only valuable lab-space and lab supplies for my research, but also essential advice, guidance and countenance. Moreover, I want to thank my supervisor **Dr. Yuemin Tian**, for her continuous support of my work, her knowledge and guidance during my research.

I want to thank all members of the workgroup, who readily answered all my questions and shared their knowledge and expertise in numerous scientific methods. Specifically, I want to thank **David Corredor** for getting me into the workflow with glioblastoma cell culture and qPCR, **Dr. Yuemin Tian** for helping me establish the migration assay and theoretical help on all my experiments, **Dr. Jochen Maurer** and his research group of Molecular Gynaecology for allowing me to use the Incucyte in his laboratory, **Dr. Diana Panayotova-Dimitrova** and **Dr. Maria Feoktistova** for assisting with lentiviral overexpression of GSC lines, **Adrienne Oslender-Bujotzek** for helping me with all types of cloning and ordering questions, as well as **Dr. Dominik Wiemuth** for assistance and advice regarding CRISPR-Cas9.

Furthermore, I would like to kindly thank **Prof. Geraldine Zimmer-Bensch** for agreeing to be an examiner to my doctoral thesis and her continuous countenance.

Last, but not least, I would like to thank my **wife**, for ubiquitous support and strict revisions of my thesis, my **daughter**, for motivating me, and my **mother-in-law** for a lot of cooking and babysitting.

First Examiner: **Prof. Dr. rer. nat. Geraldine Zimmer-Bensch**

Institute of Functional Epigenetics
RWTH Aachen University

Worringerweg 3
52074 Aachen
Germany

Phone: +49 241 80 20844
E-Mail: zimmer@bio2.rwth-aachen.de

Second Examiner: **Prof. Dr. rer. nat. Stefan Gründer**

Institute of Physiology
RWTH Aachen University

Universitätsklinikum Aachen, AöR
Pauwelsstraße 30
52074 Aachen

Phone: +49 241 80-88800
E-Mail: sgruender@ukaachen.de

A. Abbreviations:

3'MACE/MACE	3' massive analysis of cDNA ends
4-HT	4-Hydroxytamoxifen
ACC	Acetyl-CoA carboxylase
ACLY	ATP citrate lyase
ad (latin)	To
ANOVA	Analysis of variance
ASIC	Acid-sensing ion channel
ATP	Adenosine triphosphate
bp	Base pairs
cDNA	Complementary DNA'
CNS	Central nervous system
DMEM	Dulbecco's modified eagle medium
DMSO	Dimethyl sulfoxide
DNA	Desoxyribonucleic acid
EC_{50}	Half maximal effective concentration
EDTA	Ethylenediaminetetraacetic acid
e.g. (latin)	exempli gratia / for example
EGFP	Enhanced green fluorescent protein
E. coli	Escherichia coli
FA	Fatty acid
FASN	Fatty acid synthetase
FDR	False discovery rate
FGF	Fibroblast growth factor
Fw	Forward primer
GALC	Galactosylceramidase
GBM	Glioblastoma multiforme
gDNA	Genomic DNA
GFAP	Glial fibrillary acidic protein
GLMM	Generalized linear mixed model
GOI	Gene of interest
gRNA	Guide RNA
GSC	GBM stem cells
GSEA	Gene set enrichment analysis
GSH	Glutathione
GSS	Gene set size
GSSG	Glutathione disulfide
HEPES	2-(4-(2-Hydroxyethyl)-1-piperazineethansulfonic acid
HCl	Hydrochloric acid
HIF	Hypoxia inducible factor
IC_{50}	Half maximal inhibitory concentration
IDH	Isocitrate dehydrogenase
IKCa	Intermediate-conductance potassium channel
ind	Induced
KCNN4	Potassium calcium-activated channel subfamily N member 4

KEGG	Kyoto Encyclopaedia for Genes and Genomes
KO	Knockout
L27	pF 5 × UAS W SV40 Puro
LDL	Low-density lipoprotein
LDLR	Low-density lipoprotein receptor
min	Minutes
MSigDB	Molecular signatures database
mSREBP2	Mature sterol-regulatory element binding protein 2
NaCl	Sodium chloride
NEB	New England Biolabs
NES	Normalized enrichment score
oe	Overexpressed
padj	P-adjusted value
PBS	Phosphate buffered saline
PC	Principal component
PCA	Pyruvate carboxylase / Principle component analysis
PCR	Polymerase chain reaction
PcTx1	Psalmotoxin-1
PDH	Pyruvate dehydrogenase
PH-domain	Pleckstrin homology domain
pH_e	Extracellular pH
pH_i	Intracellular pH
PI3K	Phosphoinositide 3-kinase
PIP_2	Phosphatidylinositol-4,5-bisphosphate
PIP_3	Phosphatidylinositol-3,4,5-triphosphate
POI	Proteins of interest
PuroR	Puromycin resistance cassette
qPCR	Quantitative polymerase chain reaction
rEGF	Recombinant epithelial growth factor
Rev	Reverse primer
RNA	Ribonucleic acid
ROS	Reactive oxygen species
rpm	Rotations per minute
RT	Room temperature
RTK	Receptor tyrosine kinase
SD	Standard deviation
SDS	Sodium dodecyl sulfate
sec	Seconds
SEM	Standard error of mean
SOX2	Sex determining region Y-box 2
SREBP	Sterol regulatory element binding protein
TAE buffer	TRIS-acetate-EDTA buffer
TCA cycle	Tricarboxylic acid cycle
TE buffer	TRIS-EDTA buffer
TM	Transmembrane domain
TMZ	Temozolomide

TNF	Tumour necrosis factor
TUBB3	Tubulin beta 3 class III
TRIS	Trisaminomethane
UAS	Upstream activation sequence
UV	Ultraviolet
v/v	Volume per volume
WT	Wild type
w/v	Weight per volume

B. Table of contents

C. Eidesstattliche Erklärung

Hiermit erkläre ich, dass diese Dissertation und die darin dargelegten Inhalte die eigenen sind und selbstständig, als Ergebnis der eigenen originären Forschung, generiert wurden.

Weiterhin erkläre ich an Eides statt

1. Diese Arbeit wurde vollständig oder größtenteils in der Phase als Doktorand dieser Fakultät und Universität angefertigt;

2. Sofern irgendein Bestandteil dieser Dissertation zuvor für einen akademischen Abschluss oder eine andere Qualifikation an dieser oder einer andere Institution verwendet wurde, wurde dies klar angezeigt;

3. Wenn immer andere eigene- oder Veröffentlichungen Dritter herangezogen wurden, wurden diese klar gekennzeichnet;

4. Wenn aus anderen eigenen- oder Veröffentlichungen Dritter zitiert wurde, wurde stets die Quelle hierfür angegeben. Diese Dissertation ist vollständig meine eigene Arbeit, mit der Ausnahme solcher Zitate;

5. Alle wesentlichen Quellen von Unterstützung wurden benannt;

6. Wenn immer ein Teil dieser Dissertation auf der Zusammenarbeit mit anderen basiert, wurde von mir klar gekennzeichnet, was von anderen und was von mir selbst erarbeitet wurde;

7. Teile dieser Arbeit wurden zuvor veröffentlicht, in den folgenden Publikationen:

Clusmann, J., Franco, KD.C., Suárez, D.A.C. et al. Acidosis induces RIPK1-dependent death of glioblastoma stem cells via acid-sensing ion channel 1a. Cell Death Dis 13, 702 (2022). (https://doi.org/10.1038/s41419-022-05139-3)

Cortés Franco, KD., Brakmann, I.C., Feoktistova, M. et al. Aggressive migration in acidic pH of a glioblastoma cancer stem cell line in vitro is independent of ASIC and KCa3.1 ion channels, but involves phosphoinositide 3-kinase. Pflugers Arch - Eur J Physiol 475, 405–416 (2023). (https://doi.org/10.1007/s00424-022-02781-w)

Aachen, 12.12.2023

_____

(Klaus-Daniel Cortés Franco)

D. Abstract

Glioblastoma multiforme (GBM) is the most commonly occurring brain tumour, which also has a very high recurrence rate after treatment combination, due to invasion of cancer cells into neighbouring healthy tissue, resulting in a very poor patient survival rate.

Three-dimensional GBM stem cells (GSCs) isolated from human tumor tissue, are a promising cell model to study GBM, as they grow in spheres and the cells are subjected to different tumor microenvironments, thus being heterogenous in behaviour and likely also in protein expression. However, methods are lacking in researching localized protein expression differences in GBM tumourspheres. Here, we developed a protocol to immobilize and slice 7-day old GSC tumourspheres for subsequent antibody staining and localization experiments.

It is not yet entirely understood, how environmental factors such as pH play a role in changing the tumor behaviour of GSCs. To determine and quantify differences in the transcriptome of GSCs incubated in physiological pH (pH 7.4) and acidic pH (pH 6.6) for 14 days, we conducted ribonucleic acid (RNA) sequencing and gene set enrichment analysis (GSEA). Expression of phosphoinositide 3-kinase (*PI3K*) was increased at pH 6.6, making it a candidate for potentially modulating pH dependent migration. We also observed enrichment of the oxidative phosphorylation pathway, reactive oxygen species (ROS) related pathways and lipid scavenging pathways, illustrating how cancer cells ensure cell survival under acidic stress conditions and deal with increased ROS. These pathways might provide vulnerabilities that could be exploited for therapeutic gain.

pH as a factor for tumor microenvironment is also essential in modulating migration, the effect of which we wanted to characterize in GSCs. In immortalized monolayer glioma and GBM cells, it has been reported that sodium-selective, proton-sensitive acid-sensing ion channels (ASICs), in particular ASIC1a and ASIC2a, mediate pH dependent GBM migration, by acting as a pH sensor. Using a sphere migration assay, we observed that acidic pH 6.6 increased migration. With inhibitors and activators of ASIC channels, CRISPR-Cas9 and lentivirally modified cell lines, we consistently showed that ASICs do not modulate pH dependent migration in GSCs. However, inhibiting PI3K decreased migration at pH 6.6. Migration at pH 7.4 was not abrogated by inhibiting PI3K.

E. German abstract / Deutsche Zusammenfassung

Glioblastoma multiforme (GBM) ist der am häufigsten vorkommender Gehirntumor, der sich durch eine sehr hohe Rezidivrate nach Behandlung auszeichnet. Dies liegt an der Invasion von Krebszellen in benachbartes gesundes Gewebe, was letztlich eine geringe Überlebensrate der Patienten zur Folge hat.

Dreidimensionale GBM Stammzellen (GBM stem cells; GSCs) immortalisiert von menschlichem Tumorgewebe sind ein vielversprechendes Modell um GBM zu erforschen, da sie in Sphären wachsen und die Tumorzellen verschiedenen Tumormilieubedingungen in der Sphäre ausgesetzt sind, wodurch sie heterogen im Verhalten und wahrscheinlich auch in der Proteinexpression sind. Bisher waren noch keine Methoden etabliert, um lokalisierte Proteinexpression von GSCs innerhalb der Tumorsphäre zu untersuchen. Wir entwickelten ein Protokoll um 7-Tage alte GSCs als Tumorsphären zu fixieren und in Scheiben zu schneiden. Diese Scheiben könnten danach mit Antikörpern gefärbt und für Lokalisierungsexperimente verwendet werden.

Es ist noch nicht vollkommen aufgeklärt wie Tumormilieufaktoren wie z.B. pH das Verhalten von GSCs moduliert. Um Unterschiede im Transkriptom von GSCs, die für 14 Tage in physiologischem Medium (pH 7.4) und saurem Medium (pH 6.6) inkubiert wurden, zu charakterisieren und quantifizieren, haben wir eine Ribonukleinsäure Sequenzierung und Genset Anreicherungsanalyse durchgeführt. Phosphoinosid-3-Kinase war in saurem Medium überexprimiert und war daher ein Kandidat für die Modulierung pH-abhängiger Migration in GBM. Ebenfalls sahen wir Anreicherung von biologischen Prozessen, welche die Funktion der oxidativen Phosphorylierung, der Modulierung von reaktiven Sauerstoffspezies und der exogenen Aufnahme von Fettsäuren ausüben. Die Anreicherung dieser Signalwege zeichnen ein genaueres Bild, wie Krebszellen ihr Überleben in saurem pH sicherstellen, und mit dem zusätzlichen Säurestress und ROS-Stress umgehen. Weiterhin könnten diese Signalwege Schwachstellen von GBM sein, und durch Inhibierung therapeutischen Nutzen finden.

pH, als Faktor für das Tumormilieu, ist auch wichtig für die Modulierung des Migrationsverhaltens der Tumorzellen, welches wir in GSCs charakterisieren wollten. In immortalisierten einschichtig wachsenden Glioma- und GBM-Zellen wurde zuvor berichtet, dass natrium-selektive protonen-aktivierte Ionenkanäle (acid-sensing ion channels; ASICs),

insbesondere ASIC1a und ASIC2, pH-abhängige Migration von GBM modulieren, indem sie als pH-Sensor agieren. Mithilfe eines Sphären-Migrationsassays sahen wir, dass GSCs in saurem Medium stärker ausmigrieren. Mit pharmakologischen Inhibitoren und Aktivatoren, als auch CRISPR-Cas9 und lentiviral modifizierten Zelllinien, konnten wir widerspruchsfrei zeigen, dass ASICs nicht die pH-abhängige Migration in unseren GSCs beeinflusst. Inhibition von Phosphoinositid-3-Kinase (PI3K), allerdings, bewirkte eine verringerte Migration der GSCs in pH 6.6. Migration in pH 7.4 wurde durch PI3K Inhibition nicht beeinflusst.

1. Introduction

1.1. Acid-sensing ion channels (ASICs)

Acid-sensing ion channels (ASICs) are voltage-insensitive sodium channels, which are sensitive to extracellular protons and belong to the DEG/ENaC gene family. Four genes have been identified in humans (*ASIC1*, *ASIC2*, *ASIC3*, *ASIC4*), with differential splicing resulting in six subunits (ASIC1a, ASIC1b, ASIC2a, ASIC2b, ASIC3, ASIC4) (Gründer and Pusch, 2015). Together they form trimeric ion channels, which can either be homo- or heterotrimers.

This variability not only changes proton affinities, but also the desensitization kinetics. In human neurons of the central nervous system (CNS), ASIC consists mainly of homotrimeric ASIC1a and heteromeric ASIC1a/2a or ASIC1a/2b channels (Wu *et al.*, 2016), whereas ASIC3 containing channels play a larger role in the peripheral nervous system (Lingueglia, 2007). While most ASIC members are proton-sensitive, subunits ASIC2b and ASIC4 are actually not proton-sensitive, but modulate other proton-sensitive channels, such as ASIC2a and ASIC3 (Rosa *et al.*, 2002; Lingueglia, 2007; Sherwood *et al.*, 2011) via formation of heteromeric channels.

Proton binding to closed ASIC1a results in a conformational change, opening the channel allowing the influx of sodium ions, and, to a lesser degree, potassium ions (P_{Na}/P_K 5-14). Additionally, ASIC1a can also conduct calcium ions (P_{Na}/P_{Ca} >15). Once open and a proton is bound, the channel is energetically unstable and enters a desensitized state, from which the channel recovers with a time constant τ. It has been proposed that ASIC can enter the desensitized state without opening. This process is termed steady-state-desensitisation and occurs at lower proton concentrations than regular activation. This process of steady-state-desensitisation is likely the result of the extremely high affinity of the channel for protons. A measure of the affinity of the channel for protons is the half-maximal effective concentration (EC_{50}), at which the channel response to the ligand is half-maximal. Another important variable is the half-maximal inhibitory concentration (IC_{50}), which describes pH at which the steady-state desensitization is half-maximal. Thus, IC_{50} values are measured at steady-state, whereas, due to desensitisation, EC_{50} values are measured immediately after a drop to lower proton concentrations (Chen, Kalbacher and Grunder, 2006).

The steady-state-desensitisation of homomeric ASIC1a channels starts below pH 7.4 and is complete at pH 7.0, with an IC_{50} of pH 7.31 ± 0.005, whereas the EC_{50} is pH 6.5 ± 0.04 (Joeres *et al.*, 2016, Figure 2). The steady-state desensitisation of ASIC2a homomeric channels has an IC_{50} of 6.39, whereas the EC_{50} is pH 3.8-4.5 (Joeres *et al.*, 2016; Soto, Ortega-Ramírez and Vega, 2018). Homomeric ASIC3 has a similar proton sensitivity as ASIC1, with EC_{50} being pH 6.4 (Soto, Ortega-Ramírez and Vega, 2018).

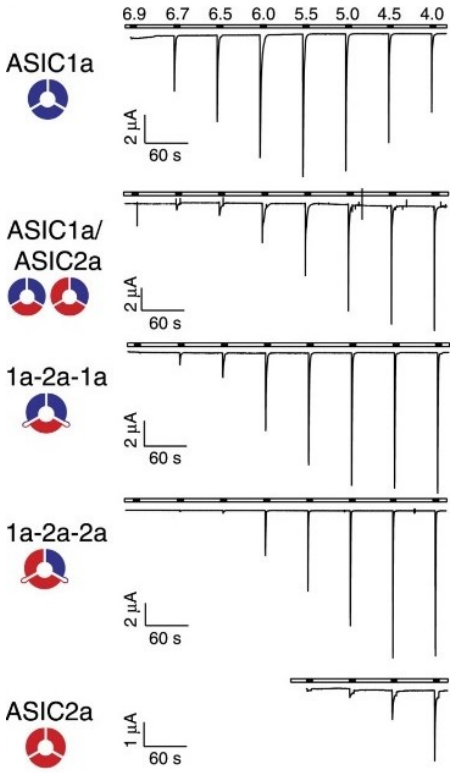

Figure 1 – pH dependent activation of homo- and heteromeric ASIC1a and ASIC2a channels. Representative current traces after 10 second activation with pH solutions, as indicated, and 50 seconds of recovery at pH 7.4 (Joeres *et al.*, 2016).

ASIC1a and ASIC1b are inhibited by Psalmotoxin1 (PcTx1), which is a polypeptide toxin isolated from the tarantula *Psalmopoeus cambridgei*. ASIC3, in turn, is inhibited by APETx2, a polypeptide toxin isolated from the sea anemone *Anthopleura elegantissima* (Baron *et al.*, 2013). For ASIC1a PcTx1 increases the affinity of the channel for protons, leading to desensitisation of the channel at pH 7.4 (Chen, Kalbacher and Grunder, 2006). MitTx is a polypeptide animal toxin from the Texas coral snake *Micrurus tener tener*, which preferentially activates ASIC1 homomers, but changes selectivity towards ASIC2a at a pH below 6.5 (Bohlen *et al.*, 2011; Osmakov *et al.*, 2020).

1.2. Intermediate-conductance calcium-dependent potassium channels (IKCas)

Calcium-dependent potassium (KCa) channels are classified into small-conductance potassium channels, intermediate-conductance potassium channels (IKCa) and big-conductance potassium channels (Vergara *et al.*, 1998). The *KCNN4* gene codes for the potassium calcium-activated channel subfamily N member 4 (KCNN4), also known as KCa3.1, which is classified as an IKCa. KCa3.1 forms a homotetrameric structure of subunits, each with six transmembrane domains and a pore segment between transmembrane domain five and six (Sforna *et al.*, 2018). The intracellular C-terminal peptide of each subunit complexes with calmodulin, allowing for the binding of four calmodulin proteins. Calmodulin in turn binds intracellular calcium ions, thereby resulting in a conformational change and opening the channel for potassium efflux. The best characterized role of KCa3.1 is the regulation of the cell membrane potential, as entry of calcium ions depolarizes the membrane, and efflux of potassium ions maintains a negative membrane potential, which allows continued influx of calcium (Wulff and Castle, 2010). KCa3.1 is not expressed in excitable tissues, including the brain, with exception of enteric neurons. However, it is expressed in brain tumours, as well as other tumour types. In cancer, KCa3.1 plays a role in migration and proliferation in GBM (Ruggieri *et al.*, 2012; d'Alessandro *et al.*, 2013) modulating desoxyribonucleic acid (DNA) repair mechanisms (Klumpp *et al.*, 2018), hepatocellular carcinoma (Liu *et al.*, 2015; Li *et al.*, 2019), radioresistance in breast cancer (Mohr *et al.*, 2019), metastasis and poor survival in patients with clear cell renal carcinoma (Rabjerg *et al.*, 2015), migration in colorectal cancer (Lai *et al.*, 2013) and migration in lung adenocarcinoma (Xu *et al.*, 2021).

1.3. Phosphatidylinositol-3 kinase (PI3K)

Phosphatidylinositol-3 kinases (PI3K) are a family of kinases that are divided into four different classes I, II, III and IV. Class I PI3Ks further separate into catalytic and regulatory proteins. Class I catalytic PI3Ks confer the actual functionality of the PI3Ks, with their ability to phosphorylate the secondary messenger phosphatidylinositol-4,5-bisphosphate (PIP_2) and as a result create the secondary messenger phosphatidylinositol-3,4,5-triphosphate (PIP_3). Proteins containing a pleckstrin homology domain (PH-domain) interact with secondary messengers PIP_2 and PIP_3, thereby modulating numerous pathways relating to cell survival, cell cycle progression and cellular growth (Vara *et al.*, 2004). Akt, also known as protein kinase B, is a collective term for three protein kinases (AKT1/2/3) that also contain the PH-domain and play a key role in

apoptosis, cell proliferation and cell migration. Akt is downstream of PI3K signalling. Class I regulatory PI3Ks modulate the catalytic functions, as Class I catalytic and regulatory PI3Ks require the formation of a heterodimer to function. Class II PI3K plays a role in endocytosis and Class III PI3K in endosomal-lysosomal trafficking and autophagy (Hawkins and Stephens, 2015). However, Class I PI3Ks have become infamous, as they are part of the PI3K/Akt pathway that is commonly upregulated or mutationally activated in cancer and associated with invasion and metastasis, angiogenesis, unlimited replicative potential, inhibition of apoptosis, regardless of tumour tissue origin. Therefore, PI3K, Akt and also downstream mTOR are popular targets for inhibition in cancer patients, which is why numerous clinical trials are currently targeting these proteins (Vara *et al.*, 2004; Weigelt and Downward, 2012; Dienstmann *et al.*, 2014). It is commonly reported that PI3K is activated by growth factor stimulation of receptor tyrosine kinases (RTKs), however PI3K can also be activated by numerous other receptors interacting with RTKs, such as tumour necrosis factor (TNF) receptor 2 (TNFR2) interacting with the RTK Etk/Bmx (Qiu *et al.*, 1998; Zhang *et al.*, 2003; Marchetti *et al.*, 2004; Al-Lamki *et al.*, 2005; Li *et al.*, 2017), with TNFR2 in turn being activated by cytokine TNF alpha and TNF superfamily member lymphotoxin alpha (Hu *et al.*, 2014; Kucka *et al.*, 2021).

1.4. Glioblastoma multiforme (GBM)

The term glioma describes primary brain tumours, which are classified by their presumed cellular origin. The term glioblastoma multiforme (GBM) refers to a type of astrocytoma, which is a type of glioma. GBM is the most common tumour affecting the CNS and also one of the most lethal human cancers. The classification of glioma cancer is determined by a pathologist and indicated as a grade from I to IV, grade I being the least aggressive and grade IV being the most aggressive (Marquet *et al.*, 2007). GBM is classified as a grade IV glioma. Age is a major risk factor and due to an aging population, the annual GBM cases are expected to rise as well (Alexopoulos *et al.*, 2022). GBM infiltrates nearby tissue aggressively, making complete surgical resection almost impossible. Furthermore, its inter- and intratumour heterogeneity has been well classified (Inda, Bonavia and Seoane, 2014). These facts, combined with the difficulty of drugs to pass the blood brain barrier, explain the low patient survival, which is ~ 7% after 5 years (Wu *et al.*, 2021). Radiotherapy and surgical resection, followed by temozolomide (TMZ) treatment is the most common treatment, but due to the

infiltration of GBM into neighbouring tissue, estimated tumour recurrence is > 86% (Oh *et al.*, 2011).

Tumours have long been reported to rely on aerobic glycolysis for adenosine triphosphate (ATP) synthesis, thereby acidifying their microenvironment (Potter, Newport and Morten, 2016). This acidic environment requires proton extrusion from the intracellular compartment of the cell, and tumours have a reversed gradient of intracellular pH (pH_i) to extracellular pH (pH_e), with a more alkaline intracellular pH than extracellular pH (Cardone, Casavola and Reshkin, 2005). Moreover, this extracellular acidification is linked to increased migration, cell-matrix remodelling, evasion from apoptosis and increased cell proliferation (Webb *et al.*, 2011; Damaghi, Wojtkowiak and Gillies, 2013). Therefore, it is important to identify the exact acid sensors involved in this process, and the downstream pathways, to find targets to inhibit increased cancer cell migration and proliferation. Numerous candidates have been identified in proton sensing, among them acid sensing ion channels (ASICs) and proton-sensing G-protein coupled receptors (Parks, Chiche and Pouyssegur, 2011; Damaghi, Wojtkowiak and Gillies, 2013). Other proteins involved in cancer migration are KCNN4/KCa3.1 channels (Ruggieri *et al.*, 2012; d'Alessandro *et al.*, 2013; Lai *et al.*, 2013; Bonito *et al.*, 2016; Li *et al.*, 2019, 2020) and phosphoinositide 3-kinase (PI3K) (Samuels and Ericson, 2006; Lien, Dibble and Toker, 2017).

mRNA expression profiles of signature markers in GBM are separated into four subtypes, namely proneural, neural, classical or mesenchymal subtypes, which can predict treatment outcomes and therefore guide treatment decisions (Figure 2; Aldape *et al.*, 2015 adapted from Verhaak *et al.*, 2010).

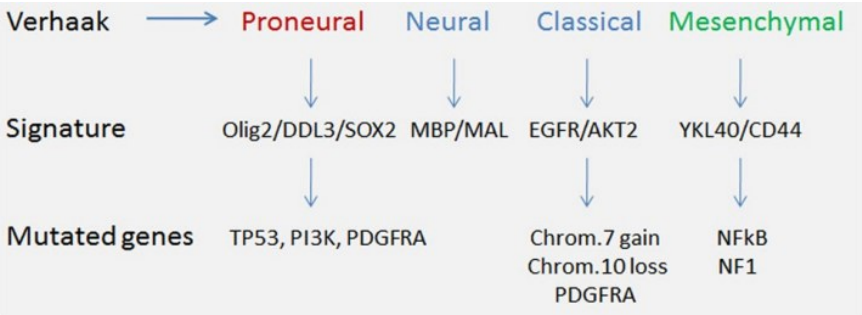

Figure 2 – Classification of GBM expression signatures. Four expression profiles are characterized in GBM: proneural, neural, classical and mesenchymal. Signature refers to genes that are enriched in their expression, compared to wild-type. Mutated genes refers to mutational changes that are characteristic for the respective subtype of GBM (Aldape *et al.*, 2015 adapted from Verhaak *et al.*, 2010).

A major challenge of GBM is the diffuse nature of the tumour, so that surgical resection of the core leaves tumour cells in the periphery, which continue to replicate and acquire chemo- and radioresistant properties. This outward migration of cells from the core of the tumour is defined as pseudopalisading behaviour. Pseudopalisading cells are hypothesised to occur due to vaso-occlusion of the tumour, causing severe hypoxia, or due to severe hypoxia by large numbers of malignant cells that are distant from arterial supply, causing necrosis. Pseudopalisading cells are rich in hypoxia inducible factor (HIF1a) and vascular endothelial growth factor, and likely act as fronts for fast neoplastic expansion and angiogenesis (Figure 3; Brat and Van Meir, 2004; Rong *et al.*, 2006).

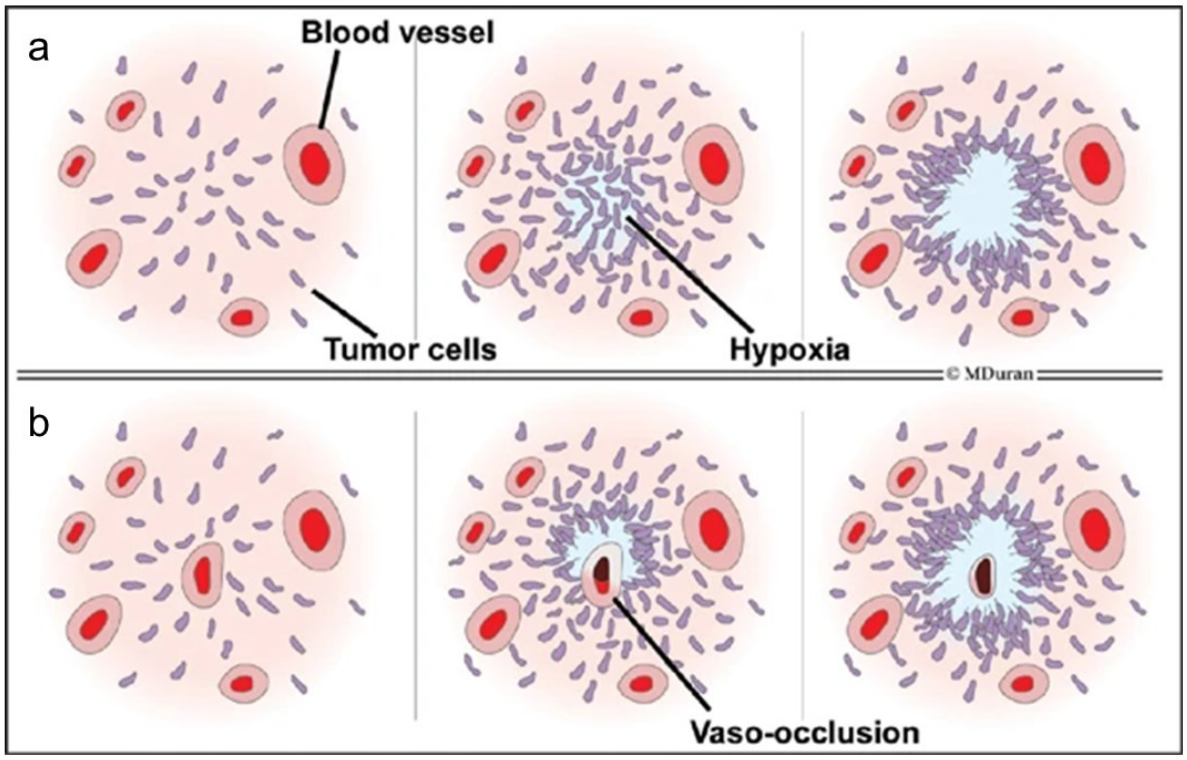

Figure 3 – a) Pseudopalisading cells after necrosis due to tumour density far from blood vessels or b) vaso-occlusion. (Brat and Van Meir, 2004)

Hypoxic cancer environments also promote acidification (Chiche, Brahimi-Horn and Pouysségur, 2010). Acidic microenvironments are reported to impact cancer stemness (Gillies *et al.*, 2019; de Bem Prunes *et al.*, 2022) and cancer differentiation, or lack thereof (Persano *et al.*, 2013; Daniele *et al.*, 2015), which in turn can affect not only local migration and invasion behaviour of cancer (Sivridis, Giatromanolaki and Koukourakis, 2005; Iwadate, 2016; Garcia, Jain and Aghi, 2021), but also chemo-/radiotherapy resistance (Haar *et al.*, 2012; Fidoamore *et al.*, 2016; Colwell *et al.*, 2017).

1.5. Glioblastoma stem cells (GSCs)

1.5.1. Glioblastoma stem cells (GSCs)

Cancer stem cells represent only a small fraction of the cancer cells and are necessary for cancer renewal, growth and differentiation (Singh *et al.*, 2004; Lobo *et al.*, 2007; Ward and Dirks, 2007; Tilghman *et al.*, 2014). $CD133^-$ mesenchymal-like GBM stem cell (GSC) line R8 and $CD133^+$ proneural-like GSC-line R54, isolated in 2007 in Regensburg (Beier *et al.*, 2007), are suspension cell lines growing in tumour spheres, contain GSCs, are heterogeneous and represent a more complex model, better resembling the *in vivo* tumour than classical GBM cell lines that grow as a monolayer. Moreover, their transcriptional profile more closely resembles tumour tissue than monolayer GBM cells (Lee *et al.*, 2006; De Witt Hamer *et al.*, 2008).

Solid core cancer cells are inherently heterogeneous, as individual cells are subject to different environmental stimuli, such as oxygen, nutrients, pH and secondary metabolites, depending on their localization (Dayan *et al.*, 2008; Bader, Voss and Rathmell, 2020). This makes spheroid cancer cells an ideal model, as they are also subject to these different environmental stimuli (Tevis, Colson and Grinstaff, 2017). Proteins relevant for cancer survival, such as acid sensing proteins, or proteins relevant for stem cell-like properties, such as SOX2, could be differentially expressed within tumourspheres (Trédan *et al.*, 2007; Ponomarev *et al.*, 2022), as expression differences are also common within different regions of solid core cancers (Wang *et al.*, 2017; Puchalski *et al.*, 2018).

1.5.2. ASIC expression in R8, R54 GSCs, and in GBM samples

ASIC1a and ASIC3, but not ASIC2a, is expressed in R8 and R54 GSCs (Tian *et al.*, 2017), with homomeric ASIC1a being the primary functional ASIC in these GSC lines. Concerning ASIC expression in GBM tissue, one dataset covering non-cancerous, glioma and GBM tissue of all grades (I-IV) is the microarray subtyping by Gravendeel et al. (Gravendeel *et al.*, 2009). Therein, ASIC2 shows decreased expression of ribonucleic acid (RNA) in GBM, compared to non-tumour tissue (Figure 4). Moreover, decreased RNA expression of ASIC1 and ASIC2 correlates with the WHO tumour grade. Unfortunately, ASIC3 is not included in the Gravendeel dataset.

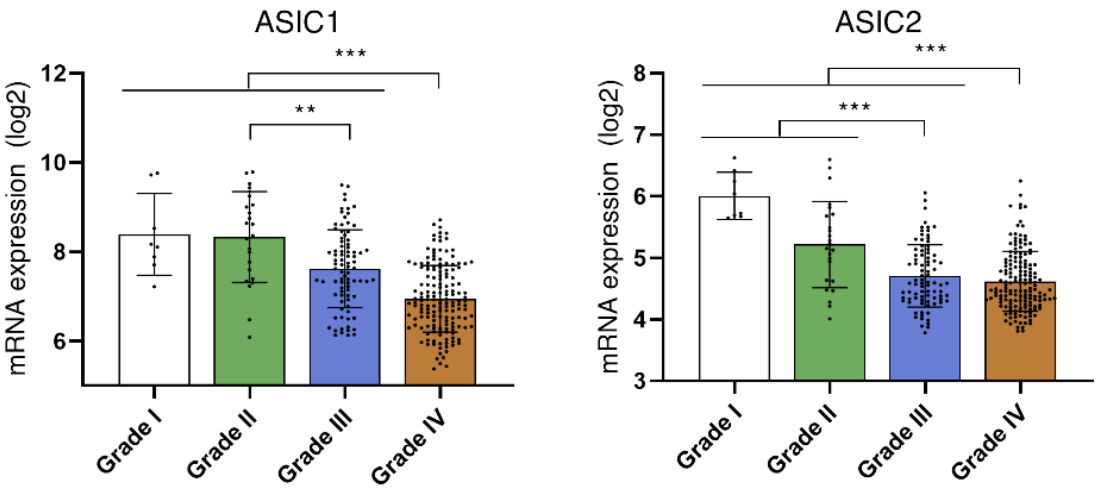

Figure 4 – RNA-level expression of ASICs from patient tumour samples, determined via array hybridization. (Gravendeel *et al.*, 2009)**.** Bar graphs show the mean ± SD. ** $p < 0.01$, *** $p < 0.001$; Tukey's HSD multiple comparison.

1.5.3. The possible role of ASICs in GSC migration

Deg/ENaC channels have been reported to play a role in epithelial cell migration (Chifflet, Hernández and Grasso, 2005) and vascular smooth muscle cell migration (Yellowhair *et al.*, 2014). Previous studies have reported ASIC1 and ASIC2 to be proton-sensors in glioma and GBM, affecting pH dependent migration and cell cycle progression (Kapoor *et al.*, 2009; Rooj *et al.*, 2011, 2012). Furthermore, ASIC1 integrin-ß1 interactions have been reported, facilitating the ASIC1 dependent effect on migration in glioma cells (Rooj *et al.*, 2015).

1.6. Aims

My thesis had the following aims:

Aim 1: To establish a protocol for generating slices from R54 spheres. We aimed to establish a method to generate R54 GSC sphere slices, which would be a helpful method that could be used for antibody staining, to localize proteins of interest (POI) within the sphere and potentially discover protein expression differences between sphere periphery and sphere core.

Aim 2: To determine expression levels of candidate genes and differences in the transcriptome of GSC lines at pH 7.4 and pH 6.6. Firstly, we aimed to confirm and expand on previous findings of ASIC expression via quantitative polymerase chain reaction (qPCR) in R8 and R54 GSCs, which would help in identifying which ASICs could potentially play a role in

protein sensing and pH dependent behavious in the R8 and R54 GBM cell models. Secondly, we aimed to do RNA sequencing of R54 GSCs, and conduct a bioinformatical analysis and gene-set enrichment analysis (GSEA), to determine the transcriptome of spheres incubated and grown at pH 7.4 or at pH 6.6 for two weeks. Thus, we would be able to identify other genes and pathways that are differentially expressed in pH 6.6. This would help us deeper understand what changes the GBM cells undergo at acidic tumor microenvironments, and also could aid in identifying proteins that might play a role in pH dependent migration.

Aim 3: To compare migration of R54 GSCs at pH 7.4 and pH 6.6 and investigate the role of candidate proteins for migration. Firstly, we aimed to establish a migration assay for R54 GSC spheroid culture and test migration in hypoxia (~ 3% O_2) and in normoxia at physiological and acidic pH conditions, to see whether migration would be pH dependent in our GBM cells. Secondly, we aimed to investigate whether ASIC1, ASIC2 or ASIC3 play a role as proton sensors in pH dependent GBM migration. Lastly, we aimed to use the RNA sequencing data to identify and test other potential modulators of pH dependent migration. Thus, we would be able to characterize our cell models more in depth, in terms of pH dependent migration, and would be able to determine potential modulators of said migration, which could be promising future therapeutic targets to inhibit cancer infiltration into neighbouring tissue.

2. Materials and methods

2.1. Cell culture

GSC lines R8 and R54 have been provided by Prof. Christoph Beier (Department of Neurology, Odense, Denmark). They are isocitrate dehydrogenase (IDH) 1 and IDH2 WT (Beier *et al.*, 2018). R8 is a $CD133^-$ mesenchymal-like GSC-line, and R54 a $CD133^+$ proneural-like GSC-line (Lottaz *et al.*, 2010). GSC-lines were regularly tested for mycoplasma contamination. pH 7.4 medium for GSC lines was prepared by 0.22 µm sterile filtration of supplements, as listed in Table 1, which were added to 500 mL of 1:1 Dulbecco's modified Eagle medium (DMEM):F12 medium, containing L-Glutamine, 15 mM 2-(4-(2-Hydroxyethyl)-1-piperazineethansulfonic acid (HEPES) and 1.2 g/L $NaHCO_3$ (PAN Biotech).

Table 1 – Supplements for GBM medium. rEGF: recombinant epithelial growth factor, FGF: fibroblast growth factor.

Ingredient (Manufacturer)	**Volume (Concentration, if applicable)**
Neuropan 27 (PAN Biotech)	10 mL
L-Glutamine (Gibco)	5 mL (200 mM)
100x Vitamin solution (Gibco)	5 mL
rEGF (Peprotech)	50 µL (200 µg/mL)
FGF (Peprotech)	50 µL (200 µg/mL)

pH 6.6 medium for GSC lines was prepared by adding the same volume and concentration of supplements to powder-prepared 1:1 DMEM:F12 medium (Thermo Fisher Scientific, Waltham, USA), containing L-Glutamine and 15 mM HEPES, and 400 mg/L added sodium bicarbonate. The correct pH was tested using the Metrohm 827 pH-meter and osmolarity was tested using the Gonotec Osmomat 030 osmometer.

2.2. *E. coli* transformation

TOP10 competent *Escherichia coli* (*E. coli*) cells were kindly prepared and aliquoted by Adrienne Oslender-Bujotzek. They have the genotype: F^- *mrc*A Δ(*mrr-hsd*RMS-*mcr*BC) ϕ80*lac*ZΔM15 Δ*lac*X74 *rec*A1 *ara*Δ139 Δ (*ara-leu*)7697 *gal*U *gal*K *rps*L(Str^R) *end*A1 *nup*G. TOP10 aliquots were taken out of -80°C storage and thawed on ice for 2 min. 1 µL or 5 µL plasmid was pipetted into the aliquot, depending on whether a retransformation with a high plasmid concentration or a new ligation was conducted. The tube was kept for another 15 or

30 minutes (min) on ice, heat shocked at 42°C for 30-45 sec, and then immediately returned to the ice for 2 min. 200 µL pre-warmed LB medium was then added per tube and the bacteria were incubated for 30 or 60 min at 37°C on a heat block. Cells were then plated on LB agar plates, containing the respective antibiotic, and the agar plates were incubated overnight at 37°C or at room temperature for 48-72 hours.

2.3. Polymerase chain reaction (PCR)

Polymerase chain reactions (PCRs) were conducted with custom DNA primers and either Taq (New England Biolabs; NEB) or Phusion Polymerase (NEB), according to the manufacturer's protocol, depending on whether diagnostic or preparative reactions for downstream application were performed. The cycler used for PCR was the Biometra T3000 Thermocycler.

2.4. Quantitative PCR (qPCR)

RNA of R8 and R54 GSCs was isolated with the NucleoSpin RNA Isolation Kit (Thermo Fisher Scientific), according to the manufacturer's instructions, which included a step for genomic DNA digestion. qPCR was conducted using either custom primers in combination with the Takyon SYBR green master mix (Eurogentec), or predesigned primers, as part of the TaqMan master mix assay (Thermo Fisher Scientific), in combination with Luna master mix (NEB) (Table 2). All TaqMan probes were FAM-minor groove binder labelled. TaqMan reactions were pipetted into 4-Strip 0.1 mL Tubes (Starlab) and transferred to the Rotor-Gene Q Thermocycler (Qiagen) for cycling. The Rotor-Gene Q Software (Version 1.7.87, Qiagen) was then used for analysis.

Table 2 – qPCR Reaction Mix. cDNA: complementary DNA.

Ingredient	**Volume**
Master Mix	5 µL
Probe / Primer	1 µL / 1 µL each
cDNA Template	1 µL
Water	Ad 10 µL

The cycling program used was the same for all TaqMan assays (Table 3), whereas the annealing temperature was modified for custom primers, depending on their estimated melting temperature.

Table 3 – qPCR cycling program for TaqMan Assays.

Step	Temperature	Hold Time	Repeat Cycles
Initial Denaturation	95°C	20 sec	1x
Denaturation	95°C	30 sec	40x
Annealing	60°C	20 sec	
Elongation	72°C	20 sec	
Final Elongation	72°C	2 min	1x

TaqMan probes were bought from Thermo Fisher Scientific for quantification of ASIC1a (Hs00952802), ASIC2 (Hs00153756), ASIC3 (Hs00245097), ASIC4 (Hs00539628), Nestin (Hs00707120), Sox2 (Hs00602736), GALC (Hs00164660), TUBB3 (Hs00801390), GFAP (Hs00909233), and GAPDH as a housekeeping gene (Hs02758991) (Table 4).

Table 4 – TaqMan™ Probes information summary. Available data provided by Thermo Fisher Scientific for the TaqMan™ qPCR probe amplicons. Exact sequence of primers and amplicons is not disclosed by the manufacturer.

Target	Chromosome location	Spans Exons	Amplicon size (bp)
ASIC1	Chr.12: 50057637 - 50083622 on Build GRCh38	yes	88
ASIC2	Chr.17: 33013087 - 34156806 on Build GRCh38	yes	99
ASIC3	Chr.7: 151048292 - 151052756 on Build GRCh38	yes	71
ASIC4	Chr.2: 219514170 - 219538772 on Build GRCh38	yes	65
Nestin	Chr.1: 156668763 - 156677397 on Build GRCh38	no	81
Sox2	Chr.3: 181711924 - 181714436 on Build GRCh38	no	121
GALC	Chr.14: 87933014 - 87993665 on Build GRCh38	yes	129
TUBB3	Chr.16: 89922009 - 89936097 on Build GRCh38	no	134
GFAP	Chr.17: 44905626 - 44915552 on Build GRCh38	yes	57
GAPDH	Chr.12: 6534405 - 6538375 on Build GRCh38	yes	93

Statistical comparison of ΔCt values was performed via unpaired two-sided t-test for R8, R54 and R54 ASIC1 knockout (KO) cells, as the ΔCt values are normalized logarithmic expression values and as such expected to be normally distributed (Friedman, Cai and Xie, 2006).

2.5. Agarose gel electrophoresis

Agarose gels were poured in 1% - 2.5% (w/v) concentrations in 1x Trisaminomethane (TRIS)-acetate-ethylenediaminetetraacetic acid (EDTA; TAE) buffer and RedSafe nucleic acid staining solution, with 1x TAE buffer also serving as running buffer. After running, the gels were imaged under ultraviolet (UV) light in the Vilber Quantum Agarose Gel Imager.

2.6. Cloning of ASICs into pcDNA3.1

Human *ASIC1a* and *ASIC2* were amplified from the pIRES vectors, containing enhanced green fluorescent protein (EGFP) and the respective ASIC, with primers containing XbaI- and EcoRI restriction sites for *ASIC1* and NotI- and EcoRI restriction sites for *ASIC2a* (Table 5). Phusion-PCR was done according to the protocol of the manufacturer (Thermo Fisher Scientific).

Table 5 – Primer sequences with restriction sites for *ASIC* cloning into pcDNA3.1 (-). Restriction sites are indicated by capital letters.

Amplicon	Forward Primer Sequence	Reverse Primer Sequence
ASIC1a	5'-aTCTAGAatggaactgaaggccgagg-3'	5'-gggtcGAATTCtcagcaggtaaagtc-3'
ASIC2a	5'-aGCGGCCGCatggacctcaaggaa-3'	5'-agaGAATCCtcagcaggcaatctcc-3'

Amplicons were then run on a 1% agarose gel and isolated via High Pure PCR Purification Kit (Roche). Digestion was done for 2 hours with the respective restriction enzymes and NEBuffer 2.1 at 37°C for the amplicons and the empty pcDNA3.1 (-) vector (Thermo Fisher Scientific). Heat inactivation followed for 20 min at 65°C, before ligation with T4 Ligase overnight at 4°C (Table 6). Insert:vector molar ratios were typically 3:1. On the following day, the ligation reaction was used for transformation of TOP10 *E. coli* cells, as described in Chapter 2.2. Plasmids were subsequently isolated and verified using pcDNA3.1 sequencing primers CMV-F (forward) and BGH-R (reverse).

Table 6 – Ligation Reaction Mix.

Ingredient	Volume or concentration
Insert	60 ng
Linearized vector	50 ng
T4 ligase	0.25 µL
T4 ligase buffer	2 µL
Sterile water	Ad 20 µL

2.7. CRISPR-Cas

ASIC1 was disrupted by the CRISPR-Cas9 method. For CRISPR-Cas, the pSpCas9(BB)-2A-GFP (PX458) vector (Addgene plasmid # 48138, Figure 5, Ran *et al.*, 2013) was purchased from Addgene and linearized with BbsI restriction endonuclease (NEB).

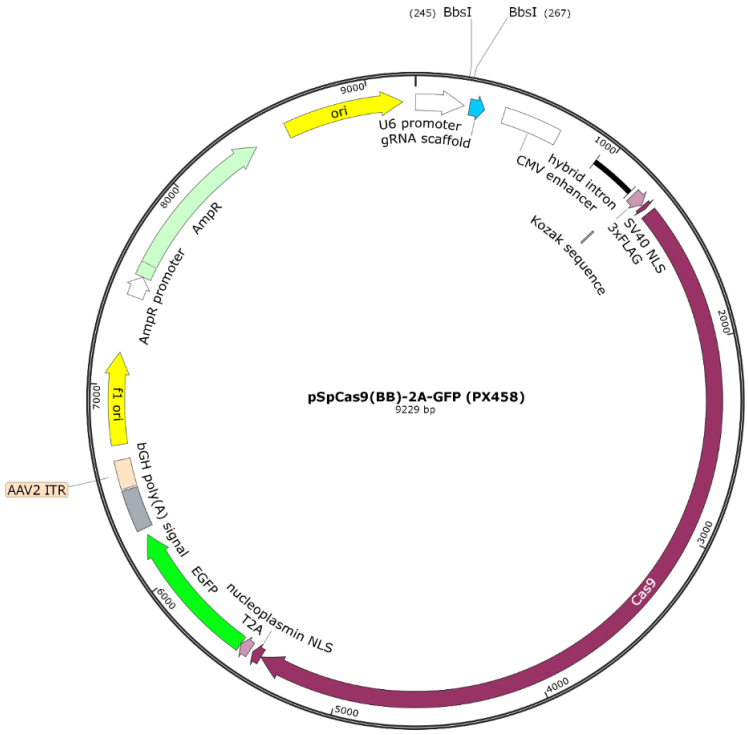

Figure 5 – Plasmid map of pSpCas9(BB)-2A-GFP (PX458). The PX458 vector contains Cas9, GFP and an ampicillin resistance cassette (Ran *et al.*, 2013). DNA guide sequence was inserted via BbsI digestion.

A double stranded DNA guide sequence was designed for the knockout and ordered as two separate, overlapping single stranded DNA strands, which were hybridized to each other, as described in Table 7. The overlaps of the leading strand were 5' – CAACG(guide sequence) – 3', whereas the lagging strand were 3' – C (guide sequence)CAAA – 5', to successfully align to the sticky ends of PX458, generated by the BbsI digestion.

Table 7 – Reaction mix for hybridization of single stranded DNA.

Ingredients	**Volume**
Each single stranded DNA Oligo (10 µM)	1 µL
T4 PNK Kinase	1 µL
T4 Ligase	1 µL
Water	6 µL

The hybridization reaction was then performed in a thermocycler, incubating at 37°C for 30 min, 95°C for 5 min and then decreasing the temperature from 95°C to 25°C at a rate of -5°C per min. The hybridized DNA guide sequence was then ligated into PX458 using T4 DNA ligase (Thermo Fisher Scientific), as described in Table 8.

Table 8 – Double stranded gDNA ligation into BbsI-linearized PX458.

Ingredients	**Volume**
50 ng BbsI-linearized PX458	As required
Dimerized oligo	2 µL
T4 ligase	1 µL
T4 ligase buffer	1 µL
Water	Ad 10 µL

After 15 min incubation at room temperature, the plasmid was transformed into TOP10 competent *E. Coli* cells, as described in Chapter 2.2. The resulting clones were picked and 4 mL LB medium was inoculated. After incubation in the shaker at 37°C, 180 rpm, for 8-12 hours a mini prep was performed, using the High Pure Plasmid Isolation Kit (Roche), according to the manufacturer's protocol. Resulting plasmids were sequenced using the U6 fw primer (5' - GAGGGCCTATTTCCCATGATTCC - 3') to confirm correct guide DNA sequence in the plasmid. Upon confirmation of sequence identity, a maxi prep was performed, using a Maxi Prep Kit (Qiagen), according to the manufacturer's instructions.

R54 cells were transfected with the resulting plasmid, using Lipofectamine 2000 Transfection Reagent (Thermo Fisher Scientific), according to the manufacturer's instructions.

After 48 hours, cells were sorted with a BD FACSAria III cell sorter (BD Biosciences), by means of GFP fluorescence, into flat-bottom 96-well plates (Falcon). Single clones were expanded for two weeks and when confluent, cells were split by pipetting and used for genomic DNA (gDNA) isolation. For gDNA isolation, cells were transferred to 1.5 mL plastic tubes and centrifuged for 1 min at maximal speed, before discarding the supernatant. The pellet was then resuspended in 500 µL proteinkinase K buffer (5 mL 1M TRIS, 5 mL 0.5M EDTA at pH 8.0, 10% (v/v) of 10% (w/v) sodium dodecyl sulfate (SDS), 100 mL 1M sodium chloride (NaCl), in 500 mL water for a final pH of 8.5), containing 0.20 mg/mL proteinkinase K. Tubes were then incubated for 3 hours at 55°C, 300 rpm in a heat block, before being centrifugated for 20 min at max speed. Supernatant was then transferred into a new 1.5 mL plastic tube, making sure that protein debris, recognisable as viscous liquid, was not transferred with the supernatant. 500 µL isopropanol was added to the supernatant and the mix was incubated for 20 min at room temperature, before being centrifuged for 10 min at max speed. The supernatant was discarded and the pellet resuspended in 500 µL 70% EtOH, before again being centrifuged for

10 min at max speed. The supernatant was discarded, the tubes were tapped with open cap against a tissue to get rid of the last liquid drops, and the tube again centrifuged for 30 sec at max speed. Tubes were then positioned with open cap in the vacuum centrifuge (Eppendorf Concentrator 5301), for drying at 45°C, for 10 min or until the supernatant evaporated. The pellet of gDNA was resuspended in 50-100 µL TRIS-EDTA (TE) buffer (pH 8.0) and stored at -20°C. The gDNA of potential candidates was screened by SYBR Green qPCR (Eurogentec) and subsequent melting curve analysis, described in Chapter 2.4 and Chapter 2.7, and the qPCR melt curve cycler protocol outlined in Table 9. Primers used for the melting curve analysis are shown in Table 10.

Table 9 – qPCR melt curve protocol.

Step	**Temperature**	**Hold Time**	**Repeat Cycles**
Hold	95°C	20 sec	1x
Denaturing	95°C	30 sec	40x
Annealing	60°C	5 sec	
Elongation	72°C	5 sec	
Hold 2	72°C	2 min	1x
Melt	Ramp from 65°C to 95°C	0.5 °C per step and 2 second hold afterwards	-

Table 10 – Primers used for CRISPR-Cas9 qPCR melt screening.

Target	**Primer**
ASIC1	(Fw) 5’ – GTGTGTGTGCACGGAGCGT – 3’
	(Rev) 5’ – GTTGAGGTTGCACAGCGTGAC – 3’

Clones with a shift of the melting curve peak of >1 °C were chosen for TOPO-cloning. For this, a PCR was conducted, with primers flanking the targeted exon and producing a 100-300 base pairs (bp) amplicon, using the taq polymerase (NEB), and following the manufacturer's instruction. The amplicon was then run on a 2-3% Agarose gel with RedSafe nucleic acid staining solution (iNtRON), according to the manufacturer's instructions. Bands were excised and purified, using the High Pure PCR Purification Kit (Roche), and ligated into the pCR2.1 Original Cloning Vector (Thermo Fisher Scientific). Fresh amplicons were used, as the TA base pair overlaps generated by the taq-polymerase degrade over time, even at -20°C storage.

After 15 min incubation of the ligation reaction at room temperature, the plasmid was transformed into TOP10 competent *E. Coli* cells and plated on agarose plates containing ampicillin (50 µg/mL), X-Gal (120 µL, 20 mg/mL) and IPTG (40 µL, 100mM). The agarose plates were incubated at 37°C overnight. On the next morning, white colonies marked the interrupted LacZ gene, which were then picked and used for LB medium inoculation. After 8-16 hours, plasmids were isolated using the High Pure Plasmid Isolation Kit (Roche), according to the manufacturer's instructions. Plasmids were then sent for sequencing, using the M13 Rev Primer (5' – CAGGAAACAGCTATGACC – 3'). Deletions, Insertions or Indels were interpreted as inducing a functional knockout, when a frameshift was observed. Sequencing was repeated for the respective knockout clone five times, or until the identity of both alleles was verified. Two knockout cell lines of R54 *ACCN2*$^{-/-}$ were generated, as identical off-target effects due to unwanted insertions, deletions or indels would be statistically unlikely to occur in both KO cell lines.

2.8. Lentiviral transduction for ASIC2a overexpression

A tamoxifen-inducible expression system was used to overexpress ASIC2a in R54 GSCs. Inducible expression systems have the advantage of not continuously overexpressing the gene of interest, thereby not exhausting the transcription system, with cells subsequently exhibit fewer side effects, such as cell death, delayed growth or development (Kallunki *et al.*, 2019). The tamoxifen-inducible expression system is a variant of the Gal4-UAS expression system (Brand and Perrimon, 1993), containing two components (Akerberg, Stewart and Stankunas, 2014), as illustrated in Figure 6. The first component is a lentiviral vector, which expresses a fusion protein, containing the Gal4 transcriptional activator fused to the hormone binding domain of the oestrogen receptor (ER), which is modified to reduce affinity for naturally occurring oestradiol, but retains affinity for oestradiol analogues tamoxifen and 4-hydroxytamoxifen (4-HT). This fusion protein is possible, thanks to the modular nature of Gal4. The fusion protein also contains the viral transcription factor VP16 (GEV16), fused to the DNA binding domain of the Gal4, which makes the transcriptional activation of Gal4 far more potent. Adding 4-HT activates the Gal4 transcription factor within 3 hours of treatment (Gerety *et al.*, 2013), subsequently expressing the gene of interest (GOI).

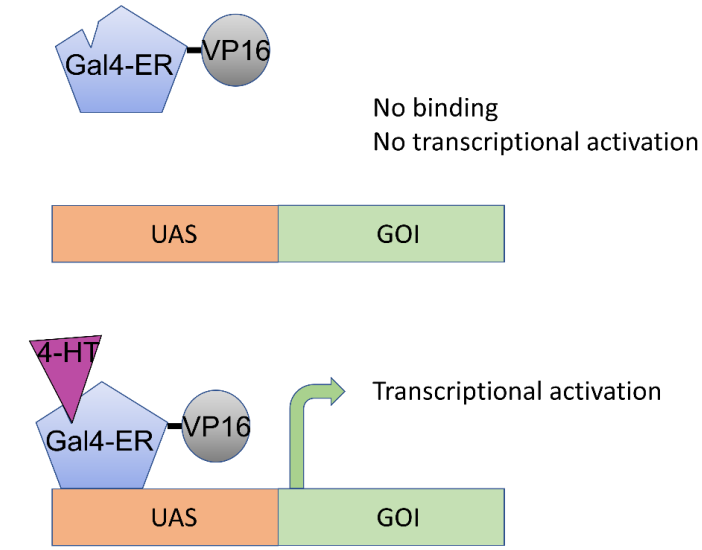

Figure 6 – The tamoxifen-inducible Gal4-UAS expression system. The transcriptional activator Gal4 is modified with both a modified oestrogen receptor (ER) binding site, thereby necessitating activation by oestradiol analogues such as tamoxifen or 4-HT, and a viral VP-16 protein (GEV16), which improves the transcriptional activation. Without adding 4-HT, no binding of the transcription factor and no transcriptional activation takes place (upper panel). Addition of 4-HT activates the Gal4 fusion protein and transcriptional activation occurs, expressing the GOI (lower panel). UAS: Upstream activation sequence. GOI: Gene of interest.

The second component is lentiviral vector pF 5 × UAS W SV40 Puro (L27; Figure 7) containing a puromycin resistance cassette for selection purposes, the UAS (upstream activation sequence) expression system and the desired gene to be overexpressed in a Gal4-UAS-dependent manner.

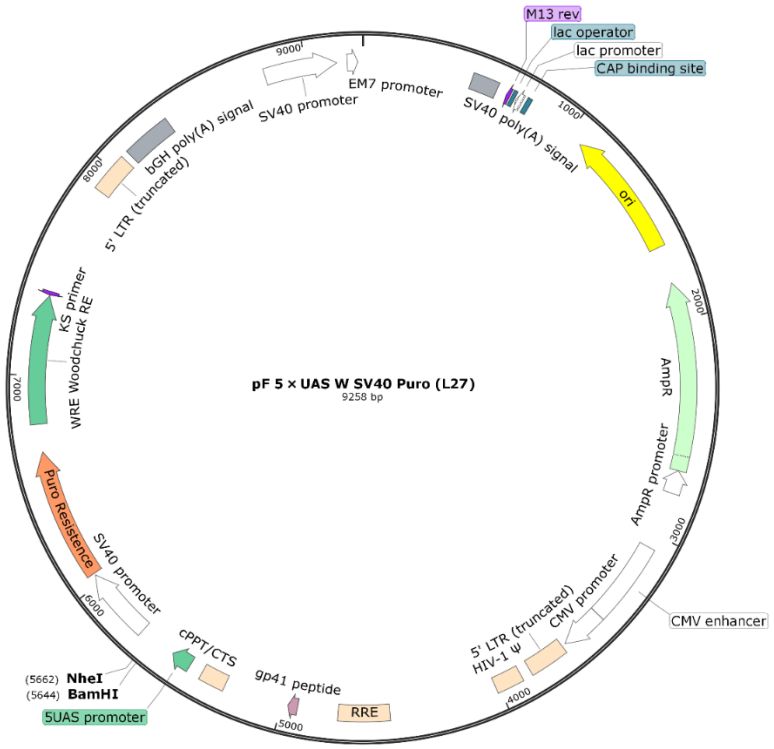

Figure 7 – pF 5 × UAS W SV40 Puro lentiviral vector (L27). L27 contains a puromycin resistance cassette for selection purposes, the UAS expression system and NheI / BamHI restriction sites used for insertion of ASIC2a. UAS: upstream expression system.

The lentiviral transfer vector, L27, was kindly provided to us by Dr. Maria Alekseevna Feokstisnova and Dr. Diana Panayotova-Dimitrova (Department of Dermatology at the University Hospital Aachen, Germany). Human ASIC2a was amplified from the previously prepared pcDNA3.1 (-) vector (Chapter 2.6), using a forward primer containing BamHI- and a reverse primer containing NheI restriction sites for ligation into L27 (Table 11). Phusion-PCR was done according to manufacturer's instructions (Thermo Fisher Scientific).

Table 11 – Primer sequences with restriction sites for cloning ASIC2a into L27. Restriction sites are indicated by capital letters.

Amplicon	**Forward Primer Sequence**	**Reverse Primer Sequence**
ASIC2a	5'-agaGGATCCatggacctcaagg-3'	5'-ataGCTAGCtcagcaggcaatct-3'

Amplicons were run on a 1% agarose gel and isolated via the High Pure PCR Purification Kit (Roche), according to the manufacturer's instructions. Amplicons and L27 vector were then digested using BamHI-High Fidelity and NheI restriction enzymes, in NEBuffer2.1 at 37°C for 2 hours. Both amplicons and L27 vector were then purified via High Pure PCR purification kit (Roche). The digested amplicons were then ligated with the linearized L27 lentiviral transfer vector with T4 Ligase (Thermo Fisher Scientific), according to the manufacturer, overnight at 4°C. On the following day, TOP10 *E. coli* cells were transformed (Chapter 2.2) with the resulting plasmids and plated on agarose plates containing ampicillin (50 µg/mL). The agarose plates were then incubated at 37°C overnight. On the next day, colonies were picked and LB cultures inoculated for 12-16 hours in the shaking incubator at 37°C and 180 rotations per minute (rpm). Afterwards plasmids were isolated via the High Pure Plasmid Isolation Kit (Roche), according to the manufacturer's protocol. Correct insertion of the genes of interest was then confirmed via sequencing, using the L27 forward primer (5'-GATCCAGTTATCCATCGCAGC-3') and the L27 reverse primer (5'-TTCCACAGGGTCGAATCG-3'), flanking the insertion site.

L27 vectors containing the genes of interest were then provided to Dr. Maria Feoktistova, together with $1 \cdot 10^6$ single-celled R54 cells. Lentiviral transduction of both lentiviral vectors was done by Dr. Maria Feoktistova. For this, she generated lentiviral supernatants in 293 T cells, by transfecting lentiviral packaging vectors together with the two lentiviral vectors

described above. After 48 hours the supernatants were harvested, filtered (45 mm filter; Schleicher & Schuell, Keene, USA), and added to the R54 cells via spin-infection (Cortés Franco *et al.*, 2022). The cells were then returned to us, separated into transduced and control cells, the latter not having been transfected with the lentiviral vector containing the puromycin resistance cassette. Selection was started by adding 1 µg/mL puromycin into the medium. Selection was then continued for a minimum of 5 days, and until all the cells in the control condition have died. Cell cultures were then expanded and frozen down.

2.9. Sphere migration assay

GSCs were grown for 7 days into spheres at pH 7.4 and used for the migration assay, or grown for 14 days, preincubated at pH 7.4 or pH 6.6. The day before the experiment, 24-well plates (Falcon) were coated with laminin from mouse Engelbreth-Holm-Swarm sarcoma with a volume of 180 µL and a concentration of 20 ng per µL, resulting in a final laminin density of 1-2 µg per cm^2. The plates were then incubated overnight in 4°C. The spheres were split into the respective experimental conditions, by gently spinning them down at 400 g for 1.5 min and resuspending them in different pH conditions. Some conditions additionally contained inhibitors or 4-HT. If the experiment required 4-HT induction, the spheres were preincubated for 3 days with 4-HT at a concentration of 100 nM. After the spheres had been prepared, a bystander blinded the experiment. The laminin was aspirated, the wells were washed once in phosphate buffered saline (PBS) and the spheres were gently added into the wells, at a concentration that was empirically determined with another 24-well plate. The 24-well plates were incubated at 37°C, 5% CO_2 for 5-6 hours. After sphere outgrowth, the plates were carefully placed under a microscope and pictures taken with the IC Measure program (Version 2.3.1). Diameters of spheres and numbers of migrating cells were then counted by hand, and positions of cells marked, using ImageJ (NIH, Version 1.52a). Tumourspheres with high background of freely migrating cells and adjacent tumourspheres were disregarded if cells could not be assigned to a sphere. Furthermore, only spheres with a diameter > 50 µm were quantified. After counting, the experiment was unblinded.

2.10. RNA sequencing

Spheres of the GSC line R54 were kept in four 60 mm petri dishes in pH 7.4 medium and in four 60 mm petri dishes at pH 6.6 medium for two weeks. The pH 6.6 medium was prepared from powdered DMEM/F-12 medium (Gibco), without HEPES. Medium was changed daily.

Cells were then centrifuged at 1200 rpm for 1.5 min, resuspended in 1 mL RNA-later solution (Thermo Fisher Scientific), and handed over to the Genomics Core Facility at the University Hospital Aachen, where the samples were frozen at -80°C until RNA extraction and RNA sequencing, using the 3' massive analysis of complementary DNA (cDNA) ends (3'MACE) protocol.

2.11. Sphere slice assay

Using Windows 3D Viewer (Microsoft), a mold was designed, similar as in the paper by Ivanov and Grabowska (2017) according to the limits and specifications set by the 3D printer in the RWTH University Hospital workshop. The mold (Figure 8a) was designed with the dimensions: 35.63 mm x 9.39 mm x 29.94 mm (width x depth x height). The stamp fitting into the mold (Figure 8b) had the dimensions 26.402 mm x 9.501 mm x 20.001 mm.

The mold was half-filled with 2 mL of 2% agarose gel and indented with the stamp. R54 GSC tumourspheres were fixed with 4% wt/vol Paraformaldehyde (PFA) for 16-24 hours at 2-8 °C, transferred into the agarose gel mold, sealed with low-gelling 2% agarose gel, cooled and sliced for subsequent antibody staining. The mold was then kept at -80°C and later fixed in paraffin by Sylvi Joussen, who then also performed the slicing from the block at a thickness of 200 µm, as well as the fixation, antibody staining (Horseradishperoxidase, 3,3'-Diaminobenzidine) and imaging.

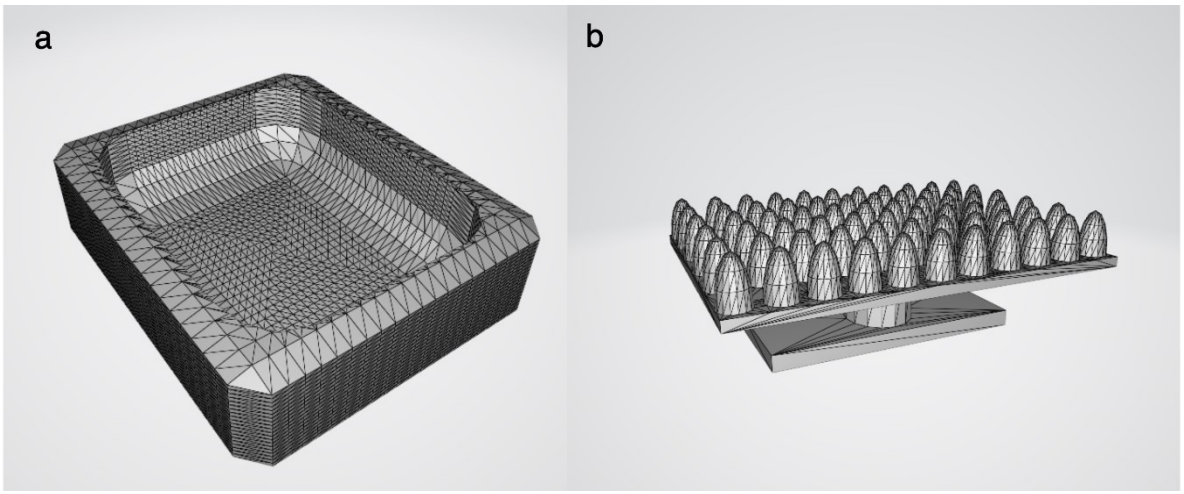

Figure 8 – a) 3D constructs of the mold and b) stamp for sphere fixation.

Immunostaining pictures were then analysed via Fiji (Schindelin *et al.*, 2012). The images were colour deconvoluted, tresholds were set for each individual image to minimize background,

and mean gray value was measured for the HRP channel. The 8-bit pixel intensities range from 0 to 255, with 0 representing the highest intensity and 255 the lowest. Based on these values, intensities of samples were quantified (negative = 181 to 255; , weak = 121 to 180; moderate = 61 to 120; strong = 0 to 60; (Cizkova *et al.*, 2021)).

2.12. Statistical analysis

2.12.1. Transcriptome analysis

Statistical analysis was performed with RStudio (Version 2022.02.1 Build 461), using the following packages: glmpca, DESeq2 (Love, Huber and Anders, 2014), BiocManager (Morgan and Ramos, 2021), tibble (Müller and Wickham, 2021), tidyverse (Wickham *et al.*, 2019), ggplot2 (Valero-Mora, 2010), dplyr (Wickham and Francois, 2018), readxl (Wickham and Brian, 2019), ComplexHeatmaps (Zuguang Gu, Roland Eils and Matthias Schlesner, 2016), pheatmaps (Kolde and Kolde, 2019), circlize (Gu *et al.*, 2014), RcolorBrewer (Neuwirth, 2014), enrichplot (Yu, 2021), fgsea (Korotkevich and Sukhov, 2016), tidyr (Wickham and Henry, 2019), openxlsx (Walker, 2018), goseq (Young *et al.*, 2010), pathview (Luo and Brouwer, 2013), ClusterProfiler (Yu *et al.*, 2012), gplots (R Warnes *et al.*, 2019), GO.db (Carlson, no date), ReactomePA (Yu and He, 2016) and Rcpp (Eddelbuettel and François, 2011).

3'MACE RNA reads were kindly provided by Dr. Ali T. Abdallah from the Genomics Core Facility at the Uniklinik Aachen, as part of the MACE sequencing service. This service included the automated annotation of reads.

The read counts were ordered into count matrices and differential expression of genes was tested in the RStudio package DESeq2, to estimate fold changes between conditions, according to the DESeq2 protocol (Love, Huber and Anders, 2014).

Expression heatmaps are shown in the supplement. Z-Scores are provided, reflecting the upregulated or downregulated expression in terms of standard deviation from the mean gene expression, with 0 indicating no up- or downregulation between pH conditions.

Normalized enrichment scores (NES) were generated for the DESeq2 resulting differentials using the RStudio package fgsea and statistically upregulated or downregulated genes (padj < 0.05) were ranked by gene set enrichment analysis (GSEA). Enrichment plots were generated

and rankings were cross-referenced with openly accessible molecular signature databases (MSigDB; www.gsea-msigdb.org/gsea/msigdb/, Database Version 7.4 and 7.5.1). Furthermore, log2 fold change enrichment of genes was plotted in Kyoto Encyclopaedia of Genes and Genomes (KEGG) pathway overviews, using the pv.out function of the RStudio package pathview.

For enrichment visualization, GSEA was re-run again on ranked reads via the GSEA-application (Version 4.2.3) (Mootha *et al.*, 2003; Subramanian, 2005), screening only gene sets with sizes 20-1000. Subsequently, Enrichment Maps for the respective signature databases were generated via the Cytoscape (Version 3.9.1) and the EnrichmentMap Cytoscape plugin (Reimand *et al.*, 2019), using a false discovery rate (FDR) of <0.25 and p-value <0.05, as recommended for phenotype analysis. Gene sets were grouped via Markov Cluster Algorithm (Van Dongen, 2008), based on shared description attributes.

2.12.2. Generalized linear mixed model (GLMM)

To determine which variables affect data differences, e.g. biological replicates, pH or experimental conditions, we used a generalized linear mixed model (GLMM) for the statistical analysis of migration assays. This also provides the advantage of more statistical power in large scale experiments with multiple comparisons. As such we generated multiple models, including and excluding variables to find the best model fit. This was done with RStudio (Version 2022.02.1 Build 461), using packages multcom (Hothorn, Bretz and Westfall, 2008), glmmADMB (Fournier *et al.*, 2012) and readxl (Wickham and Brian, 2019). Data from sphere migration assays were distributed in a negative binomial type 1 distribution (1), determined by the lowest Akaike information criterion score, except the sphere migration assay with MitTx, where the binomial distribution type 2 provided a slightly better fit (2), most likely due to the low number of technical replicates per biological replicate in this particular experiment. The difference of negative binomial distributions of type 1 and type 2 is in how the variance is calculated, as illustrated below. Var stands for variance, E is the expected value, Y a random variable and alpha the fixed variable.

$$\mathrm{Var}(\mathrm{Y}) = \mathrm{E}(\mathrm{Y}) * \mathrm{alpha} \qquad (1)$$

$$\mathrm{Var(Y)} = \mathrm{E(Y)} * (1 + \frac{\mathrm{E(Y)}}{\mathrm{alpha}}) \quad (2)$$

The best-fit model used for further statistical analysis was fitted with the glmmadmb function and is outlined in Equation (3), with m signifying the counts, b the biological replicate and t the treatment by pH and cell lines or chemicals.

$$m \sim (1 \mid b) + t \quad (3)$$

To test for differences of counts between treatment conditions, a multiple comparison was conducted, using the glht function of the multcomp package, using a one-step Tukey's all-pair comparison, resulting in Tukey's adjusted p-values, adjusted for multiple testing.

For the migration assay containing preconditioning pH and assay pH conditions, a nested model proved to be the best fit for pH comparison of control cells and wortmannin treated cells (4), respectively, where t1 is the preconditioning pH and t2 the assay pH.

$$m \sim (1 \mid b) + t1 + t1{:}\,t2 \quad (4)$$

3. Results

3.1. Preparing sphere slices in R54 GSC spheres

Since solid core cancer cells within spheres are inevitably exposed to different stimuli with regards to oxygen, nutrients, pH and secondary metabolites, it would be interesting to determine expression differences between cells from different localizations, i.e. periphery versus core (Wang *et al.*, 2017; Puchalski *et al.*, 2018). We aimed to test expression differences of acid sensing proteins (ASICs), and stemness marker protein SOX2, as they could be differentially expressed within tumourspheres. The difficulty was to have a method that would allow the quantification of protein expression, while maintaining the spatial relationship of cells within the sphere. Therefore, we adapted the method of Ivanov and Grabowska (2017). A 3D printed mold and stamp was used to create an agarose block with small wells, to keep spheres on the same height for high throughput slicing. Two-week old tumourspheres were fixed in PFA and individual spheres were pipetted into the agarose wells. The wells were then sealed with low-gelling agarose and given to Sylvi Joussen for paraffin fixation, slicing and antibody staining. Resulting slices from the block contained numerous slices of single spheres, which could then be tested under various conditions by antibody staining, to determine protein expression differences within spheres. Using this method, it was possible to generate GBM sphere slices, in a high-throughput manner, causing no tissue damage to the spheres. We then used these slices to perform preliminary stainings with anti-ASIC1 antibody (Avivasbio) and anti-SOX2 antibody (Abcam). Staining intensity was quantified via Fiji (Schindelin *et al.*, 2012), as described in the methods. Both antibodies showed strong staining, with no differences in intensity between cells of the core or the periphery (n = 6 spheres, n = 3 control spheres without secondary antibody).

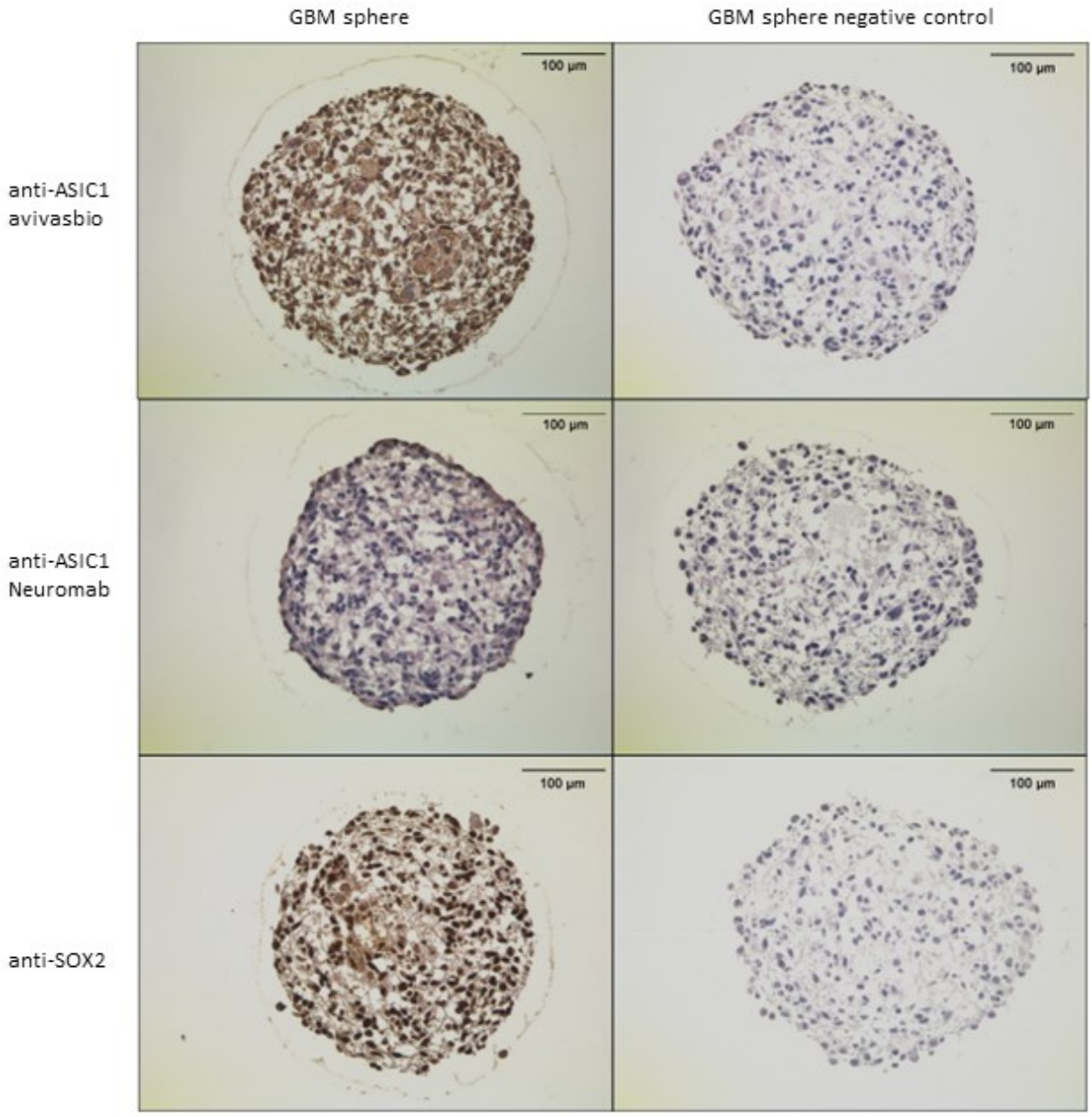

Figure 9 – Representative R54 GSCs sphere slices, stained with anti-ASIC1 antibodies from two different manufacturers and an anti-SOX2 antibody, as indicated. Fixation, slicing, antibody staining and pictures were done by Sylvi Joussen. Negative control was without addition of HRP-tagged secondary antibody. Scale bars = 100 µm.

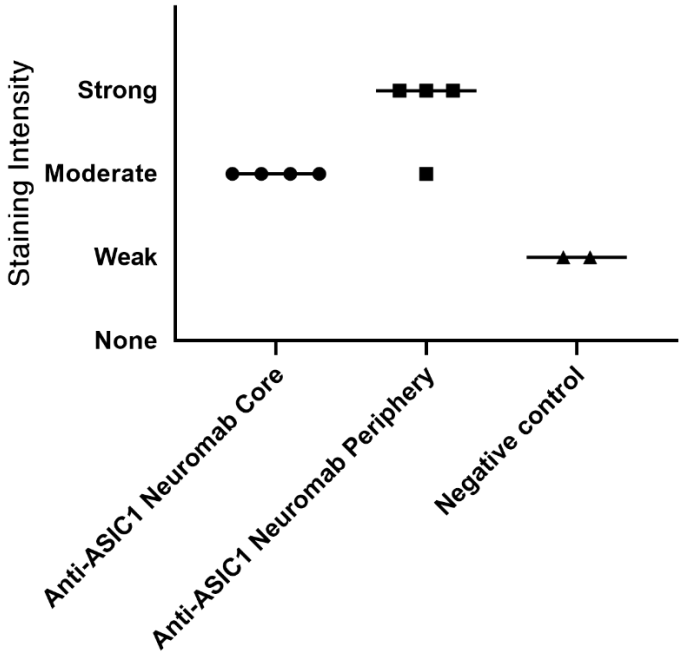

Figure 10 –Staining intensities of R54 GSCs sphere slices between core and periphery, stained with anti-ASIC1 Neuromab. Core is defined as 90% of sphere radius from the center, Periphery as the last 10% of sphere radius from the center. Negative control is defined as no addition of HRP-tagged secondary antibody. n = 4 for completely stained spheres, n = 2 for negative control.

The anti-ASIC1 antibody from Neuromab (Figure 9, left) showed only moderate staining. When focussing on the core of the sphere (90% of the sphere radius) the staining intensity was moderate, with a tendency of moderate to strong staining on the perimeter of the sphere (Figure 10).

The different results from the two ASIC1 antibodies could be due to antibody specificity, or due to a too high concentration of anti-ASIC1 (avivasbio), resulting in signal oversaturation. Thus, antibody concentrations need to be optimized in future experiments. Moreover, spheres with a knockout of ASIC1a should be used as controls. These cell lines were not yet available when the stainings were performed.

In summary, we successfully established a protocol for generating sphere slices, to be used for future antibody stainings. In future experiments antibody concentrations should be optimized individually, and knockout controls should be used. It could then be confirmed, whether ASIC1 is differentially expressed in tumourspheres, like the results of the preliminary ASIC1 staining with the antibody from neuromab suggests, and whether SOX2 is not differentially expressed in the tumoursphere. Other cancer-relevant proteins could also be evaluated.

3.2. Gene expression analysis of GSCs

3.2.1. Characterizing expression of stemness and differentiation markers and ASICs in R8 and R54 GSCs at pH 7.4 and pH 6.6

qPCR was conducted on a select group of targets, namely stemness markers nestin and *SOX2*, three differentiation markers *GFAP* (astrocyte marker), *TUBB3* (marker for neuronal differentiation) and *GALC* (oligodendrocyte marker), and *ASIC1-ASIC4* channels. This was done to determine whether changes in stemness or differentiation occur after incubation of R8 and R54 GSCs in acidic pH 6.6 for three days.

ASIC1-ASIC4 subunits were tested for potential expression changes, which could indicate a change in ASIC subunit ratios and a change in ASIC proton affinity.

For initial experiments, we used R8 and R54 GSCs. R54 GSCs were then analysed in more detail.

For both, R8 and R54, Ct-values for ASIC2a were consistently below the negative control threshold. Thus, ASIC2a was not expressed in these cells, confirming a previous report (Tian *et al.*, 2017).

For R8 GSCs, no statistically significant differences in RNA expression were observed between pH conditions (Figure 11). Thus, no change in ASIC expression, as well as no change in differentiation or stemness was observed for different pH values. For *ASIC3*, despite a 2-fold change in expression, the increase at pH 6.6 was not significant (p-value = 0.0564).

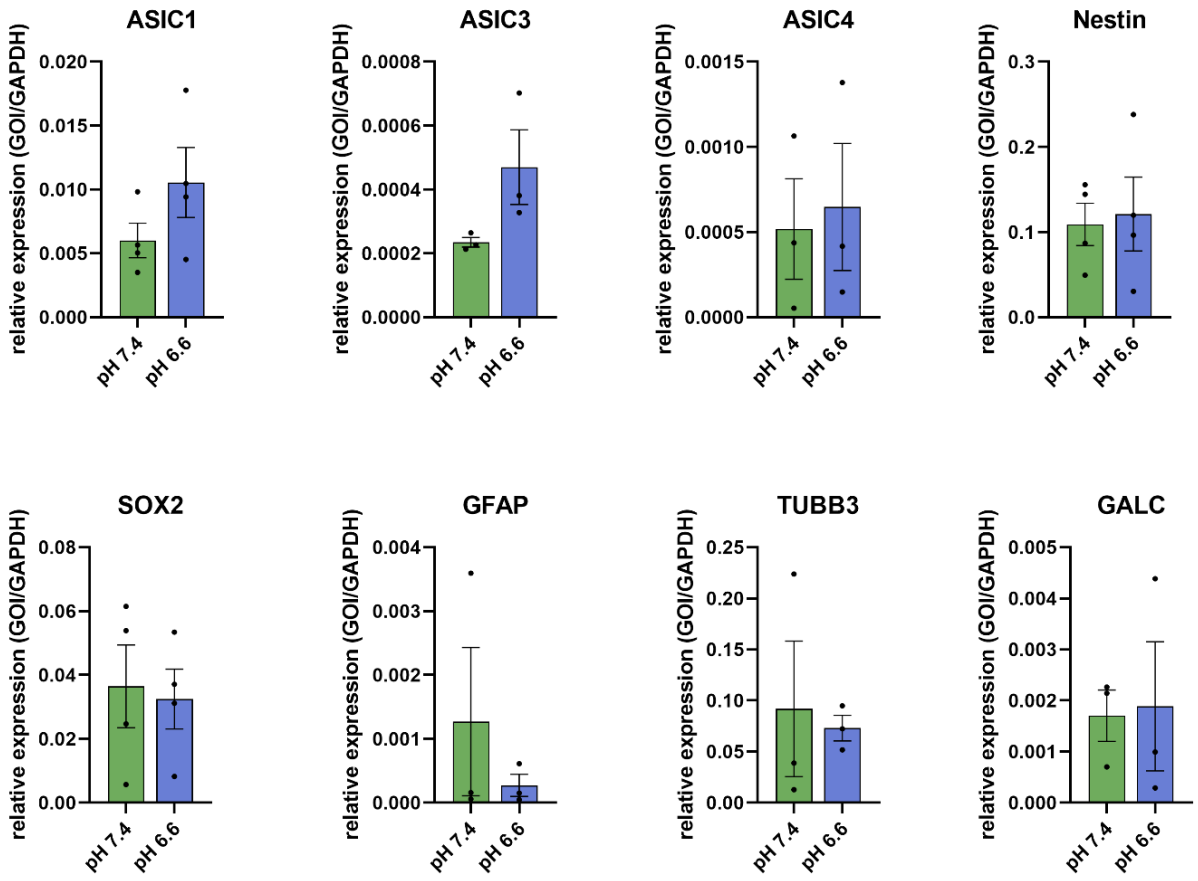

Figure 11 – qPCR of R8 cells incubated at pH 7.4 and pH 6.6 for three days. GAPDH-relative expression of *ASIC1*, *ASIC3*, *ASIC4*, stemness markers nestin and *SOX2*, and differentiation markers *GFAP*, *TUBB3* and *GALC*. n ≥ 3 biological replicates (dots(, each with three technical replicates. Bar graphs shows the mean ± SEM. Statistics were determined via two-sided t-test based on ΔCt-values, with no significances detected.

Similar to R8, in R54 GSCs all tested genes showed no significantly different expression at pH 7.4 and pH 6.6 (Figure 12). Therefore, neither stemness nor differentiation was strongly affected by environmental pH in both R8 and R54 GSCs. These results confirm the previously reported expression of ASIC1a and ASIC3 channels in R8 and R54 GSCs (Tian *et al.*, 2017).

After the generation of R54 ASIC1 KO GSCs, the results of the qPCR were supplemented with R54 ASIC1 KO GSCs, incubated at pH 7.4 for three days. The aim was to determine whether knocking out *ASIC1* would be compensated by higher expression of other subunits, and whether it would result in a difference in expression of stemness or differentiation markers. This, however, was not the case, except for *SOX2*, which was strongly upregulated in ASIC1a$^{-/-}$ spheres. This result could indicate increased stemness of ASIC1 KO cells. The reason for this change is currently unclear. ASIC1a expression was significantly reduced (Figure 12),

compared to R54 WT at pH 7.4, likely because the TaqMan™ probe did not find the ASIC1 mRNA transcript.

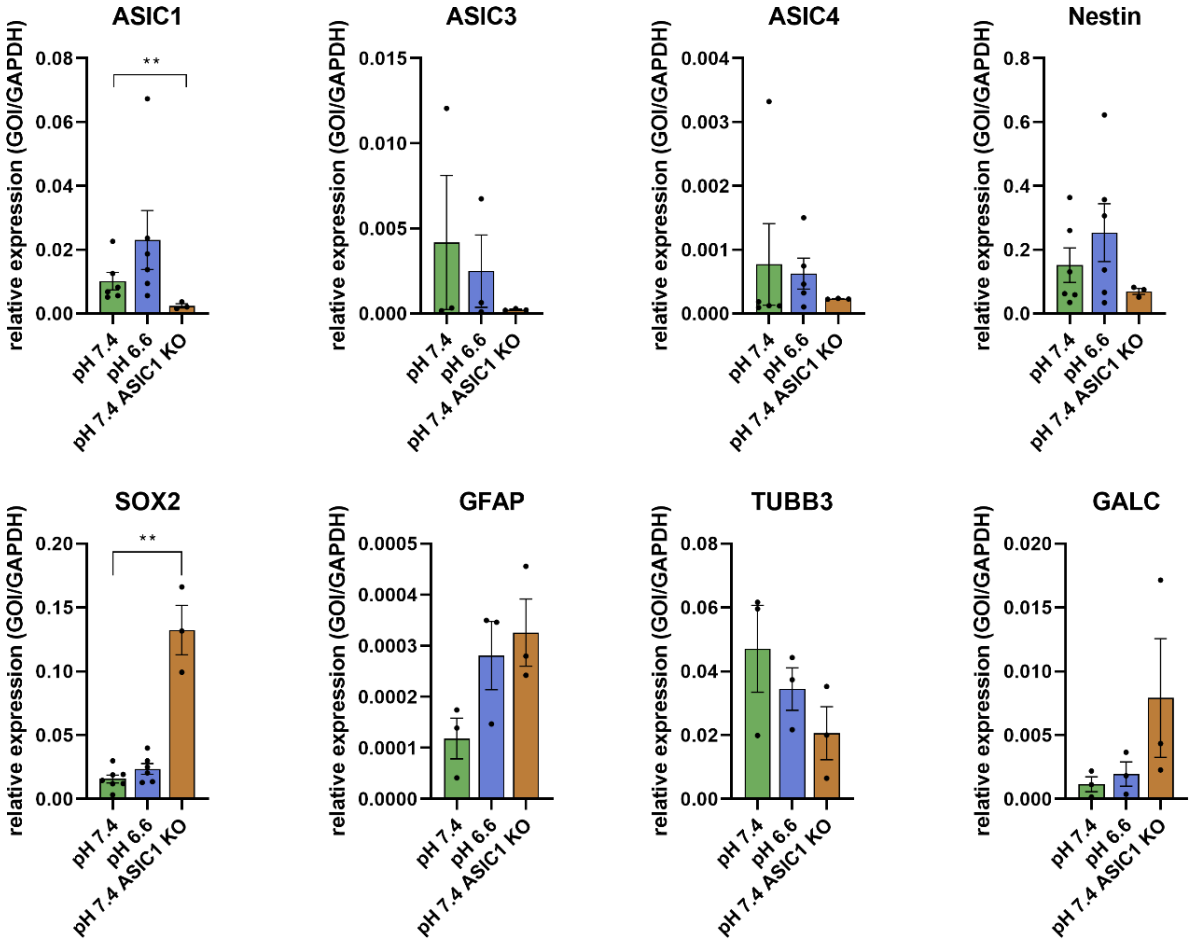

Figure 12 – qPCR of R54 cells and R54 ASIC1 KO cells (cell line 7C6) incubated at pH 7.4 or pH 6.6 for three days. Expression of *ASIC1*, *ASIC3*, *ASIC4*, stemness markers nestin and *SOX2*, and differentiation markers *GFAP*, *TUBB3* and *GALC*, relative to *GAPDH*. n ≥ 3 biological replicates (dots(, each with three technical replicates. Bar graphs shows the mean ± SEM. ** $p < 0.01$; two-sided t-test based on ΔCt-values.

3.2.2. RNA sequencing of R54 GSCs reveals KCNN4 and PI3K to be upregulated after two-week incubation at pH 6.6

Next, we conducted an RNA sequencing, with the aim to obtain a broad and unbiased picture of expression differences after two-week incubation of R54 GSCs at pH 7.4 or pH 6.6. Two-week incubation was chosen to see a strong effect on the transcriptome. Furthermore, one specific aim of RNA sequencing was to find potential targets modulating migration at pH 6.6, as ASIC1, ASIC2 and ASIC3 seemed to have no influence on GBM migration (see below, Chapter 3.3.2). Moreover, we wanted to discover potential vulnerabilities of GBM cells in acidic pH, which could be addressed in the future.

Before differential expression of genes was quantified, a generalized principal component analysis was conducted for exploratory analysis, using the RStudio package tidyverse, to determine whether the different pH treatment had a noticeable effect on the transcriptome (Figure 13).

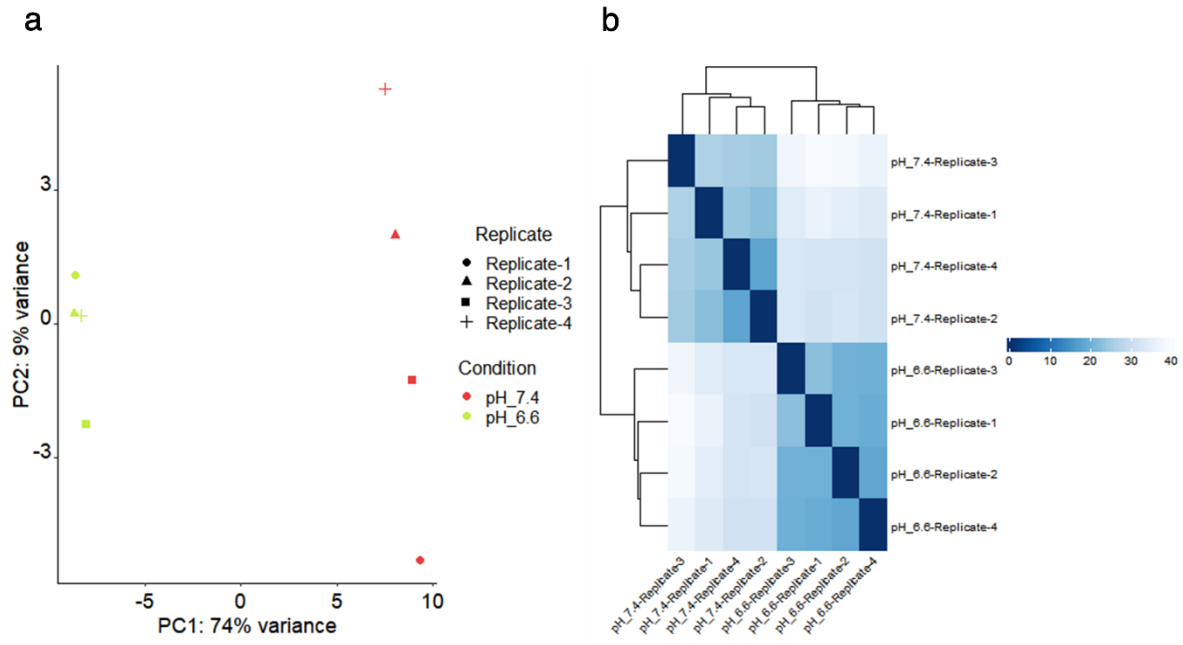

Figure 13 – Generalized principal component analysis of transcriptome data. a) shows the grouping of the four biological replicates of the treatment conditions (pH) along the axis of the two principal components. b) shows relative sample correlation, with dark blue showing highest correlation and white showing lowest correlation.

The high complexity of the dataset is thereby reduced to principal components (PC), which are created based on how much variation they cover. In this analysis, PC1 covers 74% of all variance, PC2 only 9% of variance. In theory, infinite PCs can be generated, which would then cover 100% of all variance, but which would defeat the purpose of reducing dimensionality and complexity of the dataset. As PC1 and PC2 covers > 80% of variance in this dataset, a principal component analysis is the appropriate method to visualize this dataset. The four biological replicates of the two pH conditions separated into two groups, mostly along PC1. The separation of PCs is shown in Figure 13a, with Figure 13b also showing the relative distance between samples. We can clearly see a separation of samples by pH condition, which suggests that expression differences are mainly due to the incubation at pH 7.4 or pH 6.6. We also observe some variance for different biological replicates of the pH 7.4 condition, but less variance for biological replicates of the pH 6.6 condition.

Biological variation of gene expression was further determined via a dispersion plot (Figure 14), with the utilized statistical model for gene expression analysis DESeq2 (Love, Huber and Anders, 2014) measuring the variance as:

$$\mathrm{Var} = \mu + \mathrm{alpha} * \mu^2 \quad (5)$$

with alpha being dispersion (a measure of spread or variability within the data) and μ being the expression mean. In general, if the dataset fits the DESeq2 model, data should scatter close to the expected dispersion value for gene expression strength, with dispersion being negatively correlated to mean expression strength, which was the case. Should the actual mean expression level and dispersion estimation datapoints take a different shape, than the expected dispersion behaviour, it would indicate that the data is not fitting the DESeq2 model. Since the fitted curve fit the model, we then continued to shrink the gene-wise dispersion estimates for samples with low dispersion values (black dots; below the fitted line) towards the curve. Shrinkage is the process of accounting for low reads/counts, when looking at large fold change values, and is generally recommended when ranking genes for subsequent transcriptome analysis. Samples above the curve (black dots, no blue outline) were also shrunken. Samples close to the curve or far above the curve were not shrunken (black dots with blue outline), as shrinking these values could result in false positives in the differential expression analysis, as there is a possibility that the gene has a higher variability than the model assumptions allow (Love, Huber and Anders, 2014).

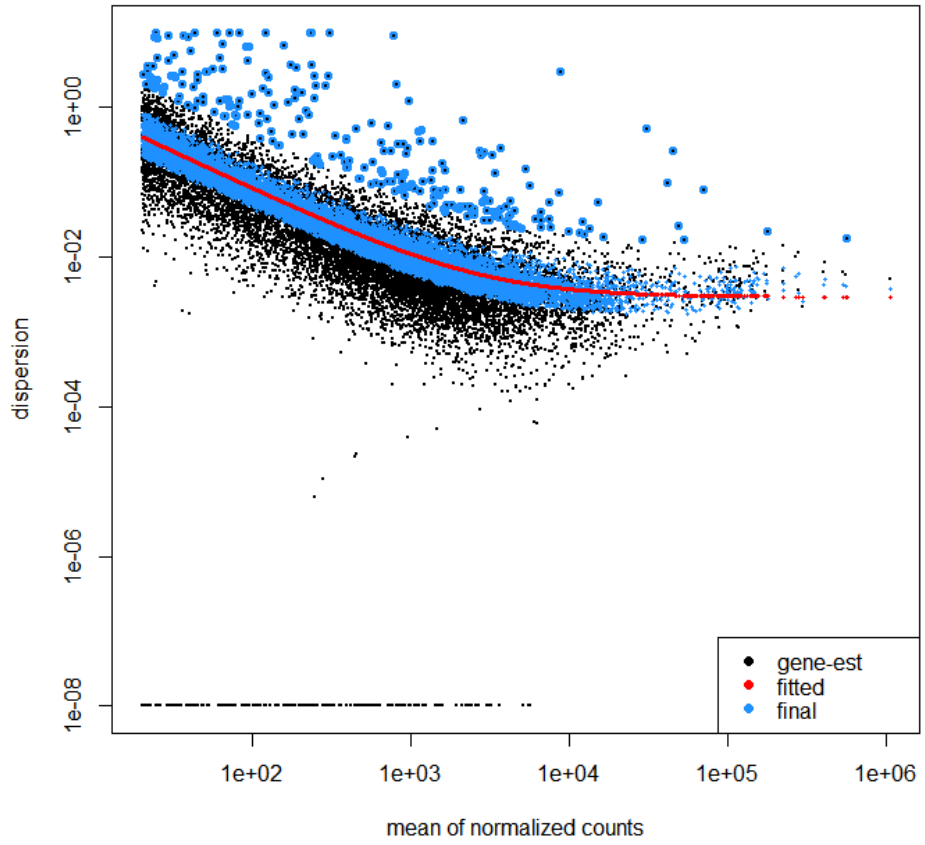

Figure 14 – Dispersion plot of DESeq2. Red line indicates the expected dispersion value for gene expression strength. Black dots indicate genes with actual mean expression level and dispersion maximum likelihood estimation, that were shrunken in their dispersion towards the fitted line of dispersion. Black dots with blue outlines are data points that are either close to the fitted line or outliers with low dispersion and are not subjected to shrinkage.

Differentially expressed genes between pH 7.4 and pH 6.6 with ≥ 20 mean base reads were plotted in a Volcano Plot, resulting in 15,479 data points (Figure 15). The gene *FAM156B* was excluded in volcano plot illustration, for the sake of better visibility of other data points, as the $\log_2$ fold change value was > 10. 3,129 genes were upregulated, 2,800 genes downregulated (padj < 0.05). Genes shown as red datapoints in the volcano plot had a $\log_2$ fold change >1 or < -1, which was considered statistically significant. Of those genes, 274 were upregulated ($\log_2$ fold change over 1), 820 genes downregulated ($\log_2$ fold change under -1).

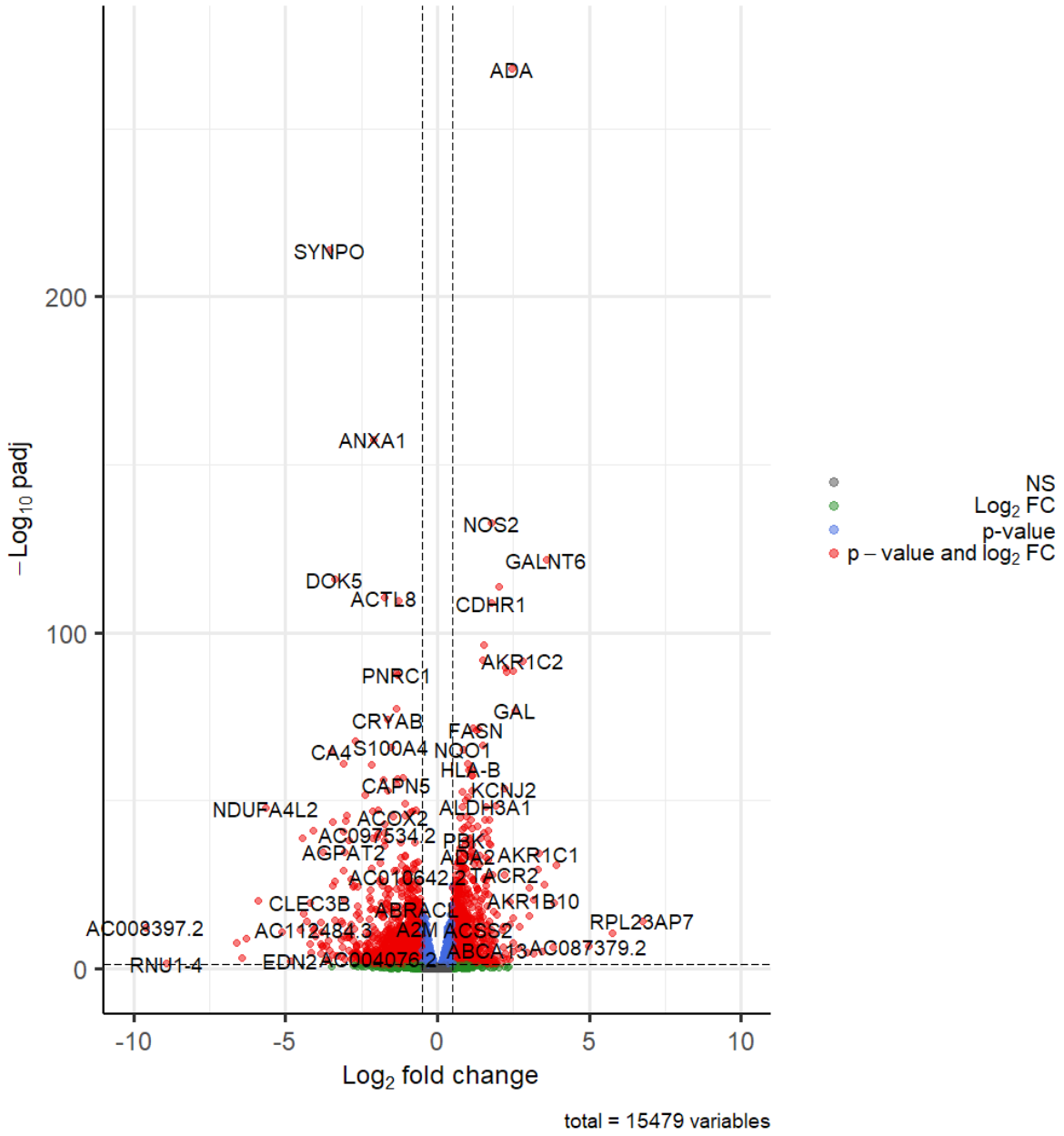

Figure 15 - Volcano plot of differentially expressed genes at pH 6.6 versus pH 7.4 conditions. Only genes with a base mean ≥20 base mean reads were included. Cut-off: padj < 0.05, NS: not significant, Log2 FC: log2 fold change, p-value: padj value.

To find targets that might influence R54 GSC migration, we chose targets that were both significantly upregulated and have been linked by previous publications to migration in cancer. We identified *KCNN4* (log2FC 2.48, padj < 0.0001), and PI3K Class 1 catalytic subunit *PIK3CB* (log2FC 0.31, padj < 0.01) as targets for future migration assays. *KCNN4* codes the calcium-dependent potassium channel KCa3.1, reported to play a role in migration and proliferation in GBM (Ruggieri *et al.*, 2012; d'Alessandro *et al.*, 2013), and Class I catalytic PI3K *PIK3CB* codes for a functional subunit of the PI3Ks, namely Phosphatidylinositol-4,5-bisphosphate 3-kinase catalytic subunit beta, known to be commonly upregulated or mutationally activated in cancer

and a modulator of cancer migration and metastasis in brain cancer (Samuels and Ericson, 2006; Arcaro, 2016; Yang *et al.*, 2019).

3.2.3. RNA gene-set enrichment analysis (GSEA) over multiple databases visualizes potential susceptibilities of GSCs at pH 6.6

Using R, enrichment scores at acidic pH were cross-referenced against relevant Molecular Signature Databases gene sets (Table 12), namely against hallmark gene sets (H), curated gene sets (C2) and C2 gene sets that are listed in the KEGG pathway database. The most concise gene set is arguably the gene set of hallmark biological processes, with a size of only 50 pathways. 31 of these pathways showed significant differences in expression and are shown in its entirety in Figure 16. For C2, the gene set was too large and only the most significant hits are shown in Table 13. C2 is a redundant dataset and could contain clues for candidate pathways. Furthermore, network analysis was conducted for C2 to create a better overview and understanding of relevant gene sets, thereby clustering redundant pathways for analysis (Figure 17). Differentially expressed genes in the KEGG pathway database were illustrated, using the pathview R package.

Table 12 – Molecular Signature Database Gene Set Collections, Version 7.4. Gene sets used for comparison are outlined in bold.

Gene Set	**Examples**	**Gene Set Size**	**Gene Set Hits (padj < 0.05)**
H: Hallmark Gene Sets	**Hallmark_Glycolysis**	**50**	**31**
C1: Positional Gene Sets	Chr16q13	299	-
C2: Curated Gene Sets	**Oxidative Phosphorylation**	**6289**	**1114**
C2 KEGG Subset	**KEGG_CELL_CYCLE**	**186**	**50**
C3: Regulatory Target Gene Sets	MIR12116	3726	-
C4: Computational Gene Sets	MODULE_330	858	-
C5: Ontology Gene Sets	Response to Oxidative Stress	14986	1805
C6: Oncogenic Signature Gene Sets	MTOR, Wnt, Myc	189	80
C7: Immunologic Signature Gene Sets	GSE5589_LPS_VS_LPS_AND_IL10_STIM_IL10_KO_MACROPHAGE_45MIN_DN	5219	-
C8: Cell Type Signature Gene Sets	MANNO_MIDBRAIN_NEUROTYPES_BASAL	700	-

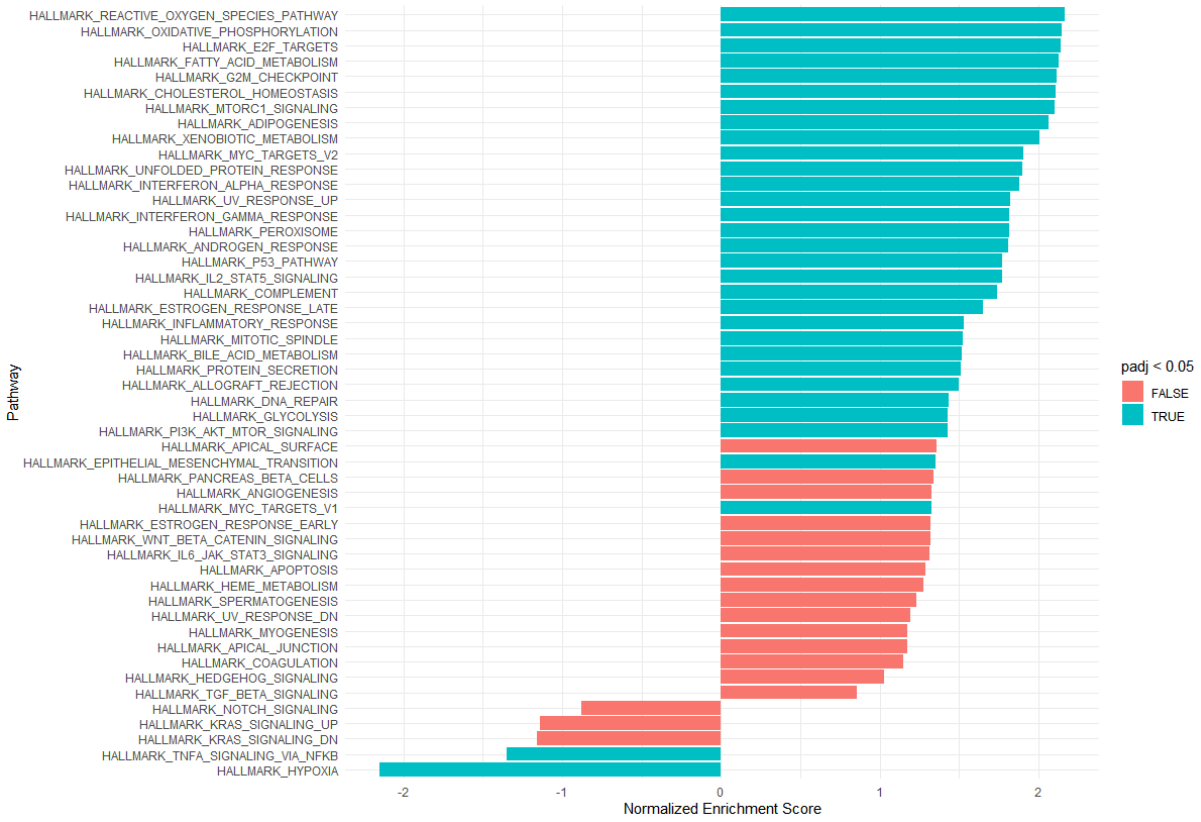

Figure 16 – MSigDB Hallmark pathways and statistically significant enrichment in acidic pH. Turquoise: padj value < 0.05, red: padj value ≥ 0.05.

Notably, 29 of 31 significantly differently expressed hallmark pathways were enriched in acidic pH, illustrating the tremendous effect acidic environment has on the transcriptome of R54 GSCs.

The two most enriched pathways of the 50 MSigDB Hallmark pathways in acidic pH were the ROS related pathway and the oxidative phosphorylation pathway. Heatmaps of these two pathways are shown in Supplementary Figure 1 and Supplementary Figure 2. Interesting are also the pathways related to cholesterol metabolism, involving mature SREB protein 2 (SREBP2) in the SREBP pathway. It has been previously reported that cholesterol synthesis is upregulated in cancer and is activated by *mTOR* and *PI3K* upregulation (Kuzu, Noory and Robertson, 2016). Our data, however, compares between cancer cells cultured in different pH conditions, and the fact that cholesterol synthesis increases as a consequence of mTOR and PI3K upregulation in acidic pH fits well with existing data, as low pH increases cholesterol metabolism by means of the PI3K/AKT/mTORC1/SREBP pathway, and mature sterol-regulatory element binding protein 2 (mSREBP2) in pancreatic cancer (Kuzu, Noory and Robertson, 2016; Huang, Song and Xu, 2020). It is notable, that in the pH 6.6 acidic condition

many genes are upregulated compared to the physiological control, whereas only few are downregulated. Downregulated pathways in the hallmark database are only hypoxia and eukaryotic translation. Downregulated in this group are ribosomal proteins, essential for transcription, and pathways correlated with nonsense mediated decay, essential for reducing errors in gene expression by elimination of erroneous mRNA transcripts.

Table 13 – Excerpt of significantly enriched C2 Curated Gene Sets. padj: p-adjusted value, NES, normalized enrichment score, GSS: gene set size.

Position	Pathway	padj	NES	GSS
1	WEST_ADRENOCORTICAL_TUMOR_UP	7.23E-09	2.51	284
2	FOURNIER_ACINAR_DEVELOPMENT_LATE_2	7.23E-09	2.45	276
3	ACOSTA_PROLIFERATION_INDEPENDENT_MYC_TARGETS_UP	7.23E-09	2.42	81
4	MANALO_HYPOXIA_DN	7.23E-09	2.40	283
5	WP_CHOLESTEROL_BIOSYNTHESIS_PATHWAY	7.23E-09	2.38	15
6	KEGG_GLUTATHIONE_METABOLISM	1.20E-06	2.37	40
7	ELVIDGE_HIF1A_TARGETS_UP	9.95E-08	2.34	64
8	WP_CHOLESTEROL_METABOLISM_INCLUDES_BOTH_BLOCH_AND_KANDUTSCHRUSSELL_PATHWAYS	2.94E-07	2.34	43
9	KEGG_CITRATE_CYCLE_TCA_CYCLE	1.75E-06	2.34	29
10	ELVIDGE_HYPOXIA_DN	7.23E-09	2.33	143

The C2 gene set database mirrors the result of the hallmark pathways, with the tricarboxylic acid (TCA) cycle, which is essential for oxidative phosphorylation, being upregulated. For better visualization of C2, gene-sets were organized in a network, where each gene set is a node and edges represent gene overlap between gene sets. This enrichment map illustrates major enriched pathways (Figure 17).

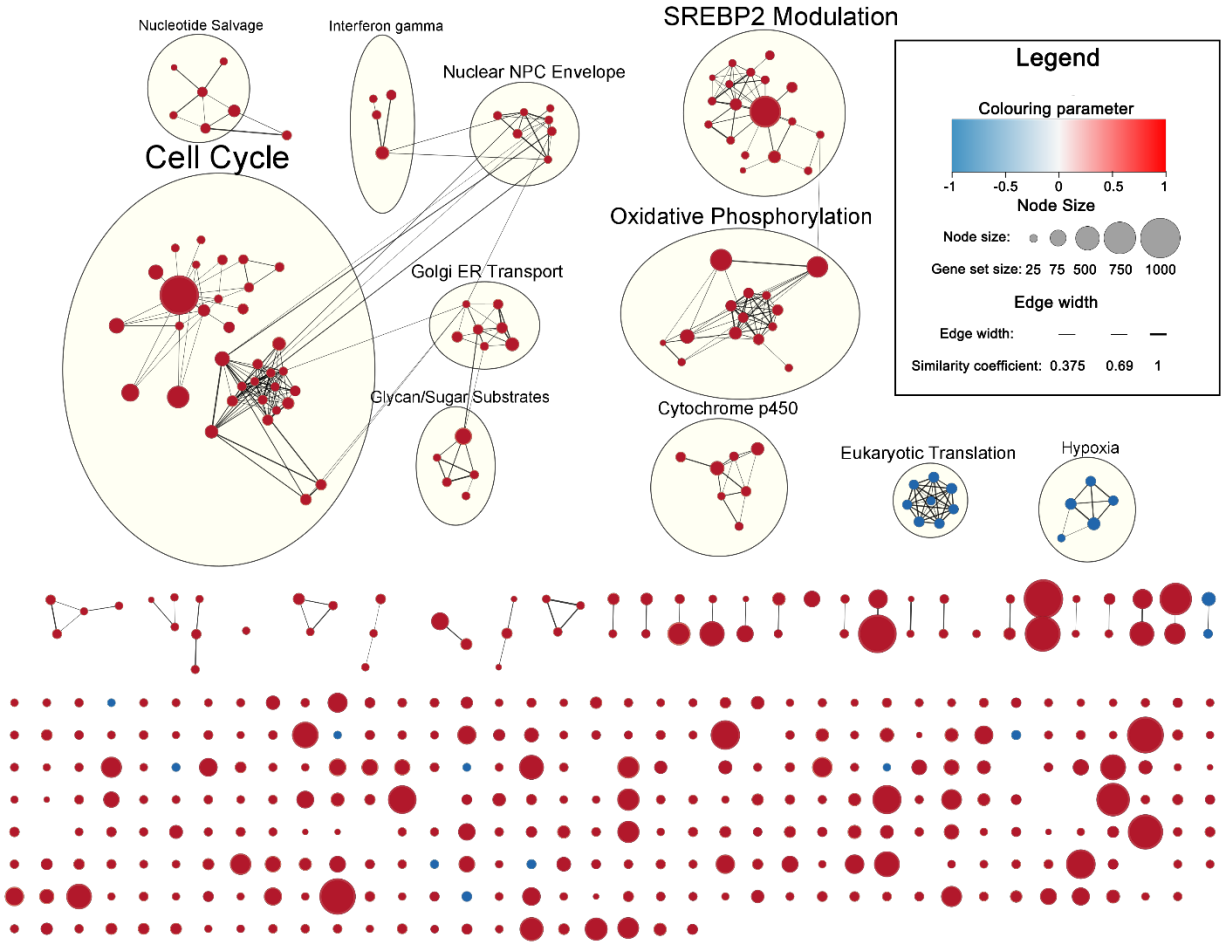

Figure 17 – Pathway enrichment visualised for C2: Curated Gene Sets. Network clusters of upregulated pathways in pH 6.6, such as (TCA) cell cycle, oxidative phosphorylation and SREBP2 modulation are visualized. Large bubbles with description indicate detected network clusters of shared pathway description attributes. Gene sets without cluster are shown at the bottom. Colour parameter is defined as 1 – adjusted p-value multiplied by the sign of the enrichment score. Thus, red indicates significant upregulation at pH 6.6, blue indicates significant downregulation at pH 6.6. Node size correlated to gene set size (minimum 20 and maximum 1039 genes in one gene set). Edge width indicates similarity coefficients (also Jaccard coefficient). Edges are shown for gene sets with similarity coefficient > 0.375. False discovery rate < 0.25, adjusted p-value < 0.05.

The KEGG Subset of C2 was analysed separately. Significant positively enriched pathways are shown in Figure 18. Only one pathway was significantly downregulated, which is shown in Figure 19, the ribosome pathway. The KEGG pathways mostly mirror previous observations done via the enrichment map. As such, most pathways are significantly upregulated at pH 6.6 and the most enriched pathways mirror the pathways previously explored via the enrichment map for C2 (Figure 17), such as the (TCA) cell cycle, oxidative phosphorylation and pathways that affect SREBP2 (such as SREBP2 signalling, cholesterol biosynthesis, fatty acid metabolism, steroid metabolism, among others).

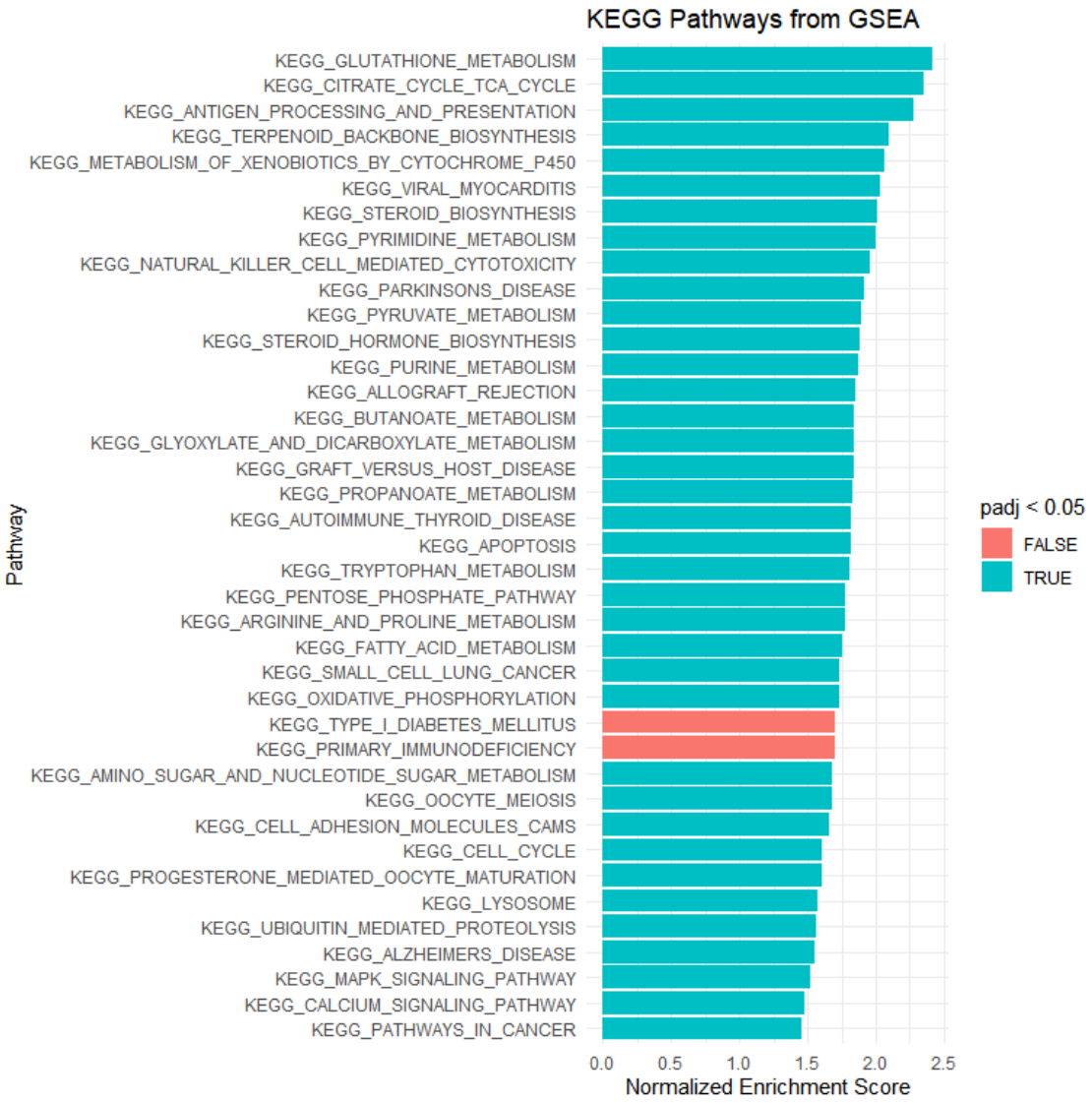

Figure 18 – C2:GO:KEGG gene set enriched pathways in the pH 6.6 condition, visualised and ranked by normalized enrichment score. Only pathways with padj < 0.1 are depicted.

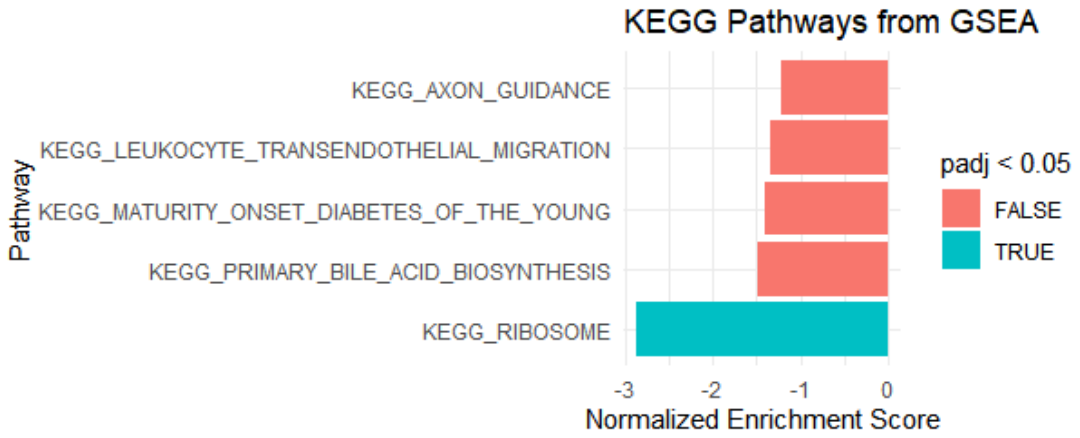

Figure 19 – C2:KEGG gene set depleted pathways in the pH 6.6 condition, visualised and ranked by normalized enrichment score. Only pathways with padj < 0.3 are depicted.

In the C2:KEGG subset, the glutathione metabolism pathway was strongly enriched. Glutathione (GSH) is an essential antioxidant, necessary for tumour cells in acidic conditions, to balance the higher amount of ROS (Bansal and Simon, 2018). On the level of individual proteins, we see an increase in glutathione peroxidase (Figure 20, 1.11.1.9), protein-disulfide reductase (1.8.4.2) and phospholipid-hydroperoxide glutathione peroxidase (1.11.1.12), necessary for oxidizing GSH to glutathione disulfide (GSSG), to protect the cancer cell from ROS damage. We also observe an increase of glutathione reductase (1.8.1.7), to reduce GSSG back to GSH, with the use of NADPH (Figure 20). It is also notable that glutathione hydrolase (2.3.2.2) and gamma-glutamyltranspeptidase (3.4.19.13) are strongly downregulated, to prevent glutathione to be used for amino acid or peptide synthesis, respectively. We also observe a strong upregulation of glutathione S-transferase (2.5.1.18), which makes up a significant part of cytosolic proteins and has been associated with detoxification and anti-cancer drug resistance (Townsend and Tew, 2003). Glutathione expression increases as a direct effect to acidosis (LaMonte *et al.*, 2013), but our RNA sequencing data provides a more detailed picture of the RNA-level activity of all proteins involved during acidosis.

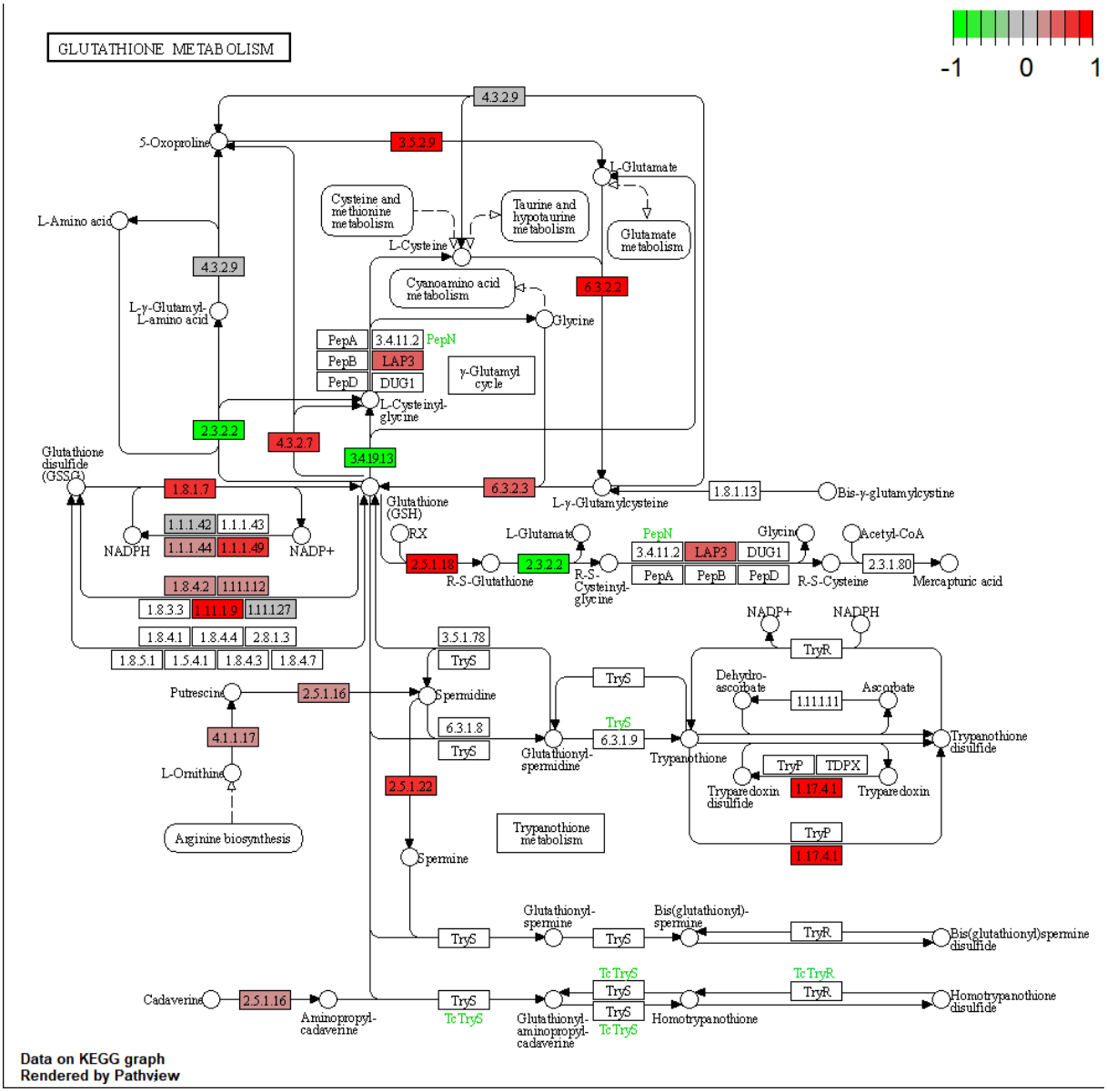

Figure 20 – KEGG: Glutathione Metabolism. Top and right centre: Amino acid metabolism, Left: ROS activity, Bottom: Arginine biosynthesis and trypanothione metabolism. Upregulation at pH 6.6 indicated in red, downregulation in green. Colour code indicates log2 fold change in expression. Values outside of -1 to 1 are truncated to the limits set by -1 or 1.

To conclude, cross-referencing the RNA-sequencing data to the three gene set databases hallmark, C2 and C2:KEGG, we observed consistent upregulation of genes involved in the TCA cycle, ROS modulation and the cholesterol metabolism at pH 6.6.

3.3. Using a migration assay to investigate the role of ASICs, KCNN4 and PI3K as modulators of migration in R54 GSC tumourspheres

3.3.1. Sphere migration assay reveals consistently higher migration at pH 6.6, and no effect of hypoxic incubation compared to normoxic incubation, in 7-day old R54 GSC tumourspheres

R54 GSC tumourspheres were incubated for 7 days at either pH 7.4 or pH 6.6. The 6-hour incubation in coated wells was then conducted in normoxic and hypoxic (~ 3% O_2) incubators, to determine whether hypoxic incubation impacts GSC migration. Few cells migrated from spheres at physiological pH, whereas at acidic pH 6.6 their number increased significantly. Our findings did not show a significant difference of migration during 6 hours in normoxic versus hypoxic culturing. Representative pictures shown in Figure 21, summary data shown in Figure 22.

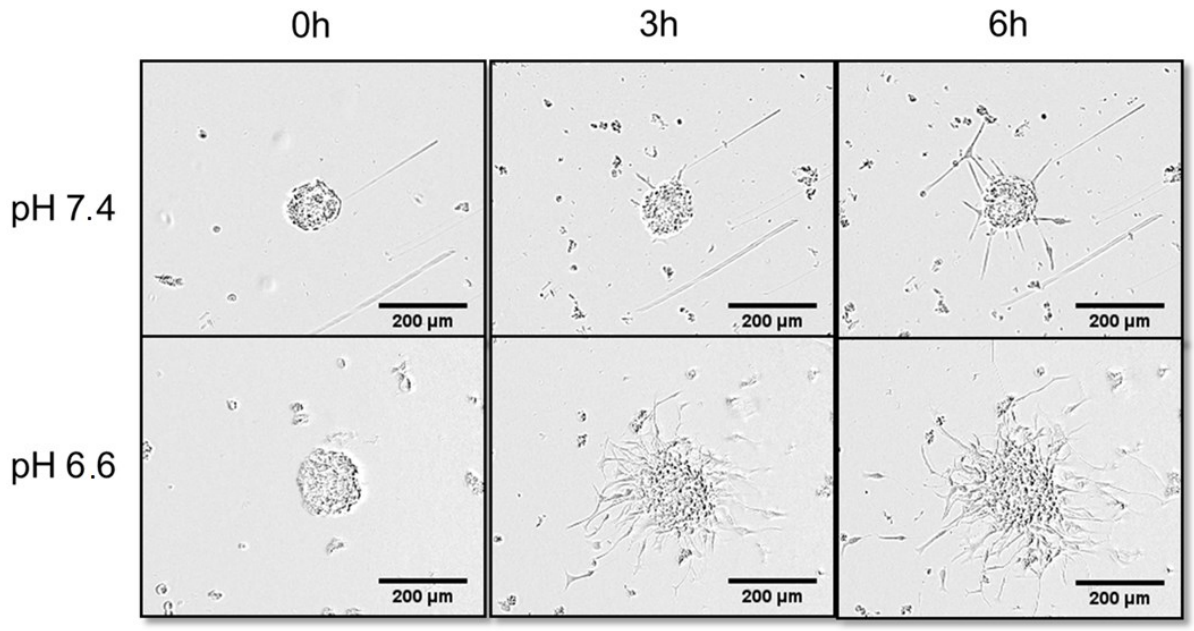

Figure 21 – Representative pictures of R54 GSC migration from spheres at pH 7.4 or pH 6.6 for 6 hours under hypoxic (~3% O_2) conditions. Scale bars = 200 µm.

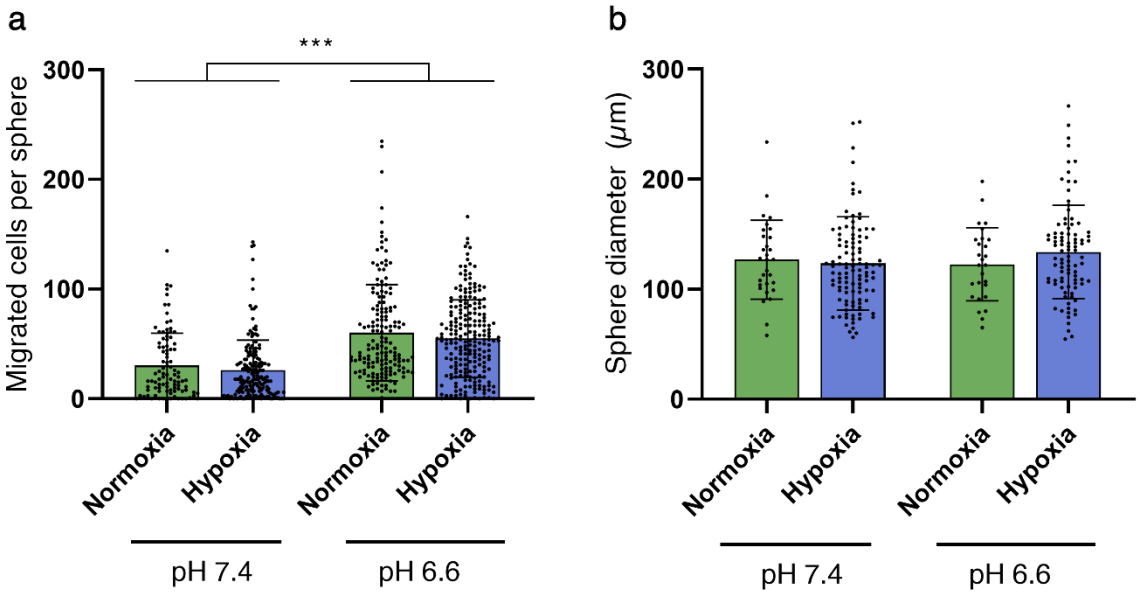

Figure 22 – Migration of R54 cells in normoxic and hypoxic (~3% O_2) conditions at pH 7.4 and pH 6.6. In a) the migrated cells per sphere are indicated. In b) the respective sphere diameters of the spheres at time point 0 are indicated. *** $p < 0.001$. Error bars indicate standard deviation (SD). Data points represent individual cells from n = 6 independent experiments for normoxia, and n = 9 independent experiments for hypoxia.

Comparing the workflow of the migration assay in normoxic with hypoxic conditions, after small-scale experiments with low n-numbers of quantified spheres we decided to conduct larger scale experiments under normoxic conditions, as normoxic conditions allowed for a higher throughput and higher n-numbers of quantified spheres for each condition. This was done for the 2-week migration assay with four pH conditions and the migration assay with ASIC2 overexpressing cells. The advantage was less statistical variability within groups due to low numbers of spheres quantified for each condition. Another advantage was better visibility of cells for quantification. The disadvantage, however, was that we were unable to image the spheres throughout the migration assay. For experiments conducted under normoxic conditions, spheres were imaged and sphere sizes measured before attachment to the plate, making it impossible to later link sphere size to particular spheres. This also prevented normalization of the number of migrated cells to sphere size. Since overall sphere sizes were not significantly different between conditions, we conducted the experiments under the assumption that differences in the size of individual spheres would be similar for all conditions.

3.3.2. ASIC1-ASIC3 do not modulate migration in 7-day old R54 GSC tumourspheres

It has previously been reported that ASIC1 modifies GBM migration (Kapoor *et al.*, 2009; Rooj *et al.*, 2012) and ASIC3 may also impact migration (Grifoni *et al.*, 2008). To investigate whether ASIC1 or ASIC3 were involved in the increase of migration at pH 6.6, a migration assay was performed with one-week-old R54 GSCs in the absence or presence of 100 nM of the ASIC1 inhibitor PcTx1 or 500 nM of the ASIC3 inhibitor APETx2 in hypoxic conditions (~3% O_2). Pictures were taken immediately (0 hours) and after 6 hours.

Surprisingly, ASIC1 and ASIC3 inhibitors did not reduce the increased migration at acidic pH. Sphere diameters measured at the beginning of the experiment were not significantly different between conditions (Figure 23b). Representative pictures of R54 GSCs in all conditions are shown in Figure 24.

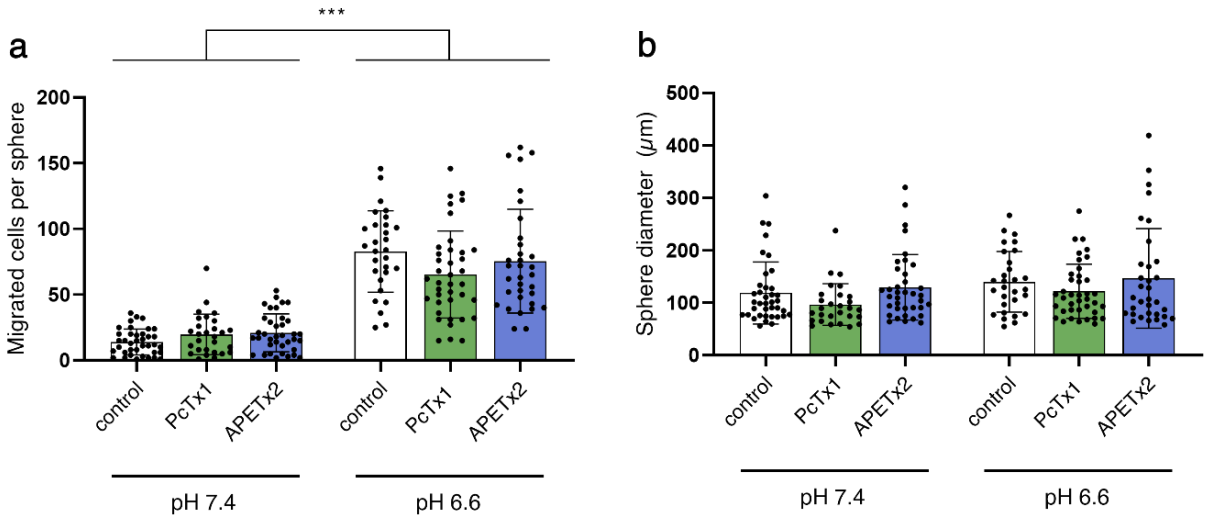

Figure 23 – Migration of R54 cells in pH 7.4 and 6.6 medium, with or without 100 nM Pctx1 or 500 nM APETx2, in hypoxic (~3% O_2) conditions. In a) the migrated cells per sphere are indicated. In b) the respective sphere diameters of the spheres at time point 0 are indicated. P-values indicated by *** $p < 0.001$. Error bars indicate standard deviation (SD).

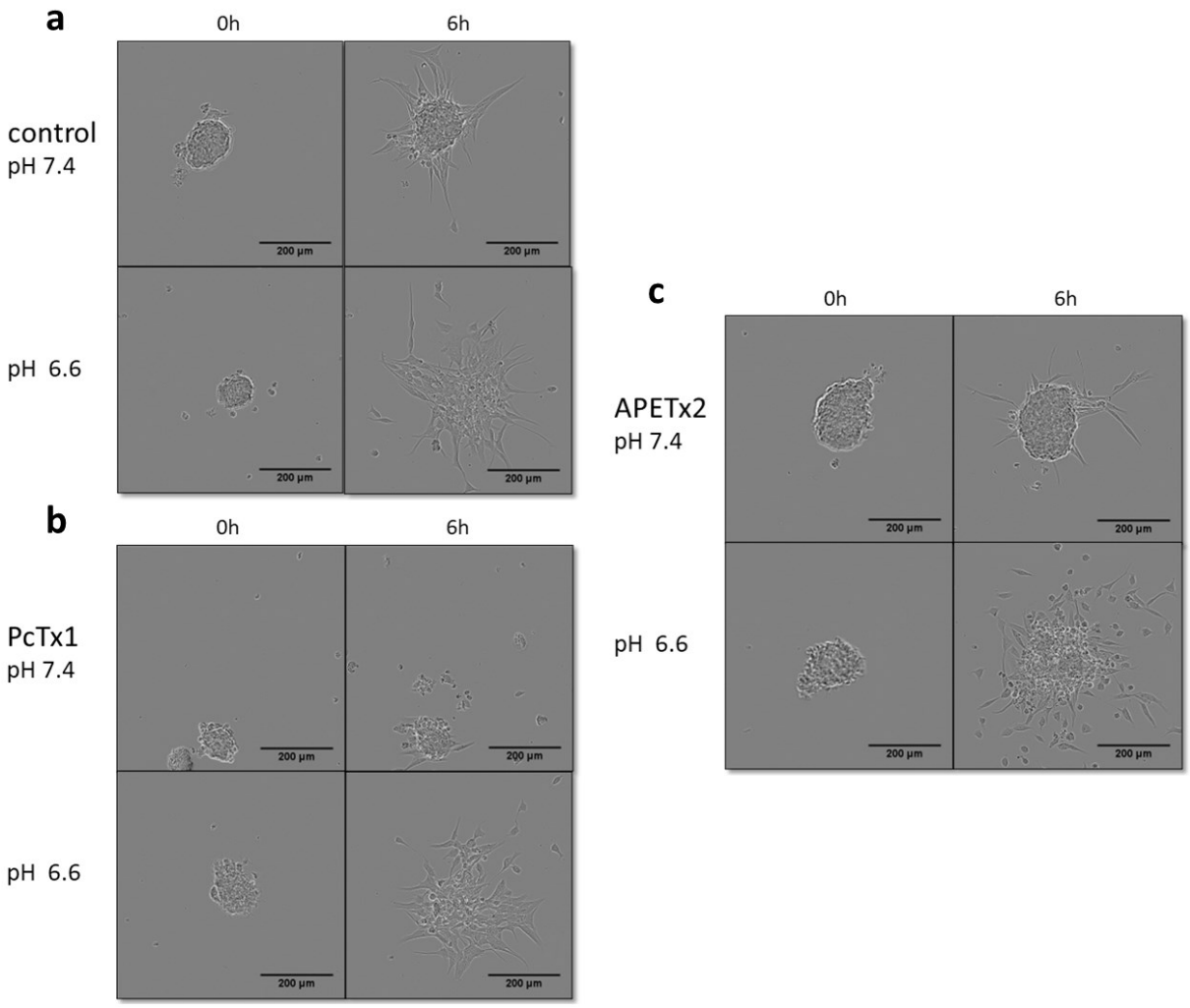

Figure 24 – Representative pictures of R54 GSCs at pH 7.4 and pH 6.6 for time points 0h and 6h in the migration assay under hypoxic conditions (~3% O_2). In a) representative pictures of control cells, b) shows cells in the presence of 100 nM of the ASIC1 inhibitor PcTx1, c) shows cells in the presence of 500 nM of the ASIC3 inhibitor APETx2. Scale bar indicates 200 µm.

The same experiment was then repeated with the ASIC1 activator MitTx (20 nM), to confirm that ASIC1 activation would not induce migration at pH 7.4 in R54 GSCs. Statistical differences were only observed between different pH groups, with absence or presence of MitTx not showing an effect (Figure 25a). Sphere diameters were not significantly different from each other (Figure 25b). Representative pictures are shown in Figure 26.

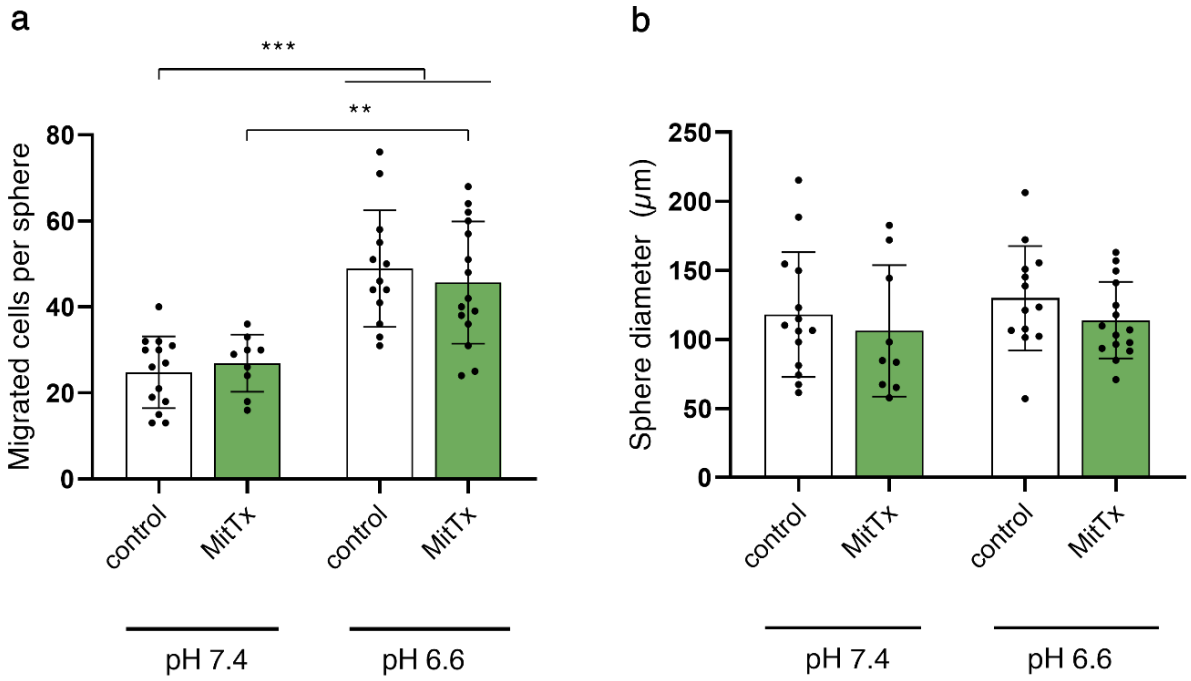

Figure 25 – Migration of R54 cells in pH 7.4 and 6.6 medium, with or without MitTx, in hypoxic (~3% O_2) conditions. In a) the migrated cells per sphere are indicated. In b) the respective sphere diameters of the spheres at time point 0 are indicated. ** $p < 0.01$, *** $p < 0.001$. Error bars indicate standard deviation (SD).

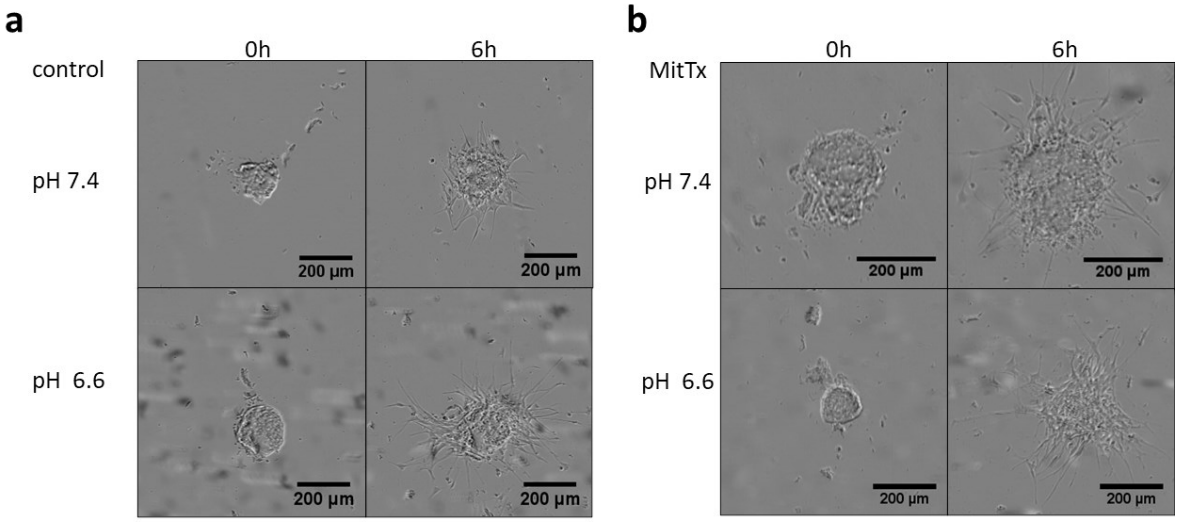

Figure 26 – Representative pictures of R54 GSCs of the ASIC1a activator MitTx experiment at pH 7.4 and pH 6.6 for time points 0h and 6h under hypoxic conditions (~3% O_2).). In a) representative pictures of control cells, b) shows cells in the presence of 20 nM of the ASIC1a activator MitTx. Scale bar indicates 200 µm.

To confirm that ASIC1a is not affecting migration, we generated a R54 ASIC1 KO cell line. For this, a single-stranded guide RNA (gRNA) sequence was designed to target exon 2 of *ASIC1* (NC_000012.12 Chromosome 12 Reference GRCh38.p13; Location: 50.058.985-50.059.004)

via CRISPR-Cas9, as indicated in Figure 27 and described in the methods. The chosen sequence was: 5’ – TGTCACCAAGCTCGACGAGG – 3’.

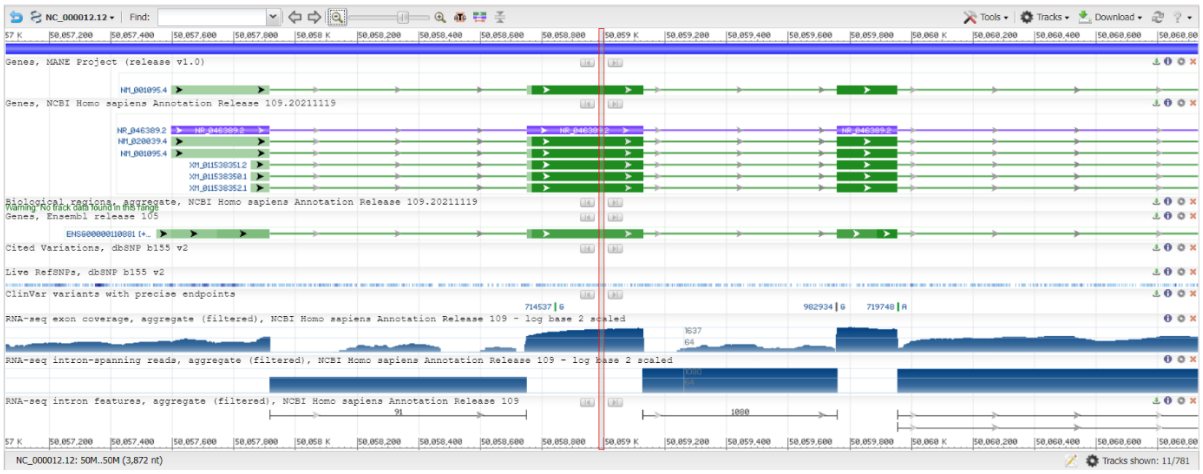

Figure 27 – Targeted sequence in genome for ASIC1 KO.

The gRNA targeted location was chosen to induce a frameshift early in the coding sequence of ASIC1 isoforms a and b. Two knockouts were generated, which were identified by frameshifts in the melting curve, as illustrated in Figure 28, namely clone 2C4 (25 bp deletion, denoted ASIC1 KO1, Figure 29) and clone 7C6 (17 bp deletion, denoted ASIC1 KO2, Figure 30),

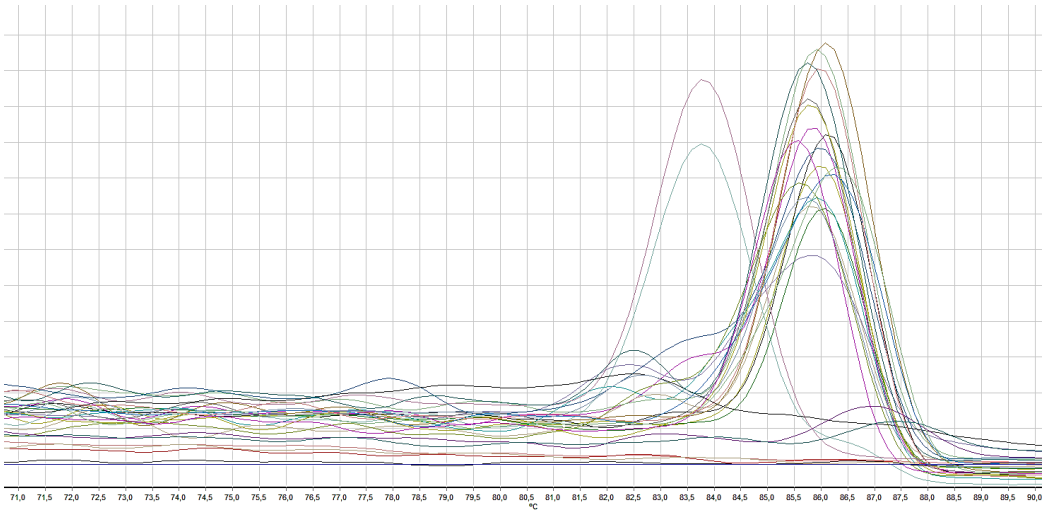

Figure 28 – Exemplary qPCR melt curve analysis result. A shift in melting temperature can be observed for two technical replicates of one sample.

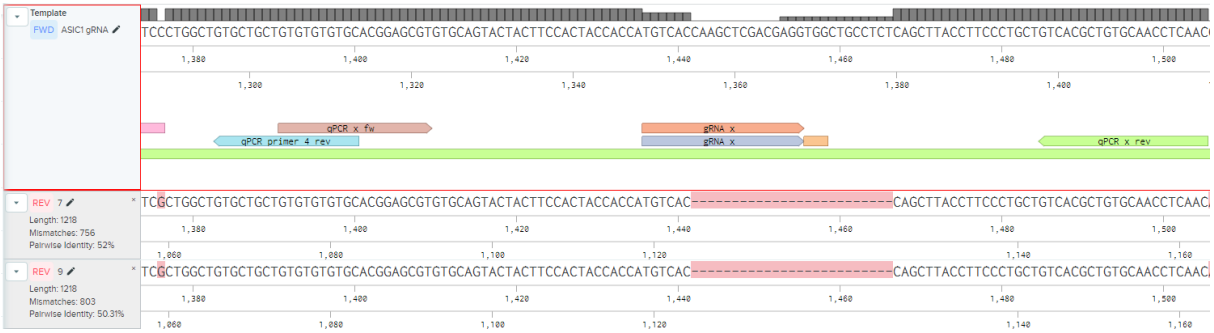

Figure 29 – ASIC1 KO 2C4 deletion validated by sequencing.

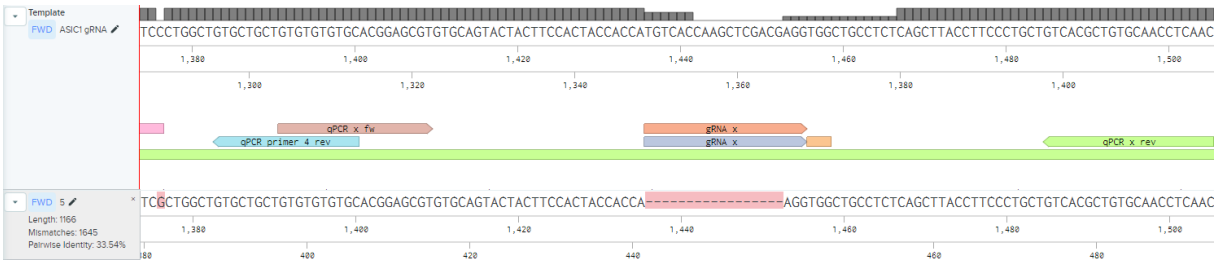

Figure 30 – ASIC1 KO 7C6 deletion validated by sequencing.

Absence of functional ASIC1a currents was confirmed by patch clamp analysis, conducted by Karolos-Philippos Pissas (data not shown).

The two monoclonal R54 GSC ASIC1 KOs were then tested in the migration assay, alongside R54 WT cells (Figure 31a). No statistical differences were observed between the ASIC1 KOs and the WT cells at the respective pH condition. Both cell lines still showed increased migration at acidic pH. This effect was slightly decreased in the control cells, compared to the ASIC1 KO cell lines, but still statistically significant. Sphere diameters were not statistically different from each other (Figure 31b). Representative pictures of R54 control and R54 ASIC1 KO cell lines are shown in Figure 32.

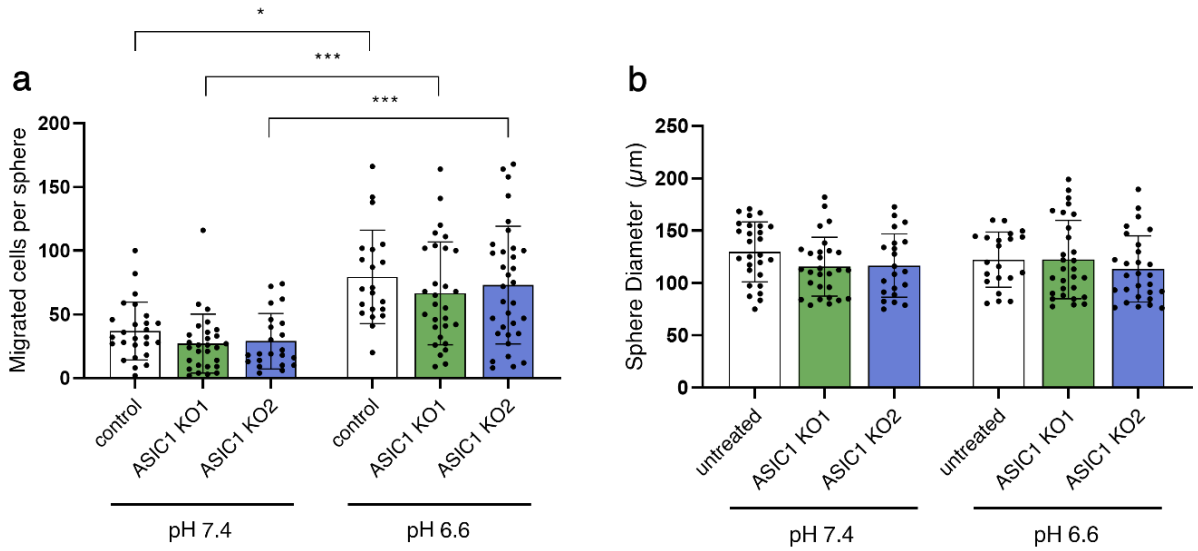

Figure 31 – R54 ASIC1 monoclonal KO cell lines 1 and 2, and control R54 cell line, in pH 7.4 and 6.6 medium, in hypoxic (~3% O_2) conditions. In a) the migrated cells per sphere are indicated. In b) the respective sphere diameters of the spheres at time point 0 are indicated. * $p < 0.05$, *** $p < 0.001$. Error bars indicate standard deviation (SD). KO: knockout.

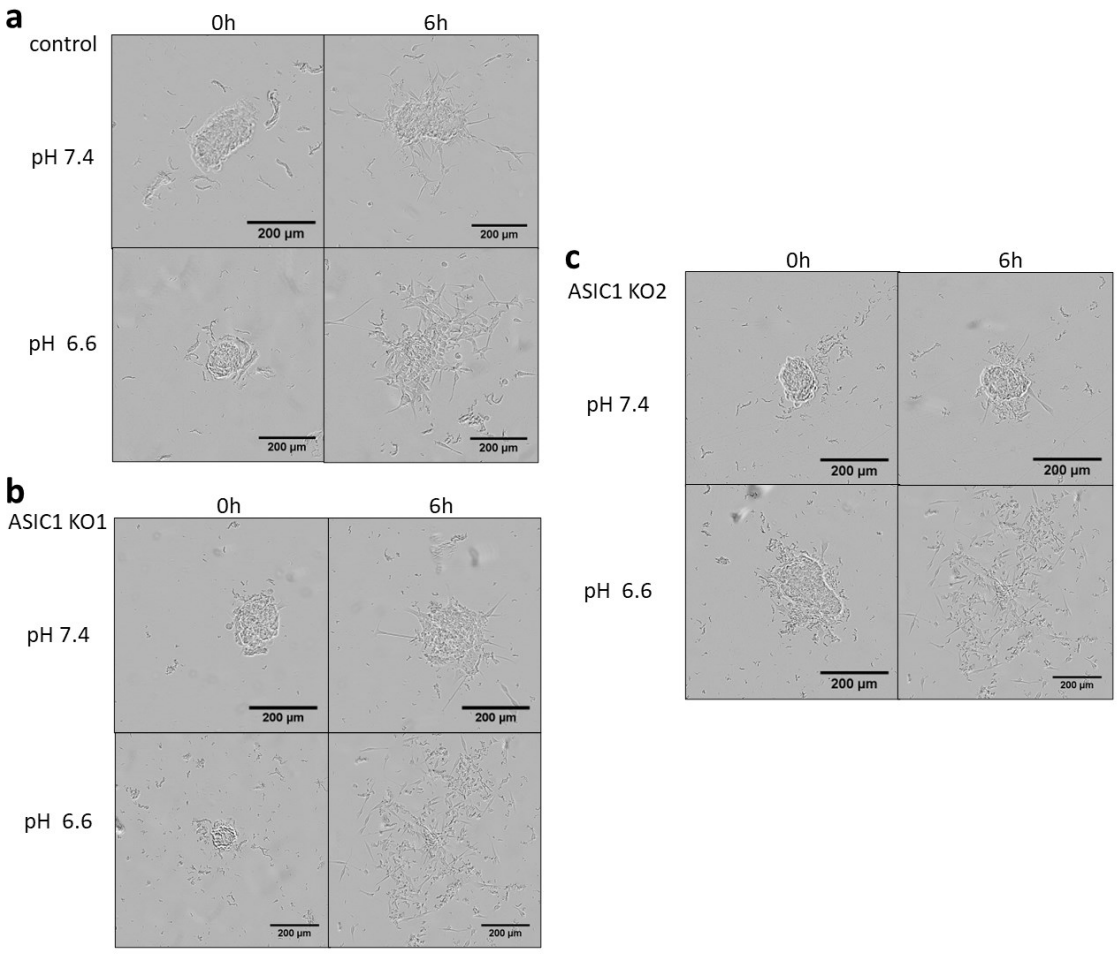

Figure 32 – Representative pictures of R54 GSCs control for the ASIC1 KO migration experiment at pH 7.4 and pH 6.6 in the migration assay for time points 0h and 6h under hypoxic conditions (~3% O_2). In a) representative pictures of control

cells, b) shows cells of the R54 GSCs ASIC1 KO1 cell line, c) shows cells of the R54 GSCs ASIC1 KO2 cell line. Scale bar indicates 200 µm.

Therefore, neither pharmacologically inhibiting or activating ASIC1 nor genetic ablation of ASIC1 influenced migration in R54 GSCs. Inhibiting ASIC3 also had no effect on migration, contrary to findings from previous studies.

ASIC2a is downregulated in GBM and is not expressed in R54 GSCs (see Chapter 3.2.1). To investigate if its downregulation plays a role in migration of R54 GSCs, we overexpressed ASIC2a via lentiviral transduction, as described in the methods. I prepared the lentiviral plasmid L27 and Dr. Maria Feoktistova spin-transfected the R54 GSCs with the lentivirus containing the two plasmid constructs, also described in the methods.

The generated GSC cultures were regarded as polyclonal cultures, as transduction efficiency varied from cell to cell. Ilka C. Brakmann characterized the polyclonal ASIC2 overexpressing (oe) R54 and control R54 GSCs via patch clamp and showed characteristic heteromeric ASIC1a/2a currents in ASIC2 oe cells, which were not present in control cells (data not shown, Cortés Franco *et al.*, 2022).

Migration was then tested in polyclonal R54 cells oe ASIC2a, and compared with control R54 cells. As observed before, cells migrated more aggressively at pH 6.6, compared to pH 7.4. However, no statistical differences were observed between control and ASIC2a oe cells (Figure 33a). Sphere diameters were not significantly different from each other (Figure 33b). Representative pictures of the ASIC2a overexpression migration experiment are shown in Figure 34. Representative pictures of experiments at hypoxic conditions are shown for the time points 0 and 6 hours. For experiments conducted in normoxic conditions, the transfer at time point 0 from the microscope to the incubator meant that spheres would be in different locations at time point 6 h. Thus, migration experiments in normoxic conditions only include representative pictures at the 6-hour time point.

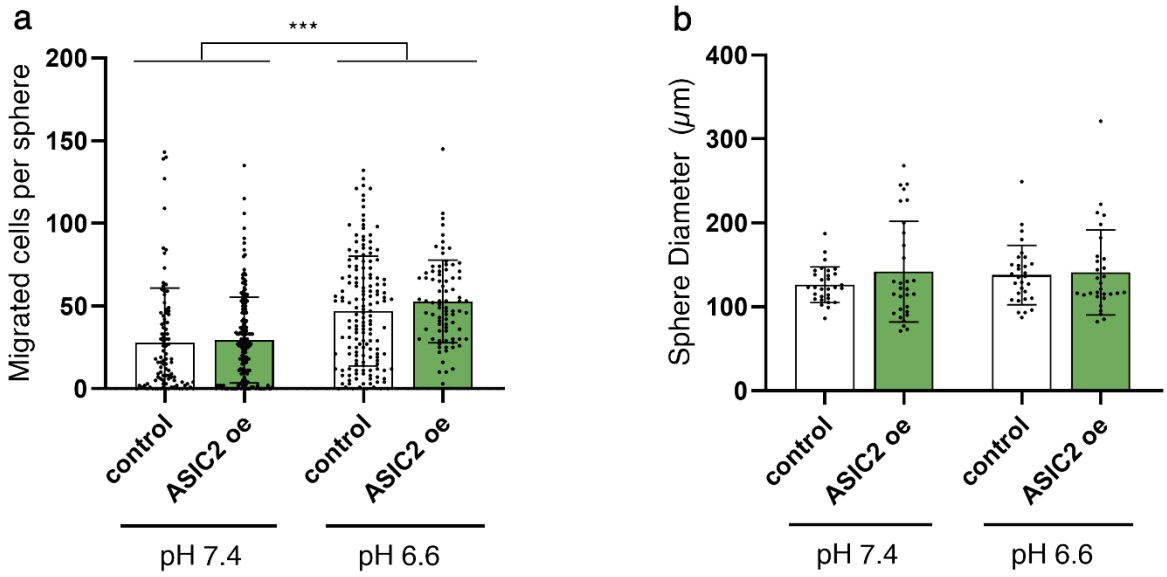

Figure 33 – R54 ASIC2a overexpressing polyclonal cell line (ASIC2 oe) and control R54 cells, in pH of 7.4 or 6.6 medium, in normoxic conditions. In a) the migrated cells per sphere are indicated. In b) the respective sphere diameters of the spheres at time point 0 are indicated. *** $p < 0.001$. Error bars indicate standard deviation (SD). oe: overexpressing.

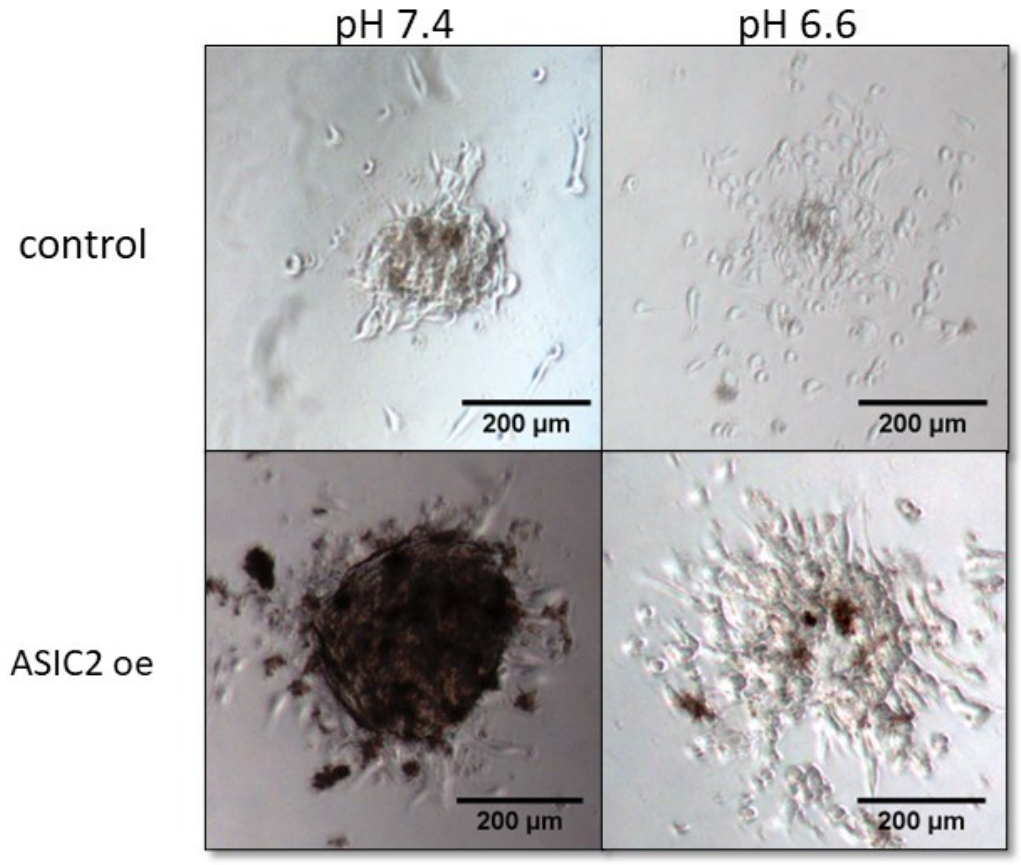

Figure 34 – Representative pictures of the ASIC2 overexpression migration experiment. Shown are control R54 GSCs and ASIC2 overexpressing (oe) R54 GSCs at pH 7.4 and pH 6.6 in the migration assay for time point 6h at normoxic conditions. Scale bar indicates 200 µm.

Therefore, overexpressing ASIC2a had no influence on migration of R54 GSCs. In summary, neither ASIC1a, ASIC3, nor upregulation of ASIC2a modulated migration of R54 GSCs.

3.3.3. Testing potential candidates KCNN4 and PI3K for a role in pH dependent GSC migration

Next, we inhibited KCNN4 (also known as KCa3.1) and PI3K, which were both significantly upregulated in the RNA sequencing screen, by using the KCNN4 inhibitor TRAM-34 (10 µM), and wortmannin (1 µM), an inhibitor of PI3K catalytic activity. We also adapted the experimental design of the migration assay, to be more in line with the experimental design of the RNA sequencing, as we were testing candidates identified in the RNA sequencing. Therefore, before conducting the migration assay, spheres were grown for two weeks, instead of one week, at pH 7.4 or pH 6.6. R54 GSC cells were then further separated into pH 7.4 and pH 6.6 groups for the migration assay. After six hours, migration was quantified (Figure 35).

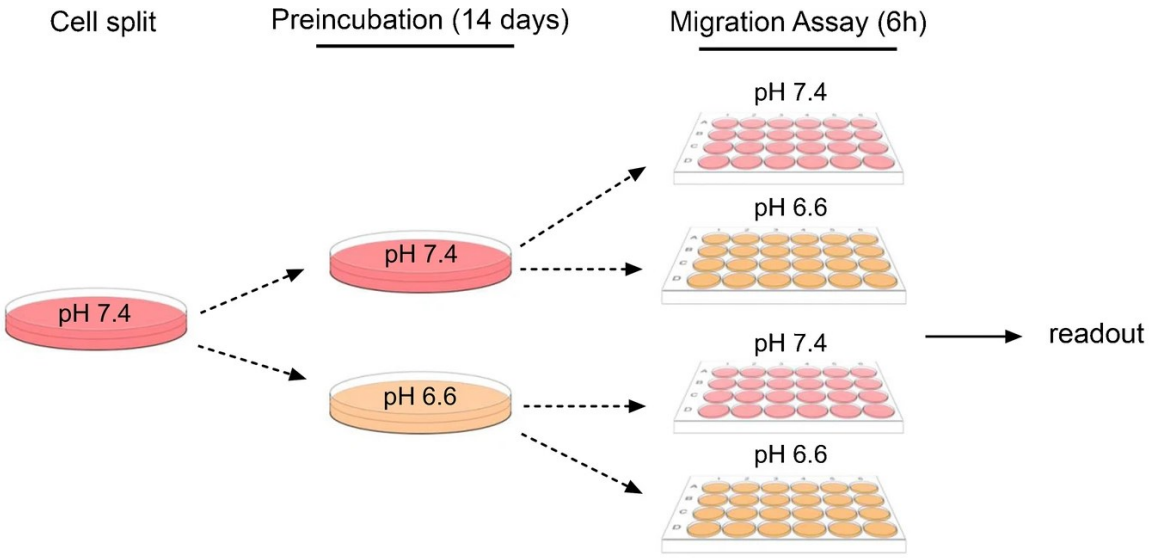

Figure 35 – Experimental setup for testing KCNN4 and PI3K in a migration assay using R54 GSC spheres grown for two weeks. R54 GSC spheres were grown for two weeks at either pH 7.4 or pH 6.6 and then again separated into pH 7.4 or pH 6.6 groups for the duration of the migration assay (6h). (Cortés Franco *et al.*, 2022)

This incubation in different pH before the migration assay was done to determine whether the pH dependent migration occurred as an acute response to acidic pH, or whether pH preconditioning would also contribute a latent effect to migration. While no difference in migration was observed between control and TRAM-34, wortmannin decreased migration, but only in assay pH 6.6, independent of the preincubation pH (Figure 36). For the control condition without inhibitors, we observed a significantly lower migration when cells had been preincubated with pH 7.4 and migration tested at pH 7.4, compared with cells that had been

preincubated with pH 6.6 and tested at pH 7.4. Migration of wortmannin-treated cells, however, did not differ depending on preincubation pH. Moreover, sphere diameters were larger for control conditions preincubated at pH 7.4 than for spheres preincubated at pH 6.6. This effect, however, was observed only for the control condition and not the TRAM-34 or wortmannin conditions (Figure 37). If anything, larger spheres should increase the number of migrated cells and can therefore not explain the lower migration in this condition. Representative pictures of all conditions are shown in Figure 38.

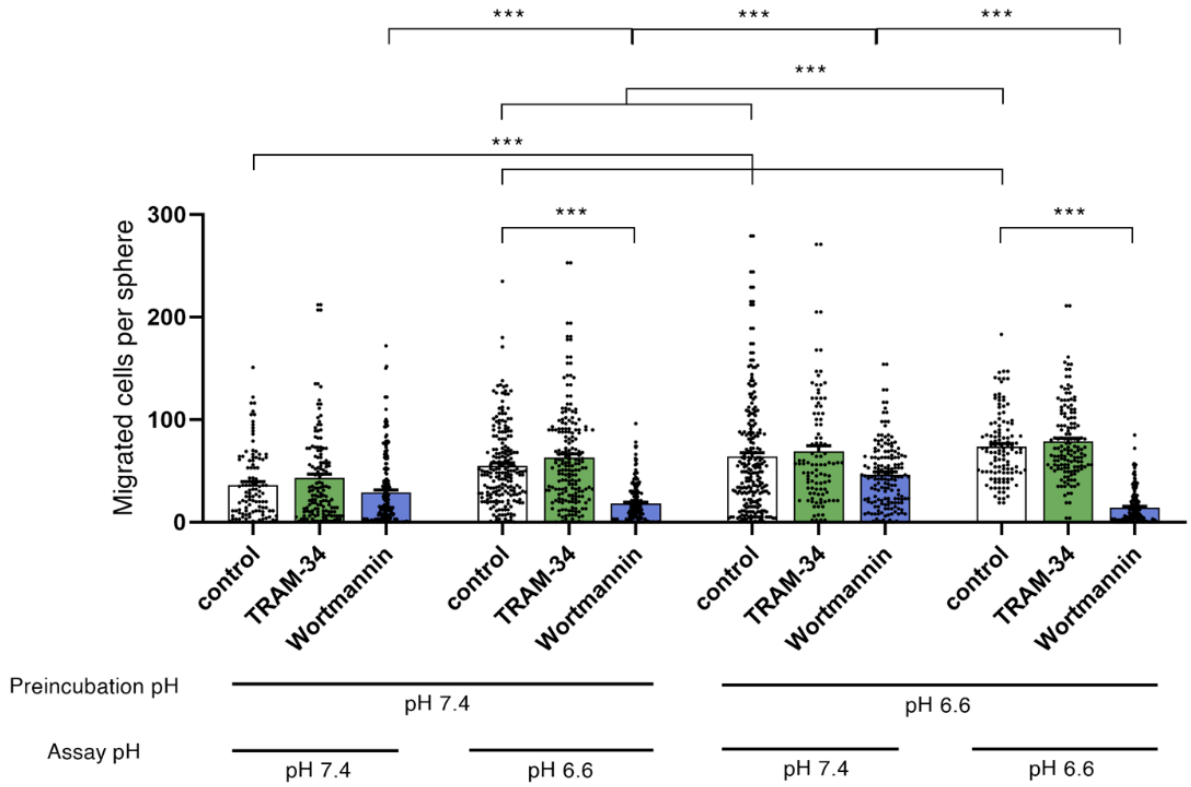

Figure 36 – Migration of R54 GSCs treated with DMSO (control), the KCNN4 inhibitor TRAM-34 (10 µM) or the PI3K inhibitor wortmannin (1 µM) after preincubation (2 weeks) and assay incubation (6 hours) at pH 7.4 and pH 6.6, in normoxic conditions. Experiment was performed in three biological replicates. The number of technical replicates varied between biological replicates, which is accounted for via generalized linear mixed modelling (GLMM). Dots indicate technical replicates. From left to right: n = 110, 141, 213, 208, 194, 191, 232, 101, 162, 119, 147, 198. Bar graphs shows the mean ± SD. Significances were determined via Tukey's glht function of multcomp package of GLMM fit, and p-adjusted values are indicated as *** $p < 0.001$. DMSO: Dimethyl sulfoxide.

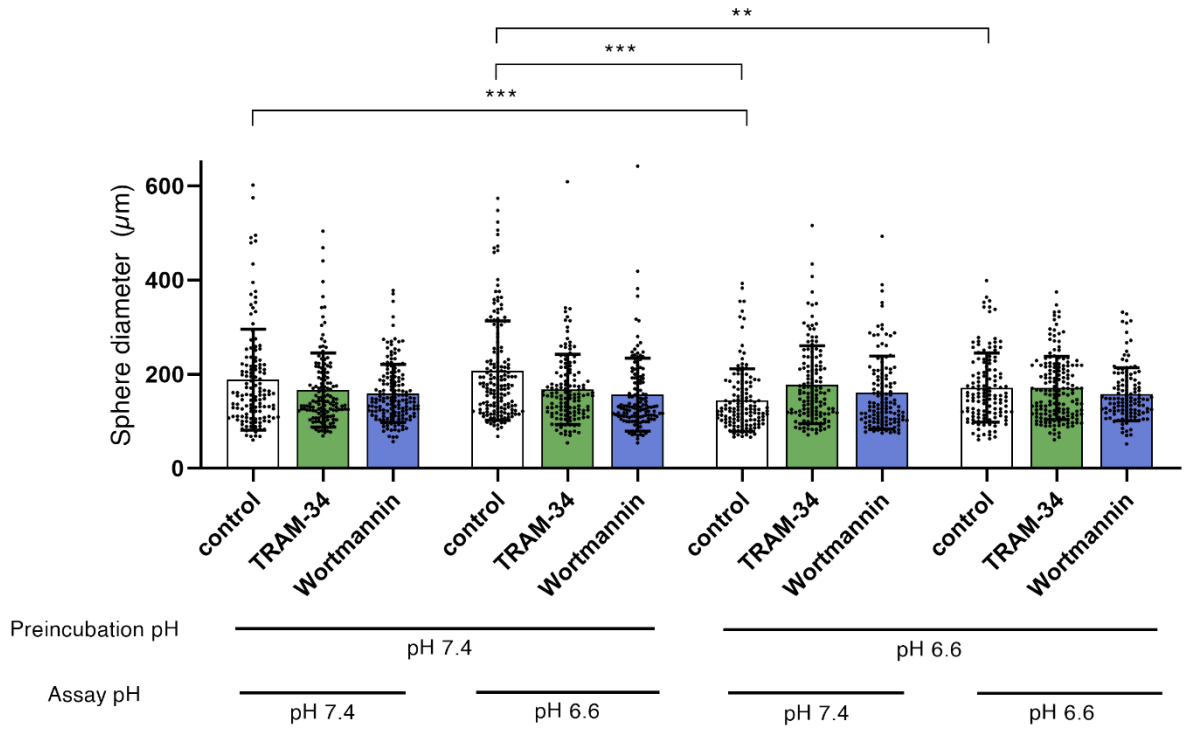

Figure 37 – Sphere diameters of R54 GSCs treated with DMSO (control), KCNN4 inhibitor TRAM-34 (10 µM) or PI3K inhibitor wortmannin (1 µM) after preincubation (2 weeks) and assay incubation (6 hours) at pH 7.4 and pH 6.6, in normoxic conditions. Dots indicate technical replicates. From left to right: n = 131, 139, 159, 165, 132, 138, 136, 133, 125, 131, 162, 121. p-values are indicated as ** $p < 0.01$, *** $p < 0.001$; One-Way ANOVA. DMSO: Dimethyl sulfoxide.

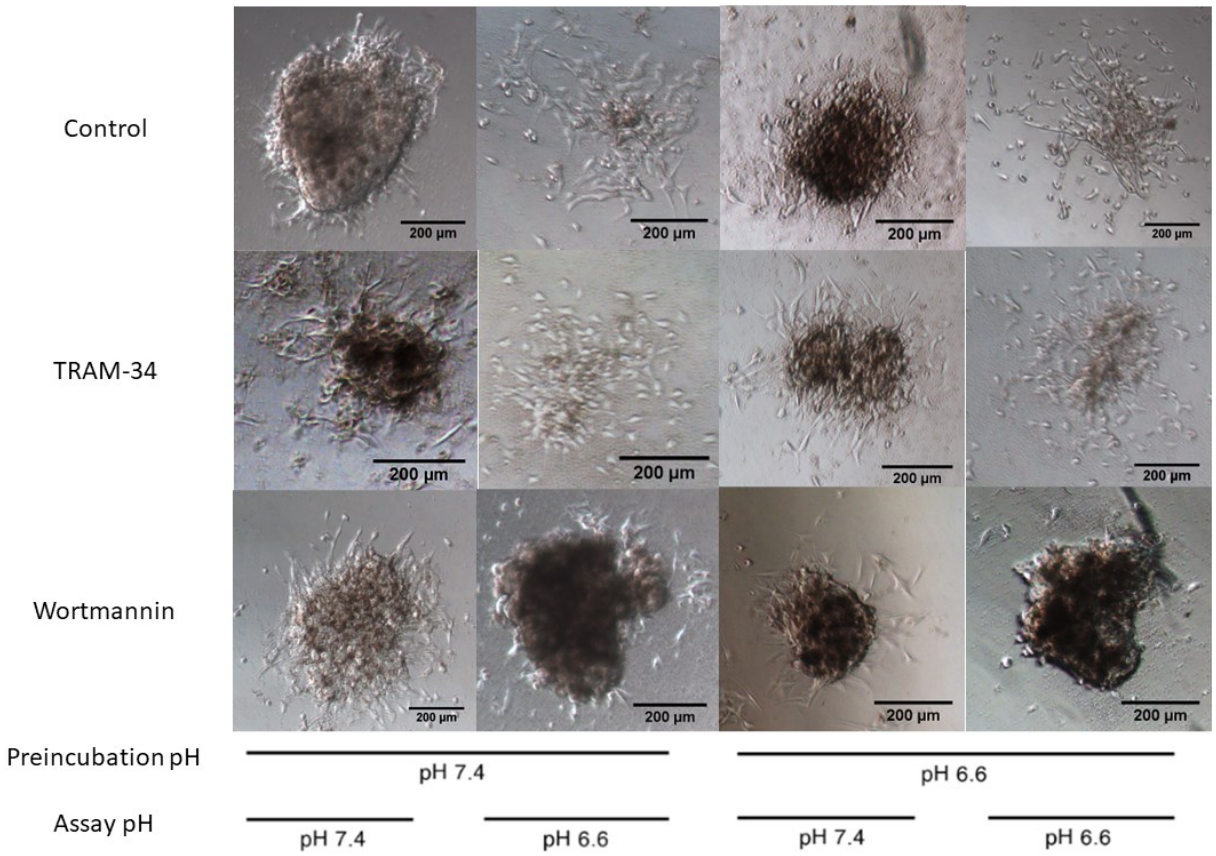

Figure 38 – Representative pictures of the two-week migration experiment. Shown are R54 GSCs, treated with DMSO (control), KCNN4 inhibitor TRAM-34 (10 µM) or PI3K inhibitor wortmannin (1 µM). Cells were preincubated for two weeks at pH 7.4 or pH 6.6 and then the migration assay was conducted for 6 hours at pH 7.4 or pH 6.6 at normoxic conditions. Scale bar indicates 200 µm.

To conclude, while the KCNN4 inhibitor TRAM-34 had no effect on migration, inhibiting PI3K via wortmannin resulted in a consistent inhibition of migration of GBM R54 GSC spheres, but only when subjected to pH 6.6 for the duration of the migration assay. Thus, PI3K appears to modulate pH dependent migration.

4. Discussion

4.1. Sphere slice assay as a method for detecting protein expression differences in core versus periphery of tumourspheres

We were able to establish a method for fixing and slicing R54 GSC spheres, using a 3D printed mold that would keep same sized spheres on the same height for optimal slicing results. Moreover, the resulting slices left the structure of the sphere intact. These slices were tested by staining with ASIC1 and SOX2 antibodies. The results are inconsistent for ASIC1, which is likely due to differences in specificity and affinity of the ASIC1 antibodies tested. Anti-ASIC1 (avivasbio) showed strong uniform staining of cells within the sphere, whereas anti-ASIC1 (neuromab) showed strong staining only for cells in the periphery of the sphere, the latter indicating a differential of expression within the sphere, based on different microenvironment stimuli. The staining signal for SOX2 was very intense, with no difference in staining between sphere core and periphery, suggesting that there is no difference in stemness within the tumoursphere. Antibodies need to be more carefully selected for specificity, concentrations need to be further optimized and this experiment needs to be redone at a larger scale, and include GBM KO-controls for each tested protein, to validate the antibodies, confirm results and clarify inconsistencies regarding different results of the two anti-ASIC1 antibodies.

4.2. Determining expression levels and transcriptome differences at pH 7.4 and pH 6.6 in GSC lines

4.2.1. qPCR analysis confirms expression of ASIC1 and ASIC3, and absence of ASIC2 in R8 and R54 GSCs

The qPCR analysis confirmed expression of *ASIC1* and *ASIC3* in R8 and R54 GSCs. Expression of *ASIC1* was 30-fold higher than that of *ASIC3* in R8 GSCs, and approximately 4-fold higher in R54 GSCs, mostly due to the *ASIC3* expression being 14-fold higher in R54 GSCs. That is also why *ASIC4* expression was approximately 2-fold higher than *ASIC3* in R8 GSCs, whereas it was 5-fold lower in R54 GSCs. Expression of stem cell markers nestin and *SOX2* was generally robust for R8 and R54 GSCs. Of the three differentiation markers, expression was only robust for *TUBB3*, with *GFAP* and *GALC* expression being orders of magnitude smaller. In R54 GSCs, *TUBB3* and *GFAP* expression was 2 and 2.5-fold lower than in R8 GSCs, with no large changes in *GALC* expression between tested cell lines. This comparative decrease of differentiation

markers between R54 and R8 is surprising, as R54 is the $CD133^+$ cell line of proneural subtype, which exhibits neuronal differentiation and is associated with better chances of survival, compared with the R8 $CD133^-$ cell line of the mesenchymal subtype (Olar and Aldape, 2014). Thus, we would instead have expected higher expression of neuronal differentiation marker *TUBB3* in R54 GSCs.

ASIC2a was expressed in neither R8 nor R54 GSCs. *ASIC1* and *ASIC3* expression in R8 and R54 GSCs was lower than previously reported (Tian *et al.*, 2017), but consistent over repeats. Our results also fit well with the RNA sequencing results at pH 7.4, concerning the magnitude of expression (data not shown). Comparing gene expression in the same cell line at pH 7.4 and pH 6.6 yielded no statistically significant differences.

As anticipated, the ASIC1 qPCR signal decreased in ASIC1 KO cells, due to a large deletion inhibiting primer binding. In ASIC1 KO cells the expression increased significantly for *SOX2*, which could mean an increased stemness. How exactly ASIC1 KO increases *SOX2* expression is unclear.

4.2.2. RNA sequencing of R54 GSCs identified KCNN4 and PI3K as potential candidates for pH 6.6 dependent migration

The large transcriptomic dataset of the RNA sequencing experiment was analysed via DESeq2. Candidate genes with increased expression at pH 6.6, compared to pH 7.4 in R54 GSCs were considered for testing their potential modulation of acid-dependent migration. Based on existing publications and consistent upregulation, we decided to inhibit KCNN4 and PI3K in the sphere migration assay.

4.2.3. Using transcriptomic analysis to identify potential vulnerabilities of GBM in acidic tumour environments

Overall, after cross-referencing transcriptome data of R54 GSCs against multiple databases for gene-set enrichment, the same motifs kept appearing. Regarding metabolism, the most striking upregulated pathway at pH 6.6 was the TCA cycle / oxidative phosphorylation. It has been reported how tumorigenic cells in acidic pH switch from glycolysis back to oxidative phosphorylation and depend on this pathway for energy production (Wu, Ying and Hu, 2016; Michl *et al.*, 2022). This would be one of the obvious susceptibilities that R54 GSCs exhibit,

which should be tested for both R54 and other cell lines in cell growth and cell survival experiments, using numerous specific oxidative phosphorylation inhibitors.

Another strong candidate was the glutathione pathway or ROS pathways in general. Dealing with ROS becomes more and more a necessity for cancers at acidic pH, as cancers typically engage in a balancing act. The presence of ROS helps maintain genetic drift and evolve the tumour, but too much ROS causes too much DNA damage and kills the cancer cells (Pelicano, Carney and Huang, 2004; Bansal and Simon, 2018). At pH 6.6, we saw that the R54 GBM cancer cells strongly upregulated pathways to limit ROS and ROS damage. Therefore, antioxidant production and pathways managing ROS, such as glutathione, should be targeted, and tested as oxidative phosphorylation inhibitors described above.

The third consistently observed pathway and potential target was the cholesterol metabolism for lipid scavenging, which was upregulated in R54 GSCs at pH 6.6.

This pathway is often aberrant in cancer, and is linked with citrate synthesis and fatty acid (FA) metabolism pathways. Glutamine is necessary for citrate production in the TCA cycle, which in turn produces acetyl-groups in the FA metabolism. Citrate is an essential building block for FAs and is required for *de novo* production of FAs, along with the ATP citrate lyase (ACLY), the acetyl-CoA carboxylase (ACC) and the fatty acid synthase (FASN), as indicated in Figure 39.

FA synthesis is necessary for sustaining the lipid metabolism of the cell, including the synthesis of cell membrane lipids (phospholipids), as well as other lipids, such as sterols. FAs are synthesized from TCA cycle metabolite carbon sources (citrate), which in adult humans occurs mainly in the liver, adipose tissue and lactating breast, or taken up exogenously from lipid vesicles. To fuel cancer tumour growth, cancer cells require receptor-mediated uptake of exogenous FAs and lipid vesicles. This exogenous uptake is controlled by sterol regulatory element binding proteins (SREBPs), which are transcription factors for enzymes in the cholesterol biosynthesis pathway and the low-density lipoprotein receptor (LDLR), as shown in Figure 39 (Metallo *et al.*, 2012; Ackerman and Simon, 2014; Röhrig and Schulze, 2016). Lipid scavenging of cancer increases, when the cancer is hypoxic, as glucose is diverted to be used for glycolysis (Michalopoulou, Bulusu and Kamphorst, 2016). We found the exogenous lipid uptake pathway increased at pH 6.6, although the cells at pH 6.6 were less hypoxic than the cells in the pH 7.4 condition (Figure 17, pathway at the bottom of the figure). This stipulates,

that GSCs at pH 6.6 are also dependent on the lipid scavenging pathway and would be potentially vulnerable to therapeutic inhibition.

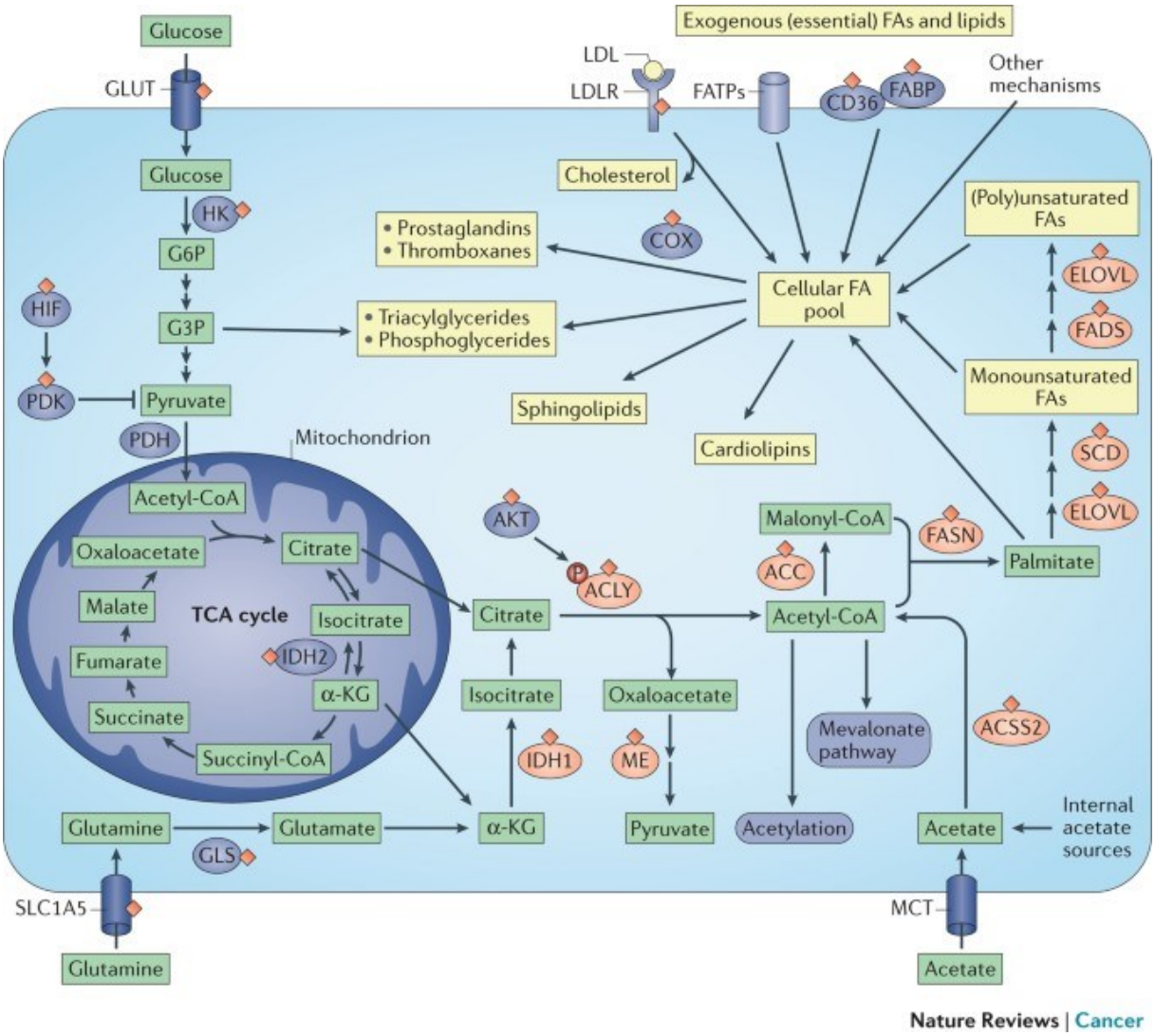

Figure 39 – Fatty acid synthesis pathways. The TCA cycle is producing citrate, which is turned into Acetyl-CoA and Malonyl-CoA, and then used by FASN for FA synthesis. FA extracellular uptake can also occur by binding of LDL by LDL-receptors, FA transporters (FATPs) or other mechanisms. Figure from Röhrig and Schulze, 2016. TCA: tricarboxylic acid, FASN: fatty acid synthetase, LDL: low density lipoprotein.

To conclude, we completed our objective in conducting a bioinformatical analysis of our RNA sequencing data, using GSEA cross-referencing and visualizing the results via enrichment maps, R Studio and the KEGG pathview plugin, to identify potential susceptibilities of GBM spheres incubated at pH 6.6, to be tested in future experiments.

4.3. R54 GSC migration assay reveals increased migration at pH 6.6, modulated not by ASIC1-3 or KCNN4, but by PI3K

4.3.1. Migration increases at pH 6.6 compared to pH 7.4, with no differences between hypoxic and normoxic incubation conditions

We conducted migration experiments with only R54 cells, as generating overexpression and knock-out cell lines for more cell lines would have been too time-consuming.

Migration in 1-week grown R54 GSCs was consistently increased at pH 6.6, compared to pH 7.4. No statistical differences were observed between cells incubated in hypoxia (~3% O_2) or in normoxia for the duration of the migration assay (6 h). This was somewhat surprising, as hypoxia is well documented to impact migration in cervical-, colon- (Höckel *et al.*, 1996; Hongo *et al.*, 2013), glioma- and ovarian cancer (Sahlgren *et al.*, 2008), glioblastoma (Li *et al.*, 2013; Joseph *et al.*, 2015; Huang *et al.*, 2018), and breast cancer (Knowles and Harris, 2001; Chen, Imanaka and Griffin, 2010; Han *et al.*, 2015).

One potential explanation is that the duration of the incubation (6 h) was too short to affect migration. Limited access to the hypoxia-incubator prevented us from testing longer time-periods. Some studies have shown that migration in glioblastoma (U251 cells) at different pO2 did not differ short term (<2 hours) but long term (≥12 hours) (Fujimura *et al.*, 2013; Li *et al.*, 2013), as changes in hypoxia-inducible transcription factors take time. In direct contrast, another study showed increased migration after only five hours for U87 and G55 glioblastoma cells (Kathagen-Buhmann *et al.*, 2016) in hypoxic versus normoxic conditions.

It should be noted that to date all cited papers showing hypoxia-dependent migration in glioblastoma cells used adherent monolayer cells in transwell migration / invasion and scratch assays.

Using spheroids as a model system for migration is arguably a more accurate approximation for the behaviour of glioblastoma cells *in vivo* than using a scratch assay with adherent glioblastoma cell lines. However, using spheres as a cell model means having a heterogeneous population of cells, having a cell core and a periphery, where cells have varying exposures to oxygen, nutrients, and proton concentrations. In culture we have observed that spheres form necrotic cores after 1-2 weeks, similar to cancer cells forming necrotic cores *in vivo*. This effect has been previously reported (Singh *et al.*, 2020). Adhering these spheres to laminin coated

plates after one-week results in active migration of peripheral cells away from the core, resulting in pseudopalisading-like behaviour. As cells within a sphere are tightly packed, and necrotic cores are already present in one to two-week-old spheres, we argue that cells within the spheroid are already exposed to hypoxic conditions from the core, independent of the oxygen-concentration in the incubator. This is likely why we did not observe differences in migration after 6-hour incubation in normoxic or hypoxic culturing.

4.3.2. ASIC1, ASIC2 and ASIC3 do not modulate migration of R54 GSCs

We tested the effect of ASIC1 and ASIC3 on migration in R54 GSCs first by inhibiting ASIC1 in R54 GSCs using 100 nM PcTx-1 and by inhibiting ASIC3 using 500 nM APETx2. While we saw a correlation of acidic pH and migration, ASIC1 or ASIC3 inhibition did not reduce migration, contrary to what has previously been reported. Using 20 nM MitTx, to activate ASIC1a at a physiological pH, also had no effect on migration at pH 7.4. We then generated two monoclonal ASIC1 KO cell lines from R54 GSCs via CRISPR-Cas9. No differences in migration were observed between WT and KO cells in our migration assay. Therefore, ASIC1 did not affect migration in R54 GSCs and we were unable to confirm previously published findings.

ASIC2a expression decreases noticeably in higher-grade tumour cells (Gravendeel *et al.*, 2009), and ASIC2 was reported to promote migration in colorectal cancer (Zhou *et al.*, 2017) and microglia (Yu *et al.*, 2015) but to inhibit migration in glioma cells (Vila-Carriles *et al.*, 2006, 2007) and vascular smooth muscle cells (de Campos Grifoni *et al.*, 2006; Grifoni, Murphy and Drummond, 2007; Fuller and Benos, 2008; Grifoni *et al.*, 2008; Grifoni, McKey and Drummond, 2008). Lentivirally overexpressing ASIC2a in R54 GSCs, we observed no significant difference between the WT and ASIC2a oe GSCs in the sphere migration assay. Thus, ASIC2 did not modulate migration in R54 GSCs.

4.3.3. Specific inhibition of PI3K via wortmannin modulates migration solely at pH 6.6

Sphere migration was then tested in a more elaborate experiment, in which spheres were grown in medium with pH 7.4 or pH 6.6 for two weeks, with the migration assay subsequently being conducted at pH 7.4 or pH 6.6 (assay pH) for 6 hours, resulting in four pH treatment conditions. Additionally, spheres were incubated with the KCa3.1 inhibitor TRAM-34 or the PI3K inhibitor wortmannin (Figure 36). It should also be mentioned that migration of R54 GSCs kept at pH 7.4 only was higher than previously observed in experiments with 1-week old

spheres. This could be due to two-week-old spheres being larger with a more necrotic core, which in turn leads to a gradient in oxygen, nutrients, pH and secondary metabolites, resulting in a stronger signal for the cells to migrate outward. This behaviour likely decreased the difference between assay pH conditions pH 7.4 and pH 6.6, as observed in experiments with 1-week old spheres, leading to an underestimation of the statistical significance of the assay pH and short-term signalling pathways for migration. Nonetheless, this effect was still statistically significant.

TRAM-34 did not affect migration in comparison to the untreated control, suggesting that KCa3.1 does not play a role in proton-mediated migration in R54 GSCs, despite numerous publications that reported an effect of KCa3.1 on migration in tumorigenic epithelial cells (Lai *et al.*, 2013; Xu *et al.*, 2014), papillary thyroid carcinoma (Wen *et al.*, 2020), hepatocellular carcinoma (Li *et al.*, 2019), colorectal cancer (Ibrahim *et al.*, 2021), lung adenocarcinoma (Xu *et al.*, 2021) and microglia (Ferreira, Lively and Schlichter, 2014), among others.

Wortmannin-treated cells in contrast showed a significant reduction in migration only in assay pH 6.6 but the number of migrating cells from spheres did not differ depending on preincubation pH, suggesting that PI3K plays a role in fast induction of migration, but not in latent long-term induction. While the PI3K/AKT/MTOR pathway is well known to be aberrant in cancer and dependent on hypoxia, directly linking acidic pH to PI3K upregulation in cancer is a novel finding, the significance of which is further emphasized by the numerous clinical trials underway for PI3K/AKT/MTOR inhibitors. So far it has only been reported that acidosis leads to phosphorylation of AKT, the downstream target of PI3K, in human neutrophils (Martínez *et al.*, 2006).

We have been so far unable to experimentally determine a proton-sensor, upstream of PI3K, as it clearly is unrelated to ASICs or KCa3.1. It could be that PI3K is regulated by GTPase CDC42, by excluding PI3K inhibitor PTEN from the cytomembrane (Li *et al.*, 2003; Yang *et al.*, 2012). The active form of GTP-bound CDC42 is strongly reduced in low extracellular pH (Oster *et al.*, 2022).

5. Outlook

Future experiments will use the protocol for generating GSC sphere slices, to determine POI localization within GSC spheres.

Our RNA sequencing screen identified numerous pathways of interest that are enriched at pH 6.6 and warrant further experiments. Oxidative phosphorylation would be a promising target pathway, to show that GSCs rely more and more on oxidative phosphorylation in more acidic pH culture conditions, along the lines of previous studies showing the same dynamic in colorectal cancer (Michl *et al.*, 2022). This experiment would require GSCs to be cultured at different pH conditions, while under influence of oxidative phosphorylation inhibitors, for example atovaquone and rotenone. As an addition, one could also add inhibitors targeting ROS-reducing peroxidases, for example N-Acetyl-L-Cysteine and diphenyleneiodonium chloride, to give an insight into how GSCs become more dependent on ROS-reducing mechanisms for survival in acidic pH conditions. Readout of this assay would be the sphere size, representing cell growth, measured every 2 days for 14 days.

Upstream of PI3K we suspect CDC42 as a potential candidate for inhibition, which could be done by MLS-573151 and ML141. It would be interesting to see whether inhibition of migration in GSCs would occur, like with inhibition via wortmannin. Another possible experiment would be to induce TNFR2, which is strongly upregulated at pH 6.6, by addition of TNF alpha or TNF superfamily member lymphotoxin alpha (Hu *et al.*, 2014; Kucka *et al.*, 2021) and see whether this would induce migration in GSCs, as this pathway is also upstream of PI3K.

To show relevance beyond R54 GSCs, key experiments could then be repeated with another GSC cell line R8, which is a $CD133^-$ mesenchymal-like GSC-line, as opposed to R54 being a $CD133^+$ proneural-like GSC-line.

These follow-up studies would reveal potential vulnerabilities of GSCs regarding migration, with the ultimate goal being the expansion of treatment options for patients.

6. Supplementary Data

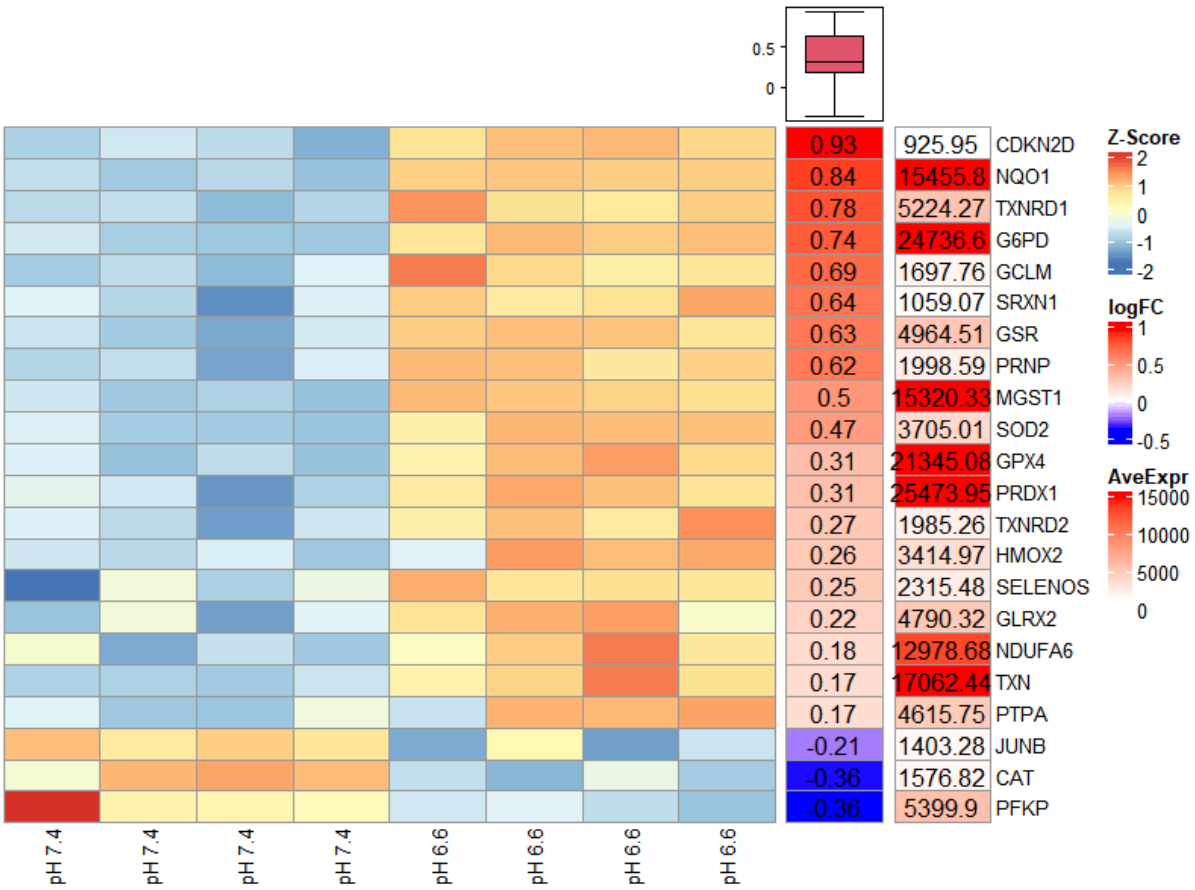

Supplementary Figure 1 – Heatmap of hallmark ROS pathway. Indicated are Z-Scores per sample, log2 fold change and average expression across all samples. Z-Scores reflect up- or downregulation in terms of standard deviation from the mean gene expression, with 0 indicating no up- or downregulation between pH conditions.

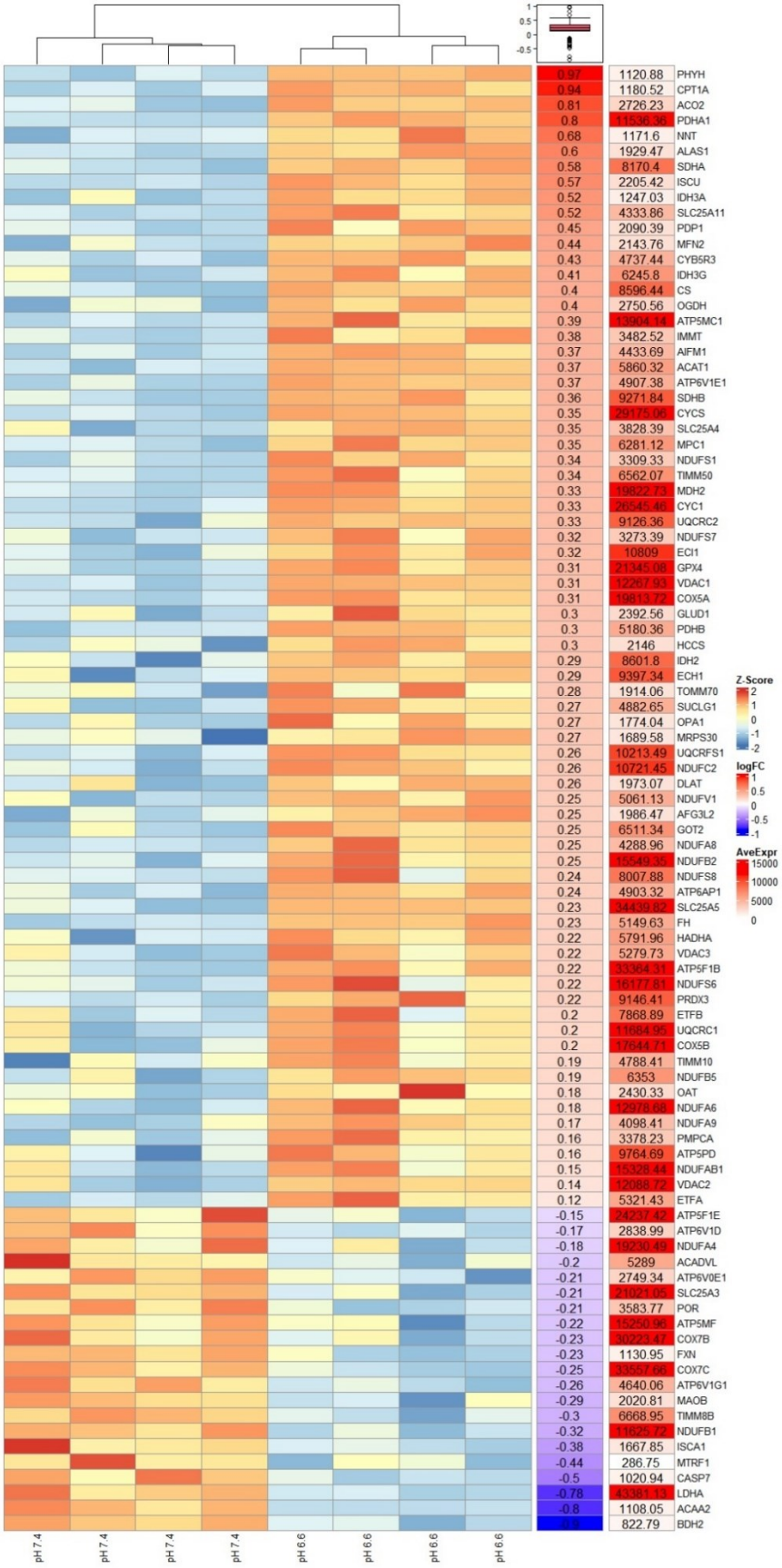

Supplementary Figure 2 – Heatmap of Hallmark Oxidative Phosphorylation Pathway. Indicated are Z-Scores per sample, log2 fold change and average expression across all samples. Z-Scores reflect up- or downregulation in terms of standard deviation from the mean gene expression, with 0 indicating no up- or downregulation between pH conditions.

7. References

Ackerman, D. and Simon, M. C. (2014) 'Hypoxia, lipids, and cancer: surviving the harsh tumor microenvironment', *Trends in cell biology*. Elsevier, 24(8), pp. 472–478.

Akerberg, A. A., Stewart, S. and Stankunas, K. (2014) 'Spatial and temporal control of transgene expression in zebrafish', *PLoS One*. Public Library of Science San Francisco, USA, 9(3), p. e92217.

Al-Lamki, R. S. *et al.* (2005) 'TNFR1-and TNFR2-mediated signaling pathways in human kidney are cell type-specific and differentially contribute to renal injury', *The FASEB Journal*. Wiley Online Library, 19(12), pp. 1637–1645.

Aldape, K. *et al.* (2015) 'Glioblastoma: pathology, molecular mechanisms and markers', *Acta neuropathologica*. Springer, 129(6), pp. 829–848.

Alexopoulos, G. *et al.* (2022) 'Long-Term Time Series Forecasting and Updates on Survival Analysis of Glioblastoma Multiforme: A 1975–2018 Population-Based Study', *Neuroepidemiology*. Karger Publishers, pp. 1–15.

Arcaro, A. (2016) 'The role of the PI3K/AKT/mTOR pathway in brain tumor metastasis', *Journal of Cancer Metastasis and Treatment*. OAE Publishing Inc., 2, pp. 80–89.

Bader, J. E., Voss, K. and Rathmell, J. C. (2020) 'Targeting metabolism to improve the tumor microenvironment for cancer immunotherapy', *Molecular cell*. Elsevier, 78(6), pp. 1019–1033.

Bansal, A. and Simon, M. C. (2018) 'Glutathione metabolism in cancer progression and treatment resistance', *Journal of Cell Biology*. Rockefeller University Press, 217(7), pp. 2291–2298.

Baron, A. *et al.* (2013) 'Venom toxins in the exploration of molecular, physiological and pathophysiological functions of acid-sensing ion channels', *Toxicon*. Elsevier, 75, pp. 187–204.

Beier, C. P. *et al.* (2018) 'Aberrant neuronal differentiation is common in glioma but is associated neither with epileptic seizures nor with better survival', *Scientific Reports*. Nature Publishing Group UK London, 8(1), p. 14965.

Beier, D. *et al.* (2007) 'CD133+ and CD133− glioblastoma-derived cancer stem cells show

differential growth characteristics and molecular profiles', *Cancer research*. AACR, 67(9), pp. 4010–4015.

de Bem Prunes, B. *et al.* (2022) 'The role of tumor acidification in aggressiveness, cell dissemination and treatment resistance of oral squamous cell carcinoma', *Life Sciences*. Elsevier, 288, p. 120163.

Bohlen, C. J. *et al.* (2011) 'A heteromeric Texas coral snake toxin targets acid-sensing ion channels to produce pain', *Nature*. Nature Publishing Group UK London, 479(7373), pp. 410–414.

Bonito, B. *et al.* (2016) 'KCa3. 1 (IK) modulates pancreatic cancer cell migration, invasion and proliferation: anomalous effects on TRAM-34', *Pflügers Archiv-European Journal of Physiology*. Springer, 468(11), pp. 1865–1875.

Brand, A. H. and Perrimon, N. (1993) 'Targeted gene expression as a means of altering cell fates and generating dominant phenotypes', *development*. Company of Biologists The Company of Biologists, Bidder Building, 140 Cowley …, 118(2), pp. 401–415.

Brat, D. J. and Van Meir, E. G. (2004) 'Vaso-occlusive and prothrombotic mechanisms associated with tumor hypoxia, necrosis, and accelerated growth in glioblastoma', *Laboratory investigation*. Nature Publishing Group, 84(4), pp. 397–405.

de Campos Grifoni, S. *et al.* (2006) 'ASIC 2 and 3 proteins are required for VSMC wound healing'. Wiley Online Library.

Cardone, R. A., Casavola, V. and Reshkin, S. J. (2005) 'The role of disturbed pH dynamics and the Na+/H+ exchanger in metastasis', *Nature reviews cancer*. Nature Publishing Group, 5(10), pp. 786–795.

Carlson, M. (no date) 'GO.db: A set of annotation maps describing the entire Gene Ontology. R package version 3.2.2.' Available at: https://bioconductor.org/packages/release/data/annotation/html/GO.db.html.

Chen, J., Imanaka, N. and Griffin, J. D. (2010) 'Hypoxia potentiates Notch signaling in breast cancer leading to decreased E-cadherin expression and increased cell migration and invasion', *British journal of cancer*. Nature Publishing Group, 102(2), pp. 351–360.

Chen, X., Kalbacher, H. and Grunder, S. (2006) 'Interaction of acid-sensing ion channel (ASIC) 1 with the tarantula toxin psalmotoxin 1 is state dependent', *The Journal of general physiology*. Rockefeller University Press, 127(3), pp. 267–276.

Chiche, J., Brahimi-Horn, M. C. and Pouysségur, J. (2010) 'Tumour hypoxia induces a metabolic shift causing acidosis: a common feature in cancer', *Journal of cellular and molecular medicine*. Wiley Online Library, 14(4), pp. 771–794.

Chifflet, S., Hernández, J. A. and Grasso, S. (2005) 'A possible role for membrane depolarization in epithelial wound healing', *American Journal of Physiology-Cell Physiology*. American Physiological Society, 288(6), pp. C1420–C1430.

Cizkova, K. *et al.* (2021) 'Comparative Analysis of Immunohistochemical Staining Intensity Determined by Light Microscopy, ImageJ and QuPath in Placental Hofbauer Cells.', *Acta histochemica et cytochemica*. Japan, 54(1), pp. 21–29. doi: 10.1267/ahc.20-00032.

Colwell, N. *et al.* (2017) 'Hypoxia in the glioblastoma microenvironment: shaping the phenotype of cancer stem-like cells', *Neuro-oncology*. Oxford University Press US, 19(7), pp. 887–896.

Cortés Franco, K.-D. *et al.* (2022) 'Aggressive migration in acidic pH of a glioblastoma cancer stem cell line in vitro is independent of ASIC and KCa3. 1 ion channels, but involves phosphoinositide 3-kinase', *Pflügers Archiv-European Journal of Physiology*. Springer, pp. 1–12.

d'Alessandro, G. *et al.* (2013) 'KCa3. 1 channels are involved in the infiltrative behavior of glioblastoma in vivo', *Cell death & disease*. Nature Publishing Group, 4(8), pp. e773–e773.

Damaghi, M., Wojtkowiak, J. W. and Gillies, R. J. (2013) 'pH sensing and regulation in cancer', *Frontiers in physiology*. Frontiers, 4, p. 370.

Daniele, S. *et al.* (2015) 'Lactate dehydrogenase-A inhibition induces human glioblastoma multiforme stem cell differentiation and death', *Scientific reports*. Nature Publishing Group, 5(1), pp. 1–17.

Dayan, F. *et al.* (2008) 'A dialogue between the hypoxia-inducible factor and the tumor microenvironment', *Cancer Microenvironment*. Springer, 1(1), pp. 53–68.

Dienstmann, R. *et al.* (2014) 'Picking the point of inhibition: a comparative review of PI3K/AKT/mTOR pathway inhibitors', *Molecular cancer therapeutics*. AACR, 13(5), pp. 1021–1031.

Van Dongen, S. (2008) 'Graph clustering via a discrete uncoupling process', *SIAM Journal on Matrix Analysis and Applications*. SIAM, 30(1), pp. 121–141.

Eddelbuettel, D. and François, R. (2011) 'Rcpp: Seamless R and C++ integration', *Journal of Statistical Software*, 40(8), pp. 1–18. doi: 10.18637/jss.v040.i08.

Ferreira, R., Lively, S. and Schlichter, L. (2014) 'IL-4 Type 1 Receptor Signaling Up-Regulates KCNN4 Expression, and Increases the KCa3.1 Current and its Contribution to Migration of Alternative-Activated Microglia', *Frontiers in cellular neuroscience*, 8, p. 183. doi: 10.3389/fncel.2014.00183.

Fidoamore, A. *et al.* (2016) 'Glioblastoma stem cells microenvironment: the paracrine roles of the niche in drug and radioresistance', *Stem cells international*. Hindawi, 2016.

Fournier, D. A. *et al.* (2012) 'AD Model Builder: Using automatic differentiation for statistical inference of highly parameterized complex nonlinear models', *Optimization Methods and Software*, 27(2), pp. 233–249. doi: 10.1080/10556788.2011.597854.

Friedman, N., Cai, L. and Xie, X. S. (2006) 'Linking stochastic dynamics to population distribution: an analytical framework of gene expression', *Physical review letters*. APS, 97(16), p. 168302.

Fujimura, A. *et al.* (2013) 'Cyclin G2 promotes hypoxia-driven local invasion of glioblastoma by orchestrating cytoskeletal dynamics', *Neoplasia*. Elsevier, 15(11), pp. 1272-IN23.

Fuller, C. M. and Benos, D. J. (2008) 'Putting the brakes on vascular smooth muscle cell migration', *American Journal of Physiology-Heart and Circulatory Physiology*. American Physiological Society, 294(5), pp. H1987–H1988.

Garcia, J. H., Jain, S. and Aghi, M. K. (2021) 'Metabolic drivers of invasion in glioblastoma', *Frontiers in cell and developmental biology*. Frontiers Media SA, 9.

Gerety, S. S. *et al.* (2013) 'An inducible transgene expression system for zebrafish and chick', *Development*. Company of Biologists, 140(10), pp. 2235–2243.

Gillies, R. J. *et al.* (2019) 'Targeting acidity in cancer and diabetes', *Biochimica et Biophysica Acta (BBA)-Reviews on Cancer*. Elsevier, 1871(2), pp. 273–280.

Gravendeel, L. A. M. *et al.* (2009) 'Intrinsic gene expression profiles of gliomas are a better predictor of survival than histology', *Cancer research*. AACR, 69(23), pp. 9065–9072.

Grifoni, S. C. *et al.* (2008) 'ASIC proteins regulate smooth muscle cell migration', *Microvascular Research*, 75(2), pp. 202–210. doi: 10.1016/j.mvr.2007.08.003.

Grifoni, S. C., McKey, S. E. and Drummond, H. A. (2008) 'Hsc70 regulates cell surface ASIC2 expression and vascular smooth muscle cell migration', *American Journal of Physiology-Heart and Circulatory Physiology*. American Physiological Society, 294(5), pp. H2022–H2030.

Grifoni, S. C., Murphy, S. and Drummond, H. A. (2007) 'Enhanced surface expression of ASIC2 inhibits VSMC migration'. Wiley Online Library.

Gründer, S. and Pusch, M. (2015) 'Biophysical properties of acid-sensing ion channels (ASICs)', *Neuropharmacology*. Elsevier, 94, pp. 9–18.

Gu, Z. *et al.* (2014) 'Circlize implements and enhances circular visualization in R', *Bioinformatics*. Oxford University Press, 30(19), pp. 2811–2812.

Haar, C. P. *et al.* (2012) 'Drug resistance in glioblastoma: a mini review', *Neurochemical research*. Springer, 37(6), pp. 1192–1200.

Han, X.-J. *et al.* (2015) 'Mitochondrial dynamics regulates hypoxia-induced migration and antineoplastic activity of cisplatin in breast cancer cells', *International journal of oncology*. Spandidos Publications, 46(2), pp. 691–700.

Hawkins, P. T. and Stephens, L. R. (2015) 'PI3K signalling in inflammation', *Biochimica et Biophysica Acta (BBA)-Molecular and Cell Biology of Lipids*. Elsevier, 1851(6), pp. 882–897.

Höckel, M. *et al.* (1996) 'Association between tumor hypoxia and malignant progression in advanced cancer of the uterine cervix', *Cancer research*. AACR, 56(19), pp. 4509–4515.

Hongo, K. *et al.* (2013) 'Hypoxia enhances colon cancer migration and invasion through promotion of epithelial-mesenchymal transition', *Journal of Surgical Research*. Elsevier, 182(1), pp. 75–84.

Hothorn, T., Bretz, F. and Westfall, P. (2008) 'Simultaneous inference in general parametric models', *Biometrical Journal*, 50(3), pp. 346–363. doi: 10.1002/bimj.200810425.

Hu, X. *et al.* (2014) 'Transmembrane TNF-α promotes suppressive activities of myeloid-derived suppressor cells via TNFR2', *The Journal of Immunology*. Am Assoc Immnol, 192(3), pp. 1320–1331.

Huang, B., Song, B. and Xu, C. (2020) 'Cholesterol metabolism in cancer: mechanisms and therapeutic opportunities', *Nature metabolism*. Nature Publishing Group, 2(2), pp. 132–141.

Huang, W. *et al.* (2018) 'Hypoxia enhances the migration and invasion of human glioblastoma U87 cells through PI3K/Akt/mTOR/HIF-1α pathway', *Neuroreport*. Wolters Kluwer, 29(18), pp. 1578–1585.

Ibrahim, S. *et al.* (2021) 'SK4 oncochannels regulate calcium entry and promote cell migration in KRAS-mutated colorectal cancer', *Cell Calcium*, 96, p. 102384. doi: 10.1016/j.ceca.2021.102384.

Inda, M.-M., Bonavia, R. and Seoane, J. (2014) 'Glioblastoma multiforme: a look inside its heterogeneous nature', *Cancers*. Multidisciplinary Digital Publishing Institute, 6(1), pp. 226–239.

Ivanov, D. P. and Grabowska, A. M. (2017) 'Spheroid arrays for high-throughput single-cell analysis of spatial patterns and biomarker expression in 3D', *Scientific Reports*, 7. doi: 10.1038/srep41160.

Iwadate, Y. (2016) 'Epithelial-mesenchymal transition in glioblastoma progression', *Oncology letters*. Spandidos Publications, 11(3), pp. 1615–1620.

Joeres, N. *et al.* (2016) 'Functional and pharmacological characterization of two different ASIC1a/2a heteromers reveals their sensitivity to the spider toxin PcTx1', *Scientific Reports*. Nature Publishing Group, 6(1), pp. 1–14.

Joseph, J. V *et al.* (2015) 'Hypoxia enhances migration and invasion in glioblastoma by promoting a mesenchymal shift mediated by the HIF1α–ZEB1 axis', *Cancer letters*. Elsevier, 359(1), pp. 107–116.

Kallunki, T. *et al.* (2019) 'How to choose the right inducible gene expression system for

mammalian studies?', *Cells*. MDPI, 8(8), p. 796.

Kapoor, N. *et al.* (2009) 'Knockdown of ASIC1 and epithelial sodium channel subunits inhibits glioblastoma whole cell current and cell migration', *Journal of Biological Chemistry*, 284(36), pp. 24526–24541. doi: 10.1074/jbc.M109.037390.

Kathagen-Buhmann, A. *et al.* (2016) 'Glycolysis and the pentose phosphate pathway are differentially associated with the dichotomous regulation of glioblastoma cell migration versus proliferation', *Neuro-oncology*. Oxford University Press US, 18(9), pp. 1219–1229.

Klumpp, L. *et al.* (2018) 'KCa3. 1 channels and glioblastoma: in vitro studies', *Current neuropharmacology*. Bentham Science Publishers, 16(5), pp. 627–635.

Knowles, H. J. and Harris, A. L. (2001) 'Hypoxia and oxidative stress in breast cancer Hypoxia and tumourigenesis', *Breast Cancer Research*. BioMed Central, 3(5), pp. 1–5.

Kolde, R. and Kolde, M. R. (2019) 'pheatmap: Pretty Heatmaps. R package version 1.0. 12 (2019)'.

Korotkevich, G. and Sukhov, V. (2016) 'Fast gene set enrichment analysis', pp. 1–29.

Kucka, K. *et al.* (2021) 'Membrane lymphotoxin-α2β is a novel tumor necrosis factor (TNF) receptor 2 (TNFR2) agonist', *Cell death & disease*. Nature Publishing Group, 12(4), pp. 1–9.

Kuzu, O. F., Noory, M. A. and Robertson, G. P. (2016) 'The Role of Cholesterol in Cancer', *Cancer research*. 2016/04/05, 76(8), pp. 2063–2070. doi: 10.1158/0008-5472.CAN-15-2613.

Lai, W. *et al.* (2013) 'KCNN4 Channels participate in the EMT induced by PRL-3 in colorectal cancer', *Medical oncology (Northwood, London, England)*, 30, p. 566. doi: 10.1007/s12032-013-0566-z.

LaMonte, G. *et al.* (2013) 'Acidosis induces reprogramming of cellular metabolism to mitigate oxidative stress', *Cancer & metabolism*. Springer, 1(1), pp. 1–19.

Lee, J. *et al.* (2006) 'Tumor stem cells derived from glioblastomas cultured in bFGF and EGF more closely mirror the phenotype and genotype of primary tumors than do serum-cultured cell lines', *Cancer cell*. Elsevier, 9(5), pp. 391–403.

Li, P. *et al.* (2013) 'Hypoxia enhances stemness of cancer stem cells in glioblastoma: an in vitro

study', *International journal of medical sciences*. Ivyspring International Publisher, 10(4), p. 399.

Li, Q.-T. *et al.* (2019) 'KCNN4 promotes invasion and metastasis through the MAPK/ERK pathway in hepatocellular carcinoma', *Journal of Investigative Medicine*, 68, p. jim-2019. doi: 10.1136/jim-2019-001073.

Li, Q.-T. *et al.* (2020) 'KCNN4 promotes invasion and metastasis through the MAPK/ERK pathway in hepatocellular carcinoma', *Journal of Investigative Medicine*. BMJ Publishing Group Limited, 68(1), pp. 68–74.

Li, Y. *et al.* (2017) 'BMX/Etk promotes cell proliferation and tumorigenicity of cervical cancer cells through PI3K/AKT/mTOR and STAT3 pathways', *Oncotarget*. Impact Journals, LLC, 8(30), p. 49238.

Li, Z. *et al.* (2003) 'Directional sensing requires Gβγ-mediated PAK1 and PIXα-dependent activation of Cdc42', *Cell*. Elsevier, 114(2), pp. 215–227.

Lien, E. C., Dibble, C. C. and Toker, A. (2017) 'PI3K signaling in cancer: beyond AKT', *Current opinion in cell biology*. Elsevier, 45, pp. 62–71.

Lingueglia, E. (2007) 'Acid-sensing Ion Channels in Sensory Perception', *The Journal of biological chemistry*, 282, pp. 17325–17329. doi: 10.1074/jbc.R700011200.

Liu, Y. *et al.* (2015) 'The blockage of KCa3. 1 channel inhibited proliferation, migration and promoted apoptosis of human hepatocellular carcinoma cells', *Journal of Cancer*. Ivyspring International Publisher, 6(7), p. 643.

Lobo, N. A. *et al.* (2007) 'The biology of cancer stem cells', *Annu. Rev. Cell Dev. Biol.* Annual Reviews, 23, pp. 675–699.

Lottaz, C. *et al.* (2010) 'Transcriptional profiles of CD133+ and CD133− glioblastoma-derived cancer stem cell lines suggest different cells of origin', *Cancer research*. AACR, 70(5), pp. 2030–2040.

Love, M. I., Huber, W. and Anders, S. (2014) 'Moderated estimation of fold change and dispersion for RNA-seq data with DESeq2', *Genome Biology*, 15(12). doi: 10.1186/s13059-014-0550-8.

Luo, W. and Brouwer, C. (2013) 'Pathview: An R/Bioconductor package for pathway-based data integration and visualization', *Bioinformatics*, 29(14), pp. 1830–1831. doi: 10.1093/bioinformatics/btt285.

Marchetti, L. *et al.* (2004) 'Tumor necrosis factor (TNF)-mediated neuroprotection against glutamate-induced excitotoxicity is enhanced by N-methyl-D-aspartate receptor activation: essential role of a TNF receptor 2-mediated phosphatidylinositol 3-kinase-dependent NF-κB pathway', *Journal of Biological Chemistry*. ASBMB, 279(31), pp. 32869–32881.

Marquet, G. *et al.* (2007) 'Grading glioma tumors using OWL-DL and NCI thesaurus', in *AMIA Annual Symposium Proceedings*. American Medical Informatics Association, p. 508.

Martínez, D. *et al.* (2006) 'Extracellular acidosis induces neutrophil activation by a mechanism dependent on activation of phosphatidylinositol 3-kinase/Akt and ERK pathways', *The Journal of Immunology*. Am Assoc Immnol, 176(2), pp. 1163–1171.

Metallo, C. M. *et al.* (2012) 'Reductive glutamine metabolism by IDH1 mediates lipogenesis under hypoxia', *Nature*. Nature Publishing Group, 481(7381), pp. 380–384.

Michalopoulou, E., Bulusu, V. and Kamphorst, J. J. (2016) 'Metabolic scavenging by cancer cells: when the going gets tough, the tough keep eating', *British journal of cancer*. Nature Publishing Group, 115(6), pp. 635–640.

Michl, J. *et al.* (2022) 'CRISPR-Cas9 screen identifies oxidative phosphorylation as essential for cancer cell survival at low extracellular pH', *Cell reports*. Elsevier, 38(10), p. 110493.

Mohr, C. J. *et al.* (2019) 'KCa3. 1 channels confer radioresistance to breast cancer cells', *Cancers*. Multidisciplinary Digital Publishing Institute, 11(9), p. 1285.

Mootha, V. *et al.* (2003) 'PGC-1 alpha-responsive genes involved in oxidative phosphorylation are coordinately downregulated in human diabetes', *Nature genetics*, 34, pp. 267–273. doi: 10.1038/ng1180.

Morgan, M. and Ramos, M. (2021) 'BiocManager: Access the Bioconductor Project Package Repository', *R package version 1.30.16*. Available at: https://cran.r-project.org/web/packages/BiocManager/index.html.

Müller, K. and Wickham, H. (2021) 'tibble: Simple Data Frames', p. v3.0.5. Available at:

https://cran.r-project.org/package=tibble.

Neuwirth, E. (2014) 'RColorBrewer: ColorBrewer palettes. R package version 1.1-2 http://CRAN', *R-project. org/package= RColorBrewer*.

Oh, J. *et al.* (2011) 'Glioblastoma: patterns of recurrence and efficacy of salvage treatments', *Canadian journal of neurological sciences*. Cambridge University Press, 38(4), pp. 621–625.

Olar, A. and Aldape, K. D. (2014) 'Using the molecular classification of glioblastoma to inform personalized treatment', *The Journal of pathology*. Wiley Online Library, 232(2), pp. 165–177.

Osmakov, D. I. *et al.* (2020) 'Animal, herb, and microbial toxins for structural and pharmacological study of acid-sensing ion channels', *Frontiers in pharmacology*. Frontiers Media SA, 11, p. 991.

Oster, L. *et al.* (2022) 'Extracellular pH Controls Chemotaxis of Neutrophil Granulocytes by Regulating Leukotriene B4 Production and Cdc42 Signaling', *The Journal of Immunology*. American Association of Immunologists, 209(1), pp. 136–144.

Parks, S. K., Chiche, J. and Pouyssegur, J. (2011) 'pH control mechanisms of tumor survival and growth', *Journal of cellular physiology*. Wiley Online Library, 226(2), pp. 299–308.

Pelicano, H., Carney, D. and Huang, P. (2004) 'ROS stress in cancer cells and therapeutic implications', *Drug resistance updates*. Elsevier, 7(2), pp. 97–110.

Persano, L. *et al.* (2013) 'Glioblastoma cancer stem cells: role of the microenvironment and therapeutic targeting', *Biochemical pharmacology*. Elsevier, 85(5), pp. 612–622.

Ponomarev, A. *et al.* (2022) 'Intrinsic and extrinsic factors impacting cancer stemness and tumor progression', *Cancers*. MDPI, 14(4), p. 970.

Potter, M., Newport, E. and Morten, K. J. (2016) 'The Warburg effect: 80 years on', *Biochemical Society Transactions*. Portland Press Ltd., 44(5), pp. 1499–1505.

Puchalski, R. B. *et al.* (2018) 'An anatomic transcriptional atlas of human glioblastoma', *Science*. American Association for the Advancement of Science, 360(6389), pp. 660–663.

Qiu, Y. *et al.* (1998) 'Etk/Bmx, a tyrosine kinase with a pleckstrin-homology domain, is an effector of phosphatidylinositol 3'-kinase and is involved in interleukin 6-induced

neuroendocrine differentiation of prostate cancer cells', *Proceedings of the National Academy of Sciences*. National Acad Sciences, 95(7), pp. 3644–3649.

R Warnes, G. *et al.* (2019) 'gplots: various R programming tools for plotting data.', (1).

Rabjerg, M. *et al.* (2015) 'High expression of KCa3. 1 in patients with clear cell renal carcinoma predicts high metastatic risk and poor survival', *PloS one*. Public Library of Science San Francisco, CA USA, 10(4), p. e0122992.

Ran, F. A. *et al.* (2013) 'Genome engineering using the CRISPR-Cas9 system', *Nature protocols*. Nature Publishing Group UK London, 8(11), pp. 2281–2308.

Reimand, J. *et al.* (2019) 'Pathway enrichment analysis and visualization of omics data using g: Profiler, GSEA, Cytoscape and EnrichmentMap', *Nature protocols*. Nature Publishing Group, 14(2), pp. 482–517.

Röhrig, F. and Schulze, A. (2016) 'The multifaceted roles of fatty acid synthesis in cancer', *Nature Reviews Cancer*, 16. doi: 10.1038/nrc.2016.89.

Rong, Y. *et al.* (2006) ''Pseudopalisading'necrosis in glioblastoma: a familiar morphologic feature that links vascular pathology, hypoxia, and angiogenesis', *Journal of Neuropathology & Experimental Neurology*. American Association of Neuropathologists, Inc., 65(6), pp. 529–539.

Rooj, A. K. *et al.* (2011) 'Regulation of Migration and Proliferation of Glioblastoma Cells by Modulating the Acid Sensitive Ion Channel-1 (ASIC-1) Activity'. Wiley Online Library.

Rooj, A. K. *et al.* (2012) 'Glioma-specific cation conductance regulates migration and cell cycle progression', *Journal of Biological Chemistry*, 287(6), pp. 4053–4065. doi: 10.1074/jbc.M111.311688.

Rooj, A. K. *et al.* (2015) 'Physical and functional interactions between a glioma cation channel and integrin-β1 require α-actinin', *American Journal of Physiology-Cell Physiology*. American Physiological Society Bethesda, MD, 309(5), pp. C308–C319.

Rosa, D. *et al.* (2002) 'Functional implications of the localization and activity of acid-sensitive channels in rat peripheral nervous system', *Proceedings of the National Academy of Sciences of the United States of America*, 99, pp. 2326–2331. doi: 10.1073/pnas.042688199.

Ruggieri, P. *et al.* (2012) 'The inhibition of KCa3. 1 channels activity reduces cell motility in glioblastoma derived cancer stem cells'. Public Library of Science San Francisco, USA.

Sahlgren, C. *et al.* (2008) 'Notch signaling mediates hypoxia-induced tumor cell migration and invasion', *Proceedings of the National Academy of Sciences*. National Acad Sciences, 105(17), pp. 6392–6397.

Samuels, Y. and Ericson, K. (2006) 'Oncogenic PI3K and its role in cancer', *Current opinion in oncology*. LWW, 18(1), pp. 77–82.

Schindelin, J. *et al.* (2012) 'Fiji: an open-source platform for biological-image analysis', *Nature Methods*, 9(7), pp. 676–682. doi: 10.1038/nmeth.2019.

Sforna, L. *et al.* (2018) 'Structure, gating and basic functions of the Ca2+-activated K channel of intermediate conductance', *Current Neuropharmacology*. Bentham Science Publishers, 16(5), pp. 608–617.

Sherwood, T. *et al.* (2011) 'Heteromeric Acid-Sensing Ion Channels (ASICs) Composed of ASIC2b and ASIC1a Display Novel Channel Properties and Contribute to Acidosis-Induced Neuronal Death', *The Journal of neuroscience : the official journal of the Society for Neuroscience*, 31, pp. 9723–9734. doi: 10.1523/JNEUROSCI.1665-11.2011.

Singh, S. K. *et al.* (2004) 'Identification of human brain tumour initiating cells', *nature*. Nature Publishing Group, 432(7015), pp. 396–401.

Singh, S. K. *et al.* (2020) 'Critical role of three-dimensional tumorsphere size on experimental outcome', *Biotechniques*. Future Science, 69(5), pp. 333–338.

Sivridis, E., Giatromanolaki, A. and Koukourakis, M. I. (2005) 'Proliferating fibroblasts at the invading tumour edge of colorectal adenocarcinomas are associated with endogenous markers of hypoxia, acidity, and oxidative stress', *Journal of clinical pathology*. BMJ Publishing Group, 58(10), pp. 1033–1038.

Soto, E., Ortega-Ramírez, A. and Vega, R. (2018) 'Protons as messengers of intercellular communication in the nervous system', *Frontiers in cellular neuroscience*. Frontiers Media SA, 12, p. 342.

Subramanian, A. e. . (2005) 'Gene set enrichment analysis: a knowledge-based approach for

interpreting genome-wide expression profiles. Proc Natl Acad Sci U S A', *Proceedings of the National Academy of Sciences*, 102, pp. 15545–15550.

Tevis, K. M., Colson, Y. L. and Grinstaff, M. W. (2017) 'Embedded spheroids as models of the cancer microenvironment', *Advanced biosystems*. Wiley Online Library, 1(10), p. 1700083.

Tian, Y. *et al.* (2017) 'Glioblastoma cancer stem cell lines express functional acid sensing ion channels ASIC1a and ASIC3', *Scientific reports*. Nature Publishing Group, 7(1), pp. 1–14.

Tilghman, J. *et al.* (2014) 'HMMR Maintains the Stemness and Tumorigenicity of Glioblastoma Stem-like CellsTargeting HMMR Inhibits Glioblastoma Stem Cells', *Cancer research*. AACR, 74(11), pp. 3168–3179.

Townsend, D. M. and Tew, K. D. (2003) 'The role of glutathione-S-transferase in anti-cancer drug resistance', *Oncogene*. Nature Publishing Group, 22(47), pp. 7369–7375.

Trédan, O. *et al.* (2007) 'Drug resistance and the solid tumor microenvironment', *Journal of the National Cancer Institute*. Oxford University Press, 99(19), pp. 1441–1454.

Valero-Mora, P. M. (2010) 'ggplot2: Elegant Graphics for Data Analysis ', *Journal of Statistical Software*, 35(Book Review 1). doi: 10.18637/jss.v035.b01.

Vara, J. Á. F. *et al.* (2004) 'PI3K/Akt signalling pathway and cancer', *Cancer treatment reviews*. Elsevier, 30(2), pp. 193–204.

Vergara, C. *et al.* (1998) 'Calcium-activated potassium channels', *Current opinion in neurobiology*. Elsevier, 8(3), pp. 321–329.

Verhaak, R. G. W. *et al.* (2010) 'Integrated genomic analysis identifies clinically relevant subtypes of glioblastoma characterized by abnormalities in PDGFRA, IDH1, EGFR, and NF1', *Cancer cell*. Elsevier, 17(1), pp. 98–110.

Vila-Carriles, W. H. *et al.* (2006) 'Surface expression of ASIC2 inhibits the amiloride-sensitive current and migration of glioma cells', *Journal of Biological Chemistry*. ASBMB, 281(28), pp. 19220–19232.

Vila-Carriles, W. H. *et al.* (2007) 'Participation of the chaperone Hsc70 in the trafficking and functional expression of ASIC2 in glioma cells', *Journal of Biological Chemistry*. ASBMB,

282(47), pp. 34381–34391.

Walker, A. (2018) 'openxlsx: Read, Write and Edit XLSX Files.'

Wang, Q. *et al.* (2017) 'Tumor evolution of glioma-intrinsic gene expression subtypes associates with immunological changes in the microenvironment', *Cancer cell*. Elsevier, 32(1), pp. 42–56.

Ward, R. J. and Dirks, P. B. (2007) 'Cancer stem cells: at the headwaters of tumor development', *Annu. Rev. Pathol. Mech. Dis.* Annual Reviews, 2, pp. 175–189.

Webb, B. A. *et al.* (2011) 'Dysregulated pH: a perfect storm for cancer progression', *Nature Reviews Cancer*. Nature Publishing Group, 11(9), pp. 671–677.

Weigelt, B. and Downward, J. (2012) 'Genomic determinants of PI3K pathway inhibitor response in cancer', *Frontiers in oncology*. Frontiers Research Foundation, 2, p. 109.

Wen, J. *et al.* (2020) 'KCNN4 is a diagnostic and prognostic biomarker that promotes papillary thyroid cancer progression', *Aging*, 12. doi: 10.18632/aging.103710.

Wickham, H. *et al.* (2019) 'Welcome to the tidyverse', *Journal of Open Source Software*, 4(43), p. 1686. Available at: https://www.r-project.org/.

Wickham, H. and Brian, J. (2019) 'readxl: Read Excel Files (Version 1.3.1)', p. R package version 1.3.1. https://cran.r-project.or. Available at: https://cran.r-project.org/package=readxl.

Wickham, H. and Francois, R. (2018) 'dplyr: A Grammar of Data Manipulation'. Available at: https://cran.r-project.org/package=dplyr.

Wickham, H. and Henry, L. (2019) 'tidyr: Tidy Messy Data', *R package version 1.0.0*.

De Witt Hamer, P. C. *et al.* (2008) 'The genomic profile of human malignant glioma is altered early in primary cell culture and preserved in spheroids', *Oncogene*. Nature Publishing Group, 27(14), pp. 2091–2096.

Wu, H., Ying, M. and Hu, X. (2016) 'Lactic acidosis switches cancer cells from aerobic glycolysis back to dominant oxidative phosphorylation', *Oncotarget*. Impact Journals, LLC, 7(26), p. 40621.

Wu, J. *et al.* (2016) 'ASIC subunit ratio and differential surface trafficking in the brain', *Molecular Brain*, 9. doi: 10.1186/s13041-016-0185-7.

Wu, W. *et al.* (2021) 'Glioblastoma multiforme (GBM): An overview of current therapies and mechanisms of resistance', *Pharmacological Research*. Elsevier, 171, p. 105780.

Wulff, H. and Castle, N. A. (2010) 'Therapeutic potential of KCa3. 1 blockers: recent advances and promising trends', *Expert review of clinical pharmacology*. Taylor & Francis, 3(3), pp. 385–396.

Xu, H. *et al.* (2014) 'Tumor-associated macrophage-derived IL-6 and IL-8 enhance invasive activity of LoVo cells induced by PRL-3 in a KCNN4 channel-dependent manner', *BMC cancer*, 14, p. 330. doi: 10.1186/1471-2407-14-330.

Xu, P. *et al.* (2021) 'KCNN4 promotes the progression of lung adenocarcinoma by activating the AKT and ERK signaling pathways', *Cancer Biomarkers*, 31, pp. 1–15. doi: 10.3233/CBM-201045.

Yang, H. W. *et al.* (2012) 'Cooperative activation of PI3K by Ras and Rho family small GTPases', *Molecular cell*. Elsevier, 47(2), pp. 281–290.

Yang, J. *et al.* (2019) 'Targeting PI3K in cancer: mechanisms and advances in clinical trials', *Molecular cancer*. BioMed Central, 18(1), pp. 1–28.

Yellowhair, T. *et al.* (2014) 'Acid Sensing Ion Channels contribute to hypoxia-induced migration in human pulmonary arterial smooth muscle cells (LB788)', *The FASEB Journal*. Wiley Online Library, 28, p. LB788.

Young, M. D. *et al.* (2010) 'Gene ontology analysis for RNA-seq: accounting for selection bias', *Genome Biology*, 11(2). doi: 10.1186/gb-2010-11-2-r14.

Yu, G. *et al.* (2012) 'ClusterProfiler: An R package for comparing biological themes among gene clusters', *OMICS A Journal of Integrative Biology*, 16(5), pp. 284–287. doi: 10.1089/omi.2011.0118.

Yu, G. (2021) 'enrichplot: Visualization of Functional Enrichment Result.', *R package version 1.12.3*. Available at: https://yulab-smu.top/biomedical-knowledge-mining-book/.

Yu, G. and He, Q. Y. (2016) 'ReactomePA: An R/Bioconductor package for reactome pathway analysis and visualization', *Molecular BioSystems*, 12(2), pp. 477–479. doi: 10.1039/c5mb00663e.

Yu, X. *et al.* (2015) 'Acid-sensing ion channels promote the inflammation and migration of cultured rat microglia', *Glia*. Wiley Online Library, 63(3), pp. 483–496.

Zhang, R. *et al.* (2003) 'Etk/Bmx transactivates vascular endothelial growth factor 2 and recruits phosphatidylinositol 3-kinase to mediate the tumor necrosis factor-induced angiogenic pathway', *Journal of Biological Chemistry*. ASBMB, 278(51), pp. 51267–51276.

Zhou, Z. *et al.* (2017) 'The acid-sensing ion channel, ASIC2, promotes invasion and metastasis of colorectal cancer under acidosis by activating the calcineurin/NFAT1 axis', *Journal of Experimental & Clinical Cancer Research*. BioMed Central, 36(1), pp. 1–12.

Zuguang Gu, Roland Eils and Matthias Schlesner (2016) 'Complex heatmaps reveal patterns and correlations in multidimensional genomic data', *Bioinformatics*.